UNIVERSITÀ VITA-SALUTE SAN RAFFAELE

CORSO DI DOTTORATO DI RICERCA
INTERNAZIONALE IN MEDICINA MOLECOLARE

Curriculum in Cellular and Molecular Biology

# Loss of Aquaporin11 affects Polycystin-1 biogenesis *via* $H_2O_2$ accumulation in the Endoplasmic Reticulum

DoS: Prof. Roberto Sitia

Second Supervisor: Prof. David Ron

Tesi di DOTTORATO DI RICERCA di Elisa Speranza

Matr. 017433

Ciclo di Dottorato XXXVI

SSD BIO11/BIO13

Anno Accademico 2022/2023

UNIVERSITÀ VITA-SALUTE SAN RAFFAELE

CORSO DI DOTTORATO DI RICERCA
INTERNAZIONALE IN MEDICINA MOLECOLARE

Curriculum in Cellular and Molecular Biology

# Loss of Aquaporin11 affects Polycystin-1 biogenesis *via* $H_2O_2$ accumulation in the Endoplasmic Reticulum

DoS: Prof. Roberto Sitia

Second Supervisor: Prof. David Ron

Tesi di DOTTORATO DI RICERCA di Elisa Speranza

Matr. 017433

Ciclo di Dottorato XXXVI

SSD BIO11/BIO13

Anno Accademico 2022/2023

# RELEASE OF PHD THESIS

| | |
|---|---|
| Il/la sottoscritto/a/ *I, the undersigned* | Elisa Speranza |
| Matricola/*Registration number* | 017433 |
| Nato/a/ *Born in* | Milano (MI) |
| Il/ *on* | 28/01/1994 |

Autore della tesi di Dottorato di ricerca dal titolo *Author of the PhD Thesis titled*

Loss of Aquaporin11 affects Polycystin-1 biogenesis via $H_2O_2$ accumulation in the Endoplasmic Reticulum

☐ AUTORIZZA la Consultazione della tesi/*AUTHORIZES the public release of the thesis*

■ NON AUTORIZZA la Consultazione della tesi per 12 mesi/DOES NOT AUTHORIZE the public release of the thesis for 12 months

a partire dalla data di conseguimento del titolo e precisamente/*from the PhD thesis date, specifically*

Dal/*from* 11/12/2023 Al/*to* 11/12/2024

Poiché/*because:*

☐ l'intera ricerca o parti di essa sono potenzialmente soggette a brevettabilità/*The whole project or part of it might be subject to patentability;*

■ ci sono parti di tesi che sono già state sottoposte a un editore o sono in attesa di pubblicazione/*Parts of the thesis have been or are being submitted to a publisher or are in press;*

☐ la tesi è finanziata da enti esterni che vantano dei diritti su di esse e sulla loro pubblicazione/*the thesis project is financed by external bodies that have rights over it and on its publication*

È fatto divieto di riprodurre, in tutto o in parte, quanto in essa contenuto/Copyright the contents of the thesis in whole or in part is forbidden

Data/*Date* 11/11/2023 Firma/*Signature* Elisa Speranza

## Declaration

This thesis has been:

- composed by myself and has not been used in any previous application for a degree. Throughout the text I use both 'I' and 'We' interchangeably.
- has been written according to the editing guidelines approved by the University.

Permission to use images and other material covered by copyright has been sought and obtained. For the following image/s (Figure 2B, 6B, 10 and 11), it was not possible to obtain permission and is/are therefore included in thesis under the "fair use" exception (Italian legislative Decree no. 68/2003).

All the results presented here were obtained by myself, except for:

1) ***Intracellular Antibodies Capture Technology screening***

   *Done in collaboration with Prof. Antonino Cattaneo and Dr. Simonetta Lisi, Scuola Normale Superiore di Pisa.*

2) ***Hyper live-imaging experiments***

   *Done in collaboration with Dr. Ilaria Sorrentino, Universidad Carlos III, Madrid.*

All sources of information are acknowledged by means of reference.

## Acknowledgments

First, I would like to thank my Director of Studies, Professor Roberto Sitia for his great support during the last three years and for being always available to enthusiastically discuss science with me.

I gratefully acknowledge Dr. Alessandra Boletta and Dr. Feng Qian for the useful exchange of reagents, ideas and exciting scientific discussion which have helped me a lot.

I would like to thank also my second supervisor, Professor David Ron, for his understanding, personal attention, and scientific advice.

My deep appreciation goes also to my irreplaceable lab mates, former and present. All of you taught me something, both from the scientific and personal side.

Last but not least I want to thank my family and friends for having always been present on this long journey.

## Dedication

*Dedico questa tesi, come qualsiasi altra cosa in cui io mi sia impegnata in passato e in cui mi impegnerò in futuro, ad Angela, Pippo, Daniela, Marco, Matilde, Luca e Arsion.*

## Abstract

Aquaporin11 (AQP11) is an ER-resident channel that allows passive transport of $H_2O_2$ from the ER-lumen to the cytosol, along a concentration gradient. Removing the channel, the flux of $H_2O_2$ that goes from one compartment to the other is blocked. As a consequence, cells with reduced expression of AQP11 display increased concentration of $H_2O_2$ in the ER $(H_2O_2)_{ER}$ and decreased $H_2O_2$ in the cytosol $(H_2O_2)_{cytosol}$, leading to ER hyper-oxidation and possibly impacting cytosolic redox signalling. *Aqp11*$^{-/-}$ mice develop an early onset Polycystic Kidney Disease (PKD) and die of renal failure within three weeks of life. The pathological mechanism proposed was the impaired maturation of Polycystin-1 (PC-1), the product of *PKD1* gene which is mutated in over four fifths of Autosomal Dominant Polycystic Kidney Disease (ADPKD) cases. During its biogenesis, PC-1 undergoes many posttranslational modifications in the early secretory pathway, including *N*-glycosylation, formation of disulfide bonds, autoproteolytic cleavage and assembly with its partner Polycystin-2 (PC-2) to generate functional polycystin complexes. This complex biogenesis is a hard task for cells: mutations in many enzymes involved in *N*-glycan assembly, protein folding, and quality control were found to affect PC-1 biogenesis and cause atypical PKD in humans. Thus, PC-1 processing seems particularly sensitive to perturbations in the folding machinery, and many conditions that are tolerated by other proteins prevent polycystin to reach its functional form. During my PhD studies, I sought to clarify how the absence of functional AQP11 causes PKD. Are the altered $H_2O_2$ fluxes ensuing from lack of AQP11 the cause of impaired polycystin maturation? To address these issues, I investigated whether and how perturbing $H_2O_2$ level and redox homeostasis impacted polycystin. My results provide new insights on how downregulation of AQP11 selectively inhibits PC-1 processing. Using tricks to manipulate $(H_2O_2)_{ER}$ independently by AQP11, I was able to demonstrate that the defect on PC-1 is manifested *via* accumulation of $(H_2O_2)_{ER}$. In addition, I found that loss of AQP11 results in defective *N*-glycan processing that affects PC-1 as well as other glycoproteins. My results confirm the fundamental role of AQP11 as a $H_2O_2$ transporter across the ER membrane, and demonstrate that subtle changes in the $(H_2O_2)_{ER}$ have dramatic consequences in PC-1 biogenesis with broad effects on glycoprotein processing.

# Table of Contents

**1 Introduction**

*1.1 Polycystic Kidney Disease*

1.1.1 ADPKD

1.1.2 Polycystin-1

1.1.3 Polycystin-2

1.1.4 The polycystin complex and other PC-1 isoforms

1.1.5 Genetic heterogeneity of ADPKD and the curious case of AQP11

*1.2 Peroxiporins*

1.2.1 Aquaporins

1.2.2 AQP11 as $H_2O_2$ transporter at the ER membrane

1.2.3 The importance of the redox-second messenger: hydrogen peroxide

1.2.3.1 Redox homeostasis maintenance

*1.3 Physiological consequences of AQP11 mutations*

1.3.1 AQPs and human kidney disorders

1.3.2 Characterization of Aqp11$^{-/-}$ mouse model

**2 Aim**

**3 Results**

*3.1 Screening for intracellular antibodies against AQP11*

*3.2 Studying the effect of AQP11$^{KD}$ on PC-1 or PC-2 maturation*

*3.3 CTF decrease depends on accumulation of $(H_2O_2)_{ER}$*

*3.4 Non-native disulfides are not detected in our system following AQP11$^{KD}$*

*3.5 AQP11$^{KD}$ does not slow down PC-1 autoproteolysis*

*3.6 AQP11$^{KD}$ affects CTF stability via $(H_2O_2)_{ER}$ but does not promote CTF degradation*

*3.7 AQP11$^{KD}$ does not promote CTF insolubility or accumulation of smaller CT-derived forms:*

*3.8 AQP11$^{KD}$ impairs a late step of sugar processing*

*3.9 AQP11$^{KD}$ generally affects sugar processing*

**4 Discussion**

*4.1 Loss of AQP11 leads to atypical Polycystic Kidney Disease*

*4.2 PC-1 is sensitive to changes in $(H_2O_2)_{ER}$ level*

*4.3 How $(H_2O_2)_{ER}$ could influence PC-1 biogenesis?*

*4.4 $AQP11^{KD}$ decreases PC-1 cleaved forms*

*4.5 $AQP11^{KD}$ affects N-linked glycan processing*

*4.6 Concluding remarks*

**5 Materials and methods**

*5.1 Cells culture and methods*

*5.2 Small interfering RNAs, plasmids and transfection procedures*

*5.3 SDS-PAGE and immunoblot*

*5.4 Real-Time qPCR*

*5.5 Radioactive pulse-chase*

*5.6 Protein synthesis and degradation inhibition*

*5.7 Deglycosylation assay*

*5.8 ELISA on secreted IgM*

*5.9 Immunofluorescence*

*5.10 Generation of Halo-DAAO-ER*

*5.11 Hyper Imaging*

*5.12 Quantification and statistical analysis*

*5.13 Intracellular Antibodies Capture Technology screening*

**6 References**

**Acronyms and abbreviations**

| | |
|---|---|
| **$^{-}$L** | medium deprived from leucine |
| **-S** | Thiol |
| **$-S^{-}$** | Thiolate |
| **$-SO_2H$** | Sulfinic acid |
| **$-SO_3H$** | Sulfonic acid |
| **-SOH** | Sulfenic acid |
| **$^{-}$W** | medium deprived from tryptophan |
| **$^{-}$WHL** | medium deprived from tryptophan, histidine, and leucine |
| **μ** | Immunoglobulin heavy chain |
| **λ** | Immunoglobulin light chain |
| **$(H_2O_2)_{cytosol}$** | amount of H2O2 in the cytosol |
| **$(H_2O_2)_{ER}$** | amount of $H_2O_2$ in the ER |
| **ADPKD** | Autosomal Dominant Polycystic Kidney Disease |
| **ADPLD** | Autosomal Dominant Polycystic Liver Disease |
| **AKI** | Acute Kidney Injury |
| **AQP** | Aquaporin |
| **AQP11** | Aquaporin 11 |
| **Ar/R** | aromatic/Arginine |
| **ARPKD** | Autosomal Recessive Polycystic Kidney Disease |
| **ATP** | Adenosine triphosphate |
| **BCA** | Bicinchoninic acid |
| **CAT** | Catalase |
| **CBS** | Cystathione β-Synthase |
| **CKD** | Chronic Kidney Disease |
| **CTF** | C-terminal Fragment |
| **CTT** | C-terminal Tail |
| **Cys** | Cysteine |
| **DTT** | Dithiotreithol |
| **DUOX** | Dual Oxidase |
| **DZIP1L** | DAZ-Interactin Protein 1-like |
| **ER** | Endoplasmic Reticulum |
| **Ero1** | Endoplasmic Reticulum oxireductin 1 |

| | |
|---|---|
| **ERp44** | ER protein 44 |
| **ERp57** | ER protein 57 |
| **ETC** | Electron Transport Chain |
| **FAO** | Fatty Acids Oxidation |
| **FBS** | Fetal Bovine Serum |
| **FL** | Full Lenght |
| **GPS** | G-Protein Coupled Receptor Proteolytic Site |
| **GPX7-8** | Glutathione Peroxidase 7-8 |
| **Grx** | Glutaredoxin |
| **$H_2O_2$** | Hydrogen Peroxide |
| **HEK** | Human Embryonic Kidney |
| **HeLa** | Henrietta Lacks tumoral immortalized cells |
| **hHcys** | Hyper Homocystinuria |
| **IACT** | Intracellular Antibodies Capture Technology |
| **IDR** | Intrinsically Disordered Region |
| **IF** | Immunofluorescence |
| **Ig** | Immunoglobulin |
| **IgM** | Immunoglobulin M |
| **Intrabodies** | Intracellular Antibodies |
| **IP3R** | Inositol 1,4,5-trisphosphate receptor |
| **KD** | Knock Down |
| **KDEL** | ER retention sequence Lys-Asp-Glu-Leu |
| **LB** | Lysis Buffer |
| **LRR** | Leucine Reach Repeat |
| **MAM** | Mitochondrial Associated Membrane |
| **MDCK** | Madin-Darby Canine Kidney |
| **MEF** | Mouse Embryonic Fibroblasts |
| **Met** | Methionine |
| **MTS** | Mitochondrial Targeting Sequence |
| **NDI** | Nephrogenic Diabete Insipidus |
| **NLS** | Nuclear Localization Sequence |
| **NOX** | NADPH Oxidase |
| **NPA** | Arginine-Proline-Alanine |

| | |
|---|---|
| **NTF** | N-termianl Fragment |
| **$O_2$** | molecular oxygen |
| **$O_2^-$** | superoxide anion |
| **PC-1** | Polycystin-1 |
| **PC-2** | Polycystin-2 |
| **PDI** | Protein Disulfide Isomerase |
| **PKD** | Polycystic Kidney Disease |
| **PKD1** | Polycystic Kidney Disease 1 gene |
| **PKD2** | Polycystic Kidney Disease 2 gene |
| **PKHD1** | Polycystic Kidney Hepatic Disease 1 |
| **PRX4** | Peroxiredoxin 4 |
| **PT** | Proximal Tubule |
| **Redoxstasis** | Redox Homeostasis |
| **ROS** | Reactive Oxygen Species |
| **RT** | Room Temperature |
| **S-S** | disulfide bond |
| **SB** | Sample Buffer |
| **SERCA** | Sarcoplasmic/Endoplasmic Reticulum Calcium ATPase |
| **ScFv** | Single Chain Fragment Variable |
| **siRNA** | small interfering RNA |
| **SOCE** | Store Operated Calcium Entry |
| **SOD** | Superoxide Dismutase |
| **Srx** | Sulfiredoxin |
| **SSG** | Oxidized glutathione |
| **TCA** | Trichloacetic acid |
| **TOP** | Tetragonal Opening for Polycystins domain |
| **TRP** | Transient Receptor Potential |
| **Trx** | Thioredoxin |
| **WB** | Western Blot |
| **WCS** | Wall integrity and Stress response Components |
| **YFP** | Yellow Fluorescent Protein |

## List of Figures and Tables

Figure 1: Primary cilia in the renal epithelium.

Figure 2: Polycystin-1.

Figure 3: Polycystin-2

Figure 4: Subselullar localization and Polycystin-1 derived isoforms

Figure 5 Mutations in enzymes involved in ER-protein folding and quality control affecting PC-1

Figure 6: AQPs structure

Figure 7: AQP11 as hydrogen peroxide transporter at the ER membrane

Figure 8: Cysteines fate upon oxidation by $H_2O_2$

Figure 9: Regulation of $H_2O_2$ homeostasis in the ER

Figure 10: Different expression of AQPs in the nephron segments and associated diseases

Figure 11: $Aqp11^{-/-}$ mice develop Polycystic Kidney due to impaired maturation of PC-1

Figure 12: Intracellular Antibodies Capture Technology screening

Figure 13: Validation of the detection system from PC-1-Myc transiently transfected HeLa cells

Figure 14: PC-1's cleaved form are decreased upon AQP11 downregulation

Figure 15: Validation of the phenotype in other cell types

Figure 16. Test whether AQP11KD impacts PC-1 maturation via PC-2

Figure 17. Association with PC-2 stabilizes PC-1 but does not abolish the requirement for AQP11

Figure 18. CBS silencing causes an increase in $(H_2O_2)_{ER}$ and a decrease in CTF accumulation resembling the absence of AQP11 phenotype.

Figure 19. Expression of ER-CAT-Myc reduces $(H_2O_2)_{ER}$ and rescues CTF/(CTF+FL) ratio in $AQP11^{KD}$ cells.

Figure 20. Comparing PC-1-Myc samples with (reduced) or without (non-reduced) addition of DTT in control and $AQP11^{KD}$ cells:

Figure 21. $AQP11^{KD}$ does not inhibit PC-1 autoproteolysis

Figure 22. CTF stability is influenced by $(H_2O_2)_{ER}$

Figure 23: Test Increased degradation of CTF upon $AQP11^{KD}$.

Figure 24. $AQP11^{KD}$ does not significantly increase PC-1 detergent insolubility

Figure 25: Stability of a 30 kDa C-terminal fragment of PC-1 (CTT?).

Figure 26. Endoglycosidases treatment of overexpressed PC-1-Myc in HeLa cells
Figure 27. Schematic representation of the QIF16 mutant and Endo-H treatment
Figure 28. Secreted QIF16 mutant shows a different N-glycan processing and slower secretion in AQP11$^{KD}$ cells
Figure 29. Secreted IgM show defective N-glycans processing in AQP11$^{KD}$ cells
Figure 30. Expression of ER-CAT-Myc in AQP11$^{KD}$ HeLa$_{\mu s\lambda}$ cells
Figure 31: Halo-DAAO-ER expression in HeLa cells
Figure 32. Analysis of PC-1 pathogenic mutations
Figure 33: Analysis of predicted IDRs and redox-conditional IDRs in human PC-1 protein sequence
Figure 34: Experimental time-line for each cell line
Figure 35: Time-line for radioactive pulse-chase experiment
Figure 36: Time line for ELISA test
Figure 37: Time-line for live-imaging with HyperProbe
Figure 38: Schematic representation of the main steps of the screening

Table 1: list of genes which mutation affect PC-1 maturation leading to ADPKD and/or ADPLD
Table 2: List of CxxC motifs
Table 3 List of the cell lines used in this work
Table 4: number of cells plated for each cell line
Table 5: List of siRNA sequences used in this work
Table 6: List of plasmids used in this work
Table 7: List of primary antibodies used in this work for immunoblot
Table 8: List of primer sequences used in this work forRT qPCR
Table 9: List of primary antibodies used in this work for immunofluorescence
Table 10: Primer used to generate Halo-DAAO-ER
Table 11: List of primers used to generate the “Baits”

# 1 Introduction

## 1.1 Polycystic Kidney Disease

### *1.1.1 ADPKD*

Polycystic Kidney Disease (PKD) is an end-stage disease characterized by the formation of fluid-filled cysts mainly in the kidney but also other organs, such as the liver, can be affected. The most diffuse form is Autosomal Dominant Polycystic Kidney Disease (ADPKD) that affects around 1:500-1.000 live births (Bergmann *et al*, 2018). The adult-onset of ADPKD is consistent with the disease being caused mainly by germline heterozygous mutations in *PKD1* (~78%) or *PKD2 (15%)* genes which encode Polycystin-1 (PC-1) and Polycystin-2 (PC-2) respectively (Hughes *et al*, 1995; Cai *et al*, 1999; Cornec-Le Gall *et al*, 2018b; Harris & Torres, 2014). At birth, renal function is normal, meaning that one healthy copy of the gene is sufficient to have normal kidney morphology and function. With aging, the insurgence of a somatic mutation that affects the healthy copy of *PKD1* or *PKD2,* or another gene important for proper PC-1 and/or PC-2 biogenesis, leads to the development of a cyst. Cysts form when the levels of functional polycystin, that is the complex formed by PC-1 and PC-2 is sufficient to guarantee the required activity. Indeed, while 0% of functional (homozygous loss of function) PC-1 is embryonically lethal and 50% (heterozygous) is enough to prevent the disease, the range in between reflects the timing and severity of cystogenesis progression (Hopp *et al*, 2012; Fedeles *et al*, 2014). PC-1 and PC-2 are abundant in the primary cilium (Igarashi & Somlo, 2002). Primary cilia are sensory single organelles that extrude from the membrane of most cell types that undergo cell cycle arrest. Their internal structure is called ciliary axoneme and consists of a circular array of nine pairs of microtubules that extend from a basal body originating from centrioles (see Figure 1A). In the kidney, primary cilia protrude from the apical surface of epithelial cells facing the tubules lumen and sensing the extracellular environment (see Figure 1B) (Lee & Somlo, 2014). Mutations that affect genes encoding for proteins important for primary cilia structure or function, such as ADPKD-related proteins, result in abnormal development of this organelle (see Figure 1C). Thus, ADPKD is categorized as a ciliopathy (Schwartz *et al*, 2011).

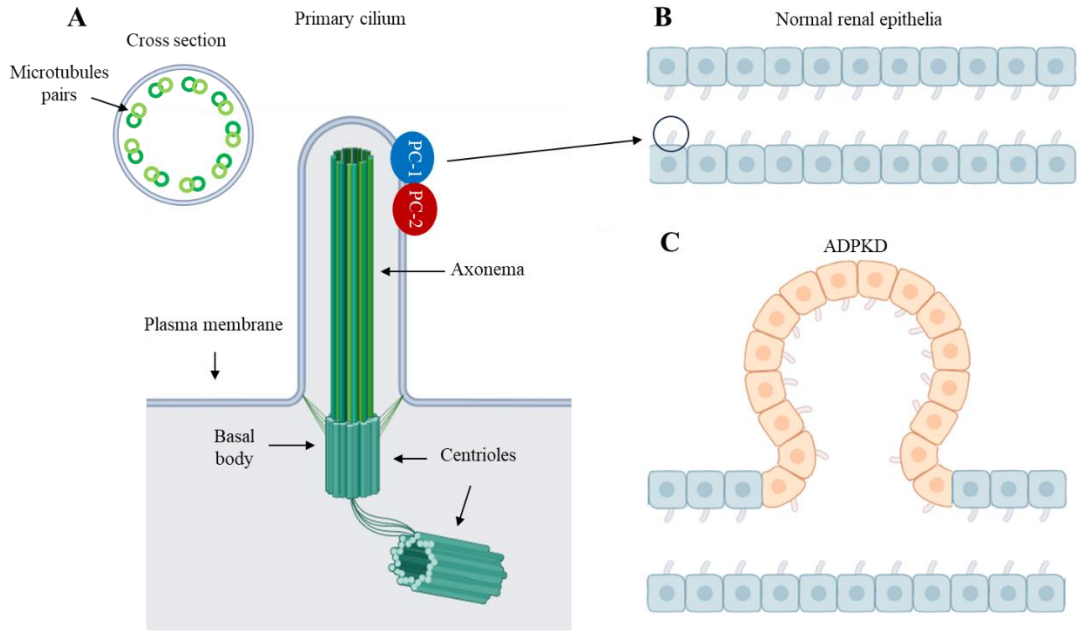



***Figure 1: Primary cilia in the renal epithelium.***
*A) Structure of the primary cilium and localization of the polycystin complex.*
*B) When functional PC-1 and PC-2 are properly localized at primary cilia of renal epithelial cells, the tissue develops normally.*
*C) Reduced polycystin complex at the primary cilia leads to cystogenesis (ADPKD).*

### *1.1.2 Polycystin-1*

Mutations affecting the biogenesis of PC-1 are the most frequent causes of ADPKD. PC-1 is widely expressed in the human body, particularly in the kidney epithelium, liver, pancreas, lung, vascular endothelium, and smooth muscles. PC-1 shows a peak of expression during embryonic kidney development, while it is expressed at lower levels postnatally and in adulthood (Ibraghimov-beskrovnaya *et al*, 1997; Geng *et al*, 1997; Padovano *et al*). PC-1 consists of 4303 amino acids and in the mature form it weighs approximately 500 kDa, owing to abundant *N*-glycosylation. It comprises an N-terminal fragment (NTF) of ≈3000 amino acids and a C-terminal fragment (CTF) of ≈1300 amino acids. The NTF contains domains involved in cell-cell and cell-matrix interactions, such as leucine-rich repeat (LRR) motifs, a cell Wall integrity and Stress response Components (WSC) homology domain, a C-type lectin domain, an LDL-A related domain and 16 PKD Immunoglobulin (Ig)-Like domains (Somlo & Guay-Woodford, 2009). The NTF also contains a Receptor for Egg Jelly (REJ) domain which integrity is important for PC-1

autoproteolysis. Indeed, the autocleavage of PC-1 at the G-Protein Coupled Receptor Proteolytic Site (GPS), is an essential event for polycystin biogenesis (Qian et al., 2002). The CTF is instead composed by 11 transmembrane regions and a cytosolic terminal tail (CTT) of ≈220 amino acids (see Figure 2A). During its biogenesis in the ER, PC-1 undergoes many processing steps that need to be strictly followed to have a functional complex at the primary cilium. PC-1 counts 60 putative *N*-glycosylation sites (Hughes *et al*, 1995), which are essential for folding and transport. In the ER, PC-1 assemble with its partner PC-2 forming the so called polycystin complex. Association with PC-2 is not a prerequisite but it stimulates PC-1 *cis*-autoproteolysis at the GPS. The GPS is formed by three aminoacidic residues: Histidine$^{3047}$, Leucine$^{3048}$ and Threonine$^{3049}$ (HLT). The catalytic mechanism starts with His$^{3047}$ that deprotonates the hydroxyl group of Thr$^{3049}$ that in turns launches a nucleophilic attack to the α-carbon of Leu$^{3048}$. This leads to the formation of an ester intermediate that finally results in the break of the peptide bond between Leu$^{3048}$ and Thr$^{3049}$ (Wei *et al*, 2007). For this reaction to start, these three amino acids need to be maintained in an optimal conformation. Among the elements that contribute to keep GPS conformation there are an extensive network of hydrophobic interactions and a disulfide bond (Cys$^{3015}$-Cys$^{3043}$) (See Figure 2B) (Trudel et al., 2016). Importantly, ≈30% of pathogenic mutations are predicted to disrupt the GPS cleavage (Trudel et al., 2015), underlining the importance of this step for PC-1 maturation and functionality. The GPS cleavage results in the dissociation between NTF and CTF that then remain non-covalently associated (Qian et al., 2002). Finally, PC-2 promotes trafficking of polycystin complex through the secretory pathway to the cell membrane (Gainullin *et al*, 2015).

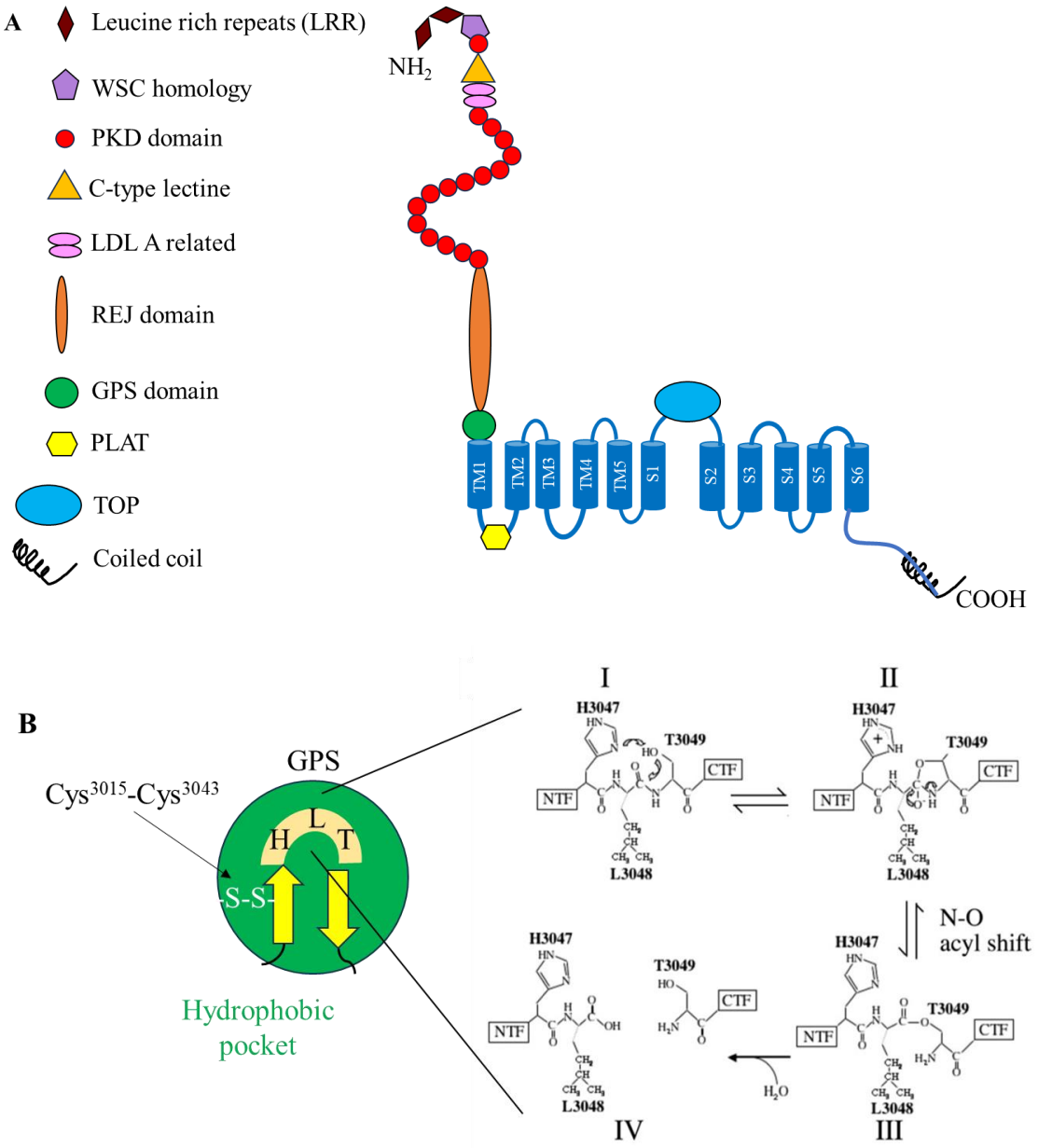



***Figure 2: Polycystin-1***.
*A) Structural domains of PC1.*
*B) Zoom on the GPS cleavage site showing the residues involved and the processing.*
*Adapted from Trudel et al.,2015: The role of G-protein-coupled receptor proteolysis site cleavage of Polycystin-1 in renal physiology and Polycystic Kidney Disease, Cells, 2016.*

### *1.1.3 Polycystin-2*

PC-2 is the second most frequently mutated protein in ADPKD. It is part of the Transient Receptor Potential (TRP) family of non-selective cation channels that *in vivo* are mainly permeable to calcium ($Ca^{2+}$). PC-2 is ubiquitous, and remains highly expressed from embryogenesis throughout adult life (Padovano et al., 2020). PC-2 is composed by 6 transmembrane regions. Both its N-terminus and the C-terminus face the cytosol. The N-terminus contains a ciliary targeting sequence, while the C-terminus an Endoplasmic Reticulum (ER)- retention sequence, as well as an EF-hand motif for $Ca^{2+}$ binding and the coiled-coil region to bind PC-1 (see Figure 3). PC-2 was found to form homotetramers by interactions of TOP domains between S1 and S2 (Grieben *et al*, 2016). These complexes are predominantly localized in the ER where they regulate release of $Ca^{2+}$ (Koulen *et al*, 2002; Shen *et al*, 2016). Also, PC-2 was found to form heterotetramers with PC-1, the so called polycystin complex. The polycystin complex displays different subcellular localization and function than PC-2 homotetramers.

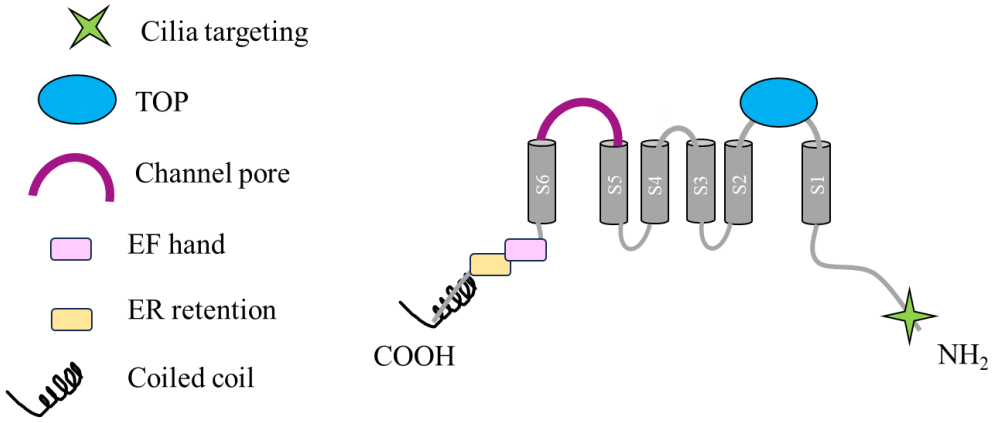



***Figure 3: Polycystin-2***
*Structural domains.*

### *1.1.4 The polycystin complex and other PC-1 isoforms*

The heterotetramer is formed by one PC-1 and three PC-2 molecules (Yu *et al*; Su *et al*, 2018). The two proteins interact mainly through coiled-coil regions in their C-terminus, but also the Tetragonal Opening for Polycystins (TOP) domains, found in the loop between S1 and S2 of both proteins, participate in the assembly (Tsiokas et al., 1997; Su et al, 2018). Subcellularly, the complex is found at the membrane of primary cilia where PC-1 is thought to act as extracellular receptor that senses the environment and transduces the stimuli intracellularly, including via $Ca^{2+}$ uptake (Ta *et al*, 2020). Polycystin complexes are also enriched at Mithocondria Assosiated Membranes (MAMs) where they are thought to regulate $Ca^{2+}$ transfer from ER to mitochondria (Padovano et al, 2017). In addition, PC-1 can localize without PC-2 at the plasma membrane to take part to the formation of tight junctions, adherens junctions and desmosomes (see Figure 4A) (Russo et al., 2005; Silberberg et al, 2005; Roitbak et al, 2004). Importantly, other cleavages occur within the CTF of PC-1 that give rise to C-terminal isoforms with different length and functions within the cell. One of these is the p100 fragment that retains the last 6 transmembrane domains of PC-1. p100 localizes in the ER and negatively regulates the Store Operated Calcium Entry (SOCE) (see Figure 4B) (Woodward et al, 2010). The precise site and the mechanism of cleavage that leads to p100 generation are not currently understood. In addition, a cleavage in the cytosolic tail by γ-secretase releases the CTT (Merrick et al., 2012), a fragment of ≈34 kDa (see Figure 4B). Thanks to a Nuclear Localization Sequence (NLS), CTT can be translocated in the nucleus where it regulates the AP-1, STAT, Wnt and other transcriptional signalling pathways (Arnould et al, 1998; Chauvet et al., 2004; Low et al, 2006; Lal et al., 2008). CTT also has a Mitochondrial Targeting Sequence (MTS). Interestingly, it and was found in the mitochondrial matrix where it regulates metabolism and redox homeostasis (Lin et al., 2018; Onuchic et al, 2023). Recently, it was observed that the mere over expression of CTT in an ADPKD mouse-model was sufficient to rescue the cystic phenotype due to the absence of PC-1 (Onuchic et al, 2023), indicating that this part of the protein is crucial to prevent cystogenesis.

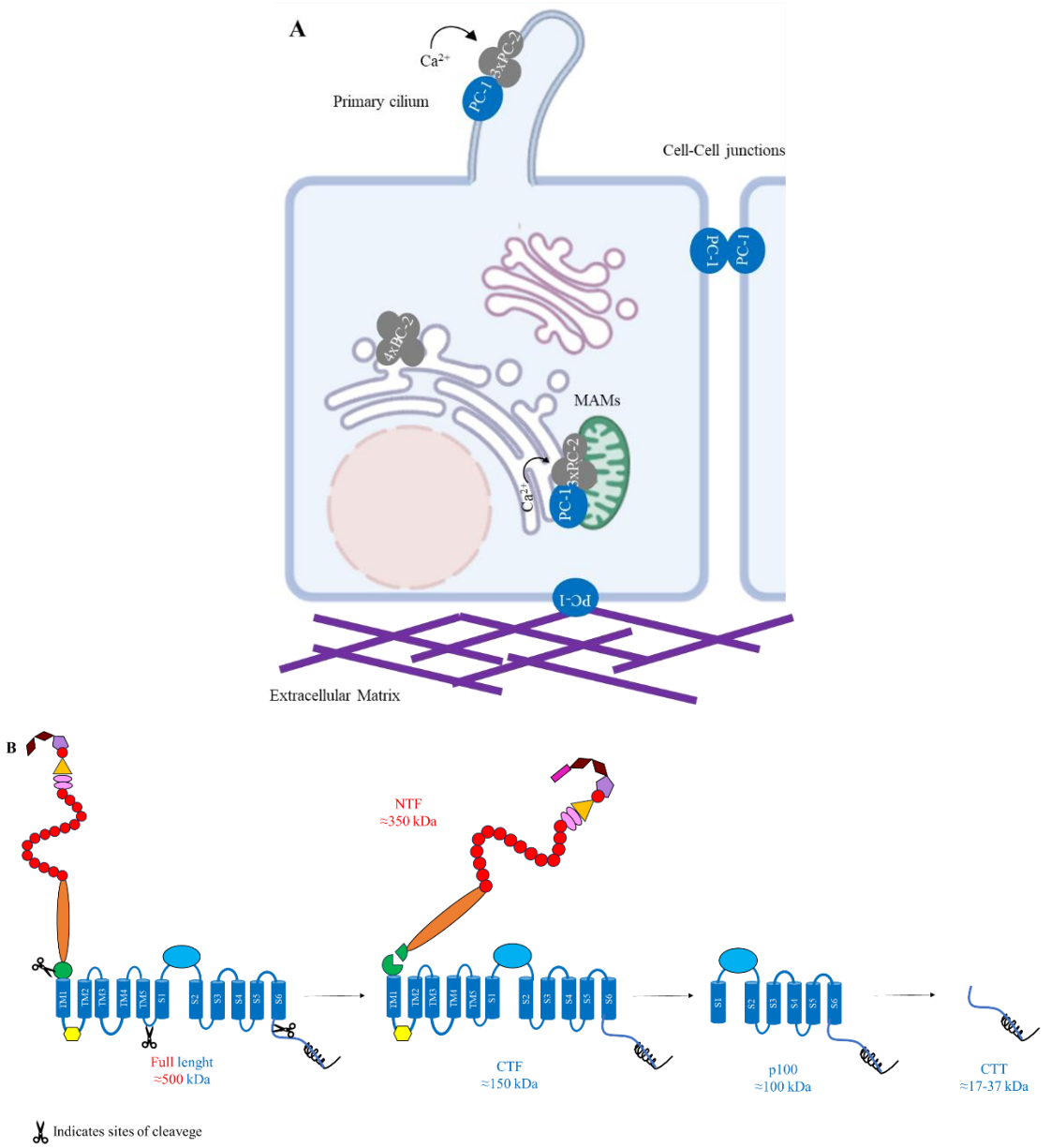



***Figure 4: Subcelullar localization and Polycystin-1 derived isoforms***

*A) Subcellular localization of polycystin complex at primary cilia and MAMs, PC-2 homotetramers in the ER and PC-1 monomer at the plasma membrane.*

*B) Isoforms derived from PC-1 cleavage.*

### *1.1.5 Genetic heterogeneity of ADPKD and the curious case of AQP11*

Pathogenic mutations in *PKD1* or *PKD2* account for the majority of ADPKD cases. In a small fraction of patients (5-10%) pathology is associated with rarer mutations that result in atypical forms of PKD. Among those genes are *ALG5*, *ALG9*, *DNAJB11*, *GANAB* and *IFT140* (Harris *et al*, 2002). Whit the exception of Intraflagellar Transport

140 (IFT140) which is a primary cilia-related protein (Senum et al., 2022), the other genes found mutated encode for ER resident proteins which are involved in *N*-glycosylation and protein folding (see Table 1 and Figure 5 for details). Importantly, these mutants share a common mechanism of cystogenesis which implies impaired maturation and trafficking of PC-1 (Cornec-Le Gall *et al*, 2018a; Besse *et al*, 2018, 2019; Lemoine *et al*, 2022). In addition, other mutations associated with genes encoding for ER-quality control enzymes were found to affect PC-1 especially, resulting in Autosomal Dominant Polycystic Liver Disease (ADPLD) with or without (w/wo) kidney cystogenesis. Among those genes are *SEC63, SEC61B, ALG8, PRKCSH* and *GANAB* (see Table 1 and Figure 5) (Fedeles et al, 2015, Fedeles et al., 2011; Besse et al, 2017). These findings suggest that in case of defective assistance of ER protein folding, marooned PC-1 is one of the proteins that majorly suffers for this impairment. Taken together, these observations suggest that its maturation requires the total attention of the quality control systems. Interestingly, also mutations in another gene that encode for an ER resident protein, Aquaporin11 (Aqp11), was found to cause a PKD in knock out mice (Inoue et al., 2014). Very recently, a casa of PKD associated with compound heterozygous variants of *AQP11* was described in human (Price *et al*, 2023). How loss of AQP11 affects PC-1 leading to PKD is currently not understood.

| *GENE* | *FUNCTION* | *DISORDER* | *REFERENCE* |
|---|---|---|---|
| ***ALG5*** *(Dolichyl-Phosphate β-Glucosyltransferase)* | Addition of the first glucose on the assembling N-glycan precursor | ADPKD | Lemoine et., 2022 |
| ***ALG9*** *(α-1,2-Mannosyltransferase)* | Addition of mannose on the assembling N-glycan precursor | ADPKD w/wo cysts in the liver | Besse et al., 2019 |
| ***DNAJB11*** *DNAJ Heat Shock Protein family Member B11)* | Co-chaperon of Bip | ADPKD w/wo cysts in the liver | Cornec-Le Gall et al., 2018; Huynh et al., 2020 |
| ***GANAB*** *(α-glucosidaseII)* | Glucose trimming from immature glycoproteins | ADPKD and ADPLD | Porath et al., 2016; Besse et al., 2017; Besse et al., 2018 |
| ***ALG8*** *(α-1,3-Glucosyltransferase)* | Addition of the second glucose on the assembling N-glycan precursor | ADPLD w/wo cysts in the kidney | Besse et al., 2017 |
| ***PRKCSH*** *(β-glucosidaseII)* | Glucose trimming from immature glycoproteins | ADPLD | Li et al., 2003; Fedeles et al., 2011 |
| ***SEC63*** | Translocon subunit | ADPLD | Davila et al., 2004; Fedeles et al., 2011; Fedeles et al., 2015 |
| ***SEC61B*** | Translocon subunit | ADPLD | Besse et al., 2017 |

***Table 1: list of genes which mutation affect PC-1 maturation leading to ADPKD and/or ADPLD***

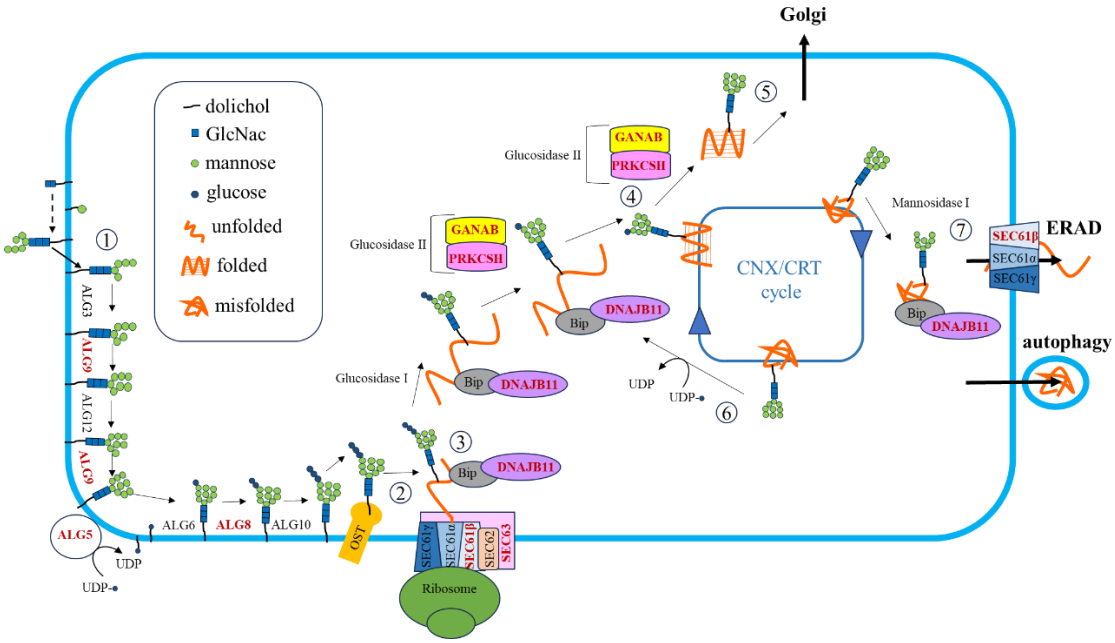



***Figure 5 Mutations in enzymes involved in ER-protein folding and quality control affecting PC-1***

*Here are depicted the principal steps of protein folding in the ER. The enzymes in red, when mutated, affect PC-1 maturation leading to Polycystic Kidney/Liver Disease.*

*1) ALG-3, ALG9, ALG12, ALG5, ALG6, ALG8 and ALG10 glycosyltransferases catalyse the biosynthesis of the oligosaccharide precursor.*

*2) The oligosaccharide precursor is attached by the Olygosaccharyl transferase (OST) complex to the nascent polypeptide emerging from the ribosome-SEC translocon complex.*

*3) Chaperones such as Bip and DNAJB11 associate to the unfolded protein preventing its misfolding.*

*4) Glucose moieties are subsequently removed by Glucosidase I and II allowing the protein to enter in the Calnexin/Calreticulin (CNX/CRT) cycle that promote proper folding by preventing premature aggregation.*

*5) Folded proteins exit the cycle by trimming of the last glucose by Glucosidase II and proceed toward the Golgi.*

*6) Misfolded proteins are re-glucosylated by UDP-glucose enzymes and retained in the CNX/CRT cycle.*

*7) Terminally misfolded proteins are deprived of one mannose moiety by Mannosidase I, retrotranslocated to the cytosol through the Sec61 complex and targeted to ER associated degradation (ERAD) or autophagy (Araki & Nagata 2011)*

*Adapted from Hu and Harris, Regulation of polycystin expression, maturation and trafficking, Cellular Signalling, 2020.*

## 1.2 Peroxiporins

### *1.2.1 Aquaporins*

AQP11 belongs to the family of aquaporins (AQPs). AQPs are channels that guarantee the passage of water across the biological membranes (Preston et al, 1993). More recently it was found that some of them can transport also other small uncharged solutes besides water, for example glycerol, urea, or hydrogen peroxide ($H_2O_2$). The human genome contains 13 AQPs (AQP0-12). All share the same homotetrameric structure, each monomer being composed of six transmembrane alpha-helices connected by short loops. Both the N and C termini face the cytosol. The 13 human AQPs are not homogeneously distributed along the body (protein atlas), possibly correlating permeability to different solutes with the specific needs of the tissue in which are expressed. The selective permeability of each AQP is given by two structural components: two Arginine-Proline-Alanine (NPA) motifs at the channel center that act as electrostatic barrier for ions (Murata *et al*, 2000), and an aromatic/Arginine (ar/R) at the extracellular face that limit the size of solutes that can cross the pore (see Figure 6) (Törnroth-Horsefield *et al*, 2010).

Among AQPs, four were shown to transport also $H_2O_2$, and for this reason are called "peroxiporins". These peroxiporins comprise AQP3, AQP8, AQP9 and AQP11 (Miller et al, 2010; Bertolotti et al, 2013; Watanabe et al, 2016; Bestetti et al, 2020). While AQP3, 8 and 9 are localized at the plasma membrane, AQP11 accumulates in the ER membrane (Bestetti *et al*, 2020).

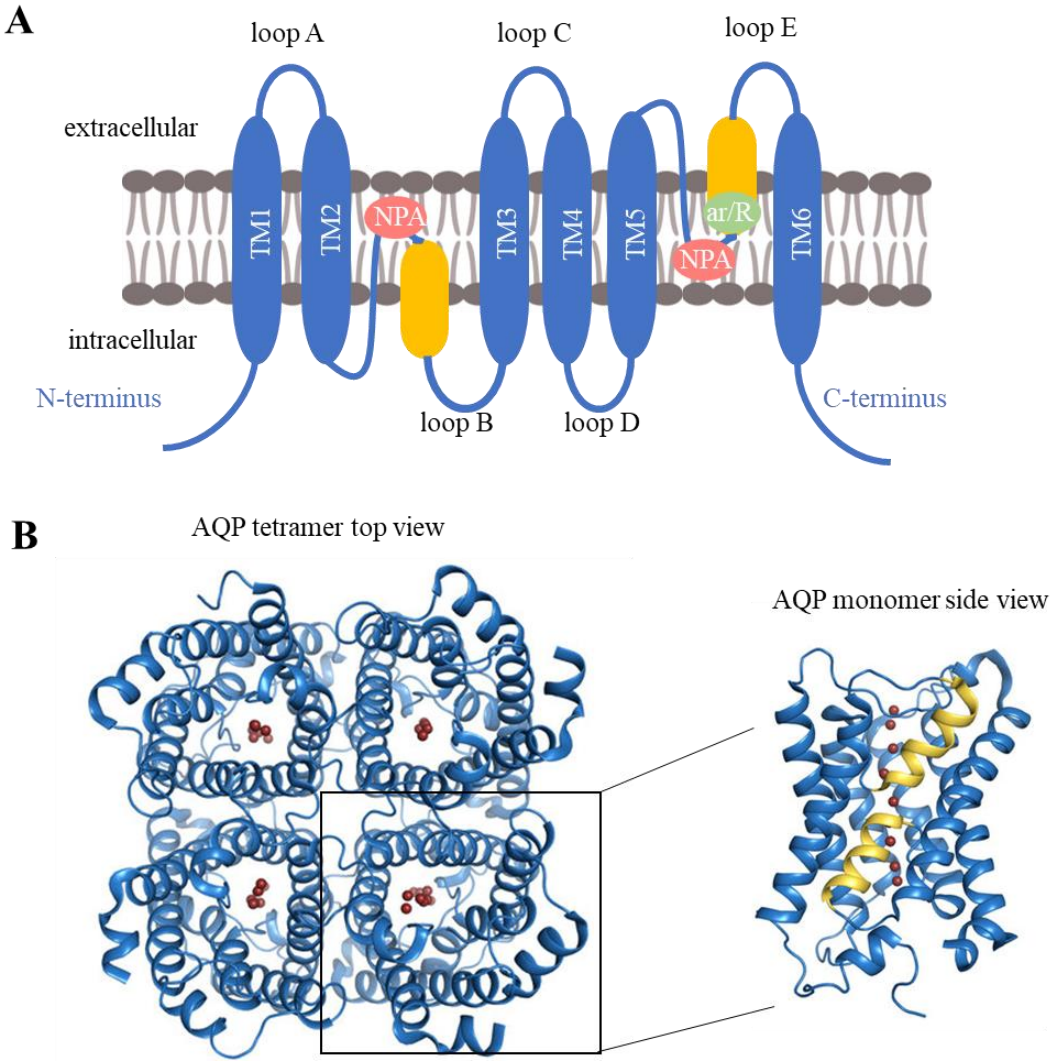



***Figure 6: AQPs structure***

*A) Lateral scheme of AQP monomer with structural domains.*

*B) 3D strture of AQP tetrament (top view) and monomer (side view). Adapted from Nesverove and Tornroth-Horsefield, Phosphorylation-dependent regulation of mammalian Aquaporins, Cells, 2019.*

### *1.2.2 AQP11 as $H_2O_2$ transporter at the ER membrane*

AQP11 is the only known AQP that stably resides at the ER. Moreover, Bestetti and colleagues demonstrated that a tagged version of AQP11, when overexpressed, was enriched at MAMs, an ER subregion that establish close contacts with mitochondria. Also, they took advantage of a ratiometric HyPer probe (Belousov *et al*, 2006) expressed in different compartments (ER-lumen or cytosol) to measure the local $H_2O_2$ environment

and the permeability of the ER membrane to this redox molecule. With this system, it was shown that AQP11 is a proteinaceous channel that can transport $H_2O_2$ across the organelle lipid bilayer. As a consequence, AQP11 silencing increased the basal $H_2O_2$ amount in the lumen of the ER $(H_2O_2)_{ER}$ because the absence of the channel traps these molecules inside the compartment. On the other side, the lack of AQP11 causes a decrease in $(H_2O_2)_{cytosol}$ (see Figure 7). Taken together, these findings revealed that AQP11 mediates a $H_2O_2$ flux from the ER to the cytosol. More recently, it was shown that AQP11 can also mediate the exchange of $H_2O_2$ between the ER and mitochondria in specific conditions (Sorrentino *et al*, 2022). Thus, this peroxiporin is key player in maintaining redox homeostasis inside the ER. Perturbing its function might interfere with the process of oxidative folding. At the same time, blocking the flux of $H_2O_2$ to the cytosol may prevent correct propagation of redox signalling. In summary, AQP11 is fundamental for both intra- and inter-organellar redox regulation.

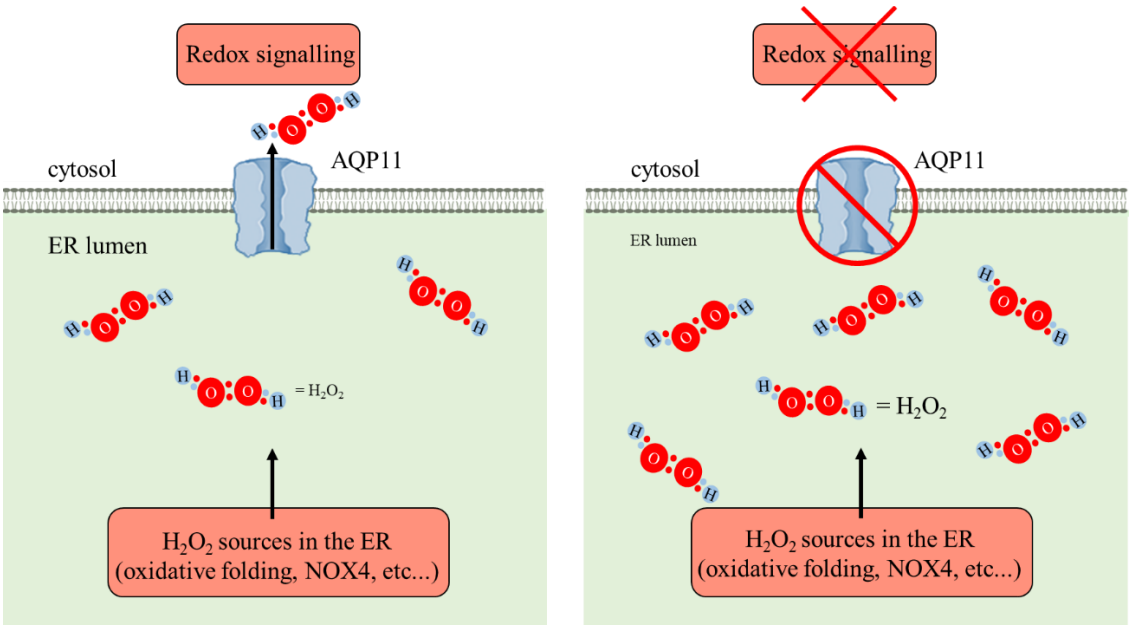



***Figure 7: AQP11 as hydrogen peroxide transporter at the ER membrane***
*$H_2O_2$ produced in the ER reaches its cytosolic targets through AQP11. Depletion of AQP11 accumulates $H_2O_2$ in the ER and reduces $H_2O_2$ in the cytosol.*

### *1.2.3 The importance of the redox-second messenger: hydrogen peroxide*

The term Reactive Oxygen Species (ROS) encloses a variety of different molecule deriving from the continuous reduction of molecular oxygen ($O_2$) Among them, $H_2O_2$ is the most stable and abundant within the cell and it works as second messenger for transmitting redox signalling (Meng *et al*, 2002). Redox reactions entail the passage of at least one electron from one molecule to another. The molecule that loses the electron is oxidized, while the one that gains the electron is reduced. In this kind of reactions, $H_2O_2$ can act as oxidizing agent which acquires two electrons from the molecule which is oxidized turning into two water molecules. In carrying out its job, $H_2O_2$ can modify proteins and lipids. For what concern proteins, it reacts with specific thiols (-S) of cysteine (Cys) or methionine (Met). The sulphur atom of methionine is oxidized producing a sulfoxide (Hoshi and Heinemann 2001). Cysteine oxidation can generate a number of moieties, including disulfide bonds (S-S). Disulfides not only are used as structural elements. Indeed, very often, S-S formation generates conformational changes that act as molecular switches and generate reversible signals. How then can redox signals be targeted in living cells, when the concentration of proteins is extremely high? The low reactivity of $H_2O_2$ makes it the best candidate to mediate specific redox reactions. Indeed, not all Cys or Met residues react similarly with $H_2O_2$. Rather, only those located in suitable protein environment would react with $H_2O_2$ and eventually generate a signal. $H_2O_2$ reacts with thiolates from Cys residues which are in the deprotonated form ($-S^-$) to form Sulfenic acid (-SOH). This modification is quite unstable. As a consequence, it is reverted to thiolate or it proceeds through subsequent reactions, including the formation of an intra- or inter-molecular disulfide bond with another Cys residue (S-S) or glutathionylation by reacting with glutathione (SSG). Both disulfides and glutathionylation can be reverted by enzymes of the thioredoxin (Trx) and glutaredoxin (Grx) system respectively. Another option for sulfenic acid is to be further oxidized by $H_2O_2$ to form sulfinic acid ($-SO_2H$) and sulfonic acid ($-SO_3H$). Sulfinic acid can still be reduced back by the Sulfiredoxin (Srx) system, while Sulfonic acid is an irreversible state (see Figure 8) (Roscoe & Sevier 2020).

Redox modifications of one or more target cysteines in a protein changes its behavior, activity and fate. For example, they can augment or inactivate their function, alter

subcellular localization, change interactors, or increase/decrease their stability (Holmström & Finkel, 2014).

Hence, redox signals are vital for cells since they regulate virtually all vital processes, including proliferation, differentiation, migration, and angiogenesis (Sies & Jones, 2020).

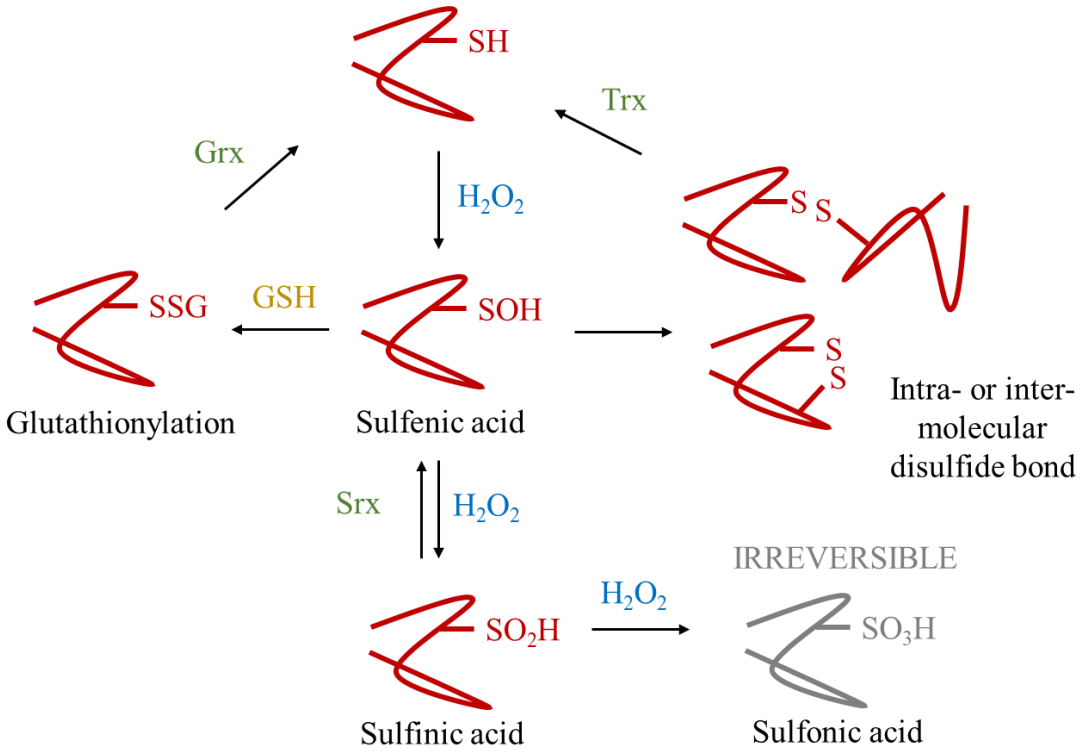



***Figure 8: Cysteines fate upon oxidation by $H_2O_2$***
*Adapted from Roscoe and Sevier, Pathway for sensing and responding to hydrogen peroxide at the endoplasmic reticulum, Cells, 2020.*

### *1.2.3.1 Redox homeostasis maintenance*

$H_2O_2$ can be defined as a pleiotropic antagonist: its pleiotropism, is given by the fact that this agent exerts many different roles within the cell, while the term antagonist refers to the fact that, according with the spatiotemporal concentration of this molecule in each specific site of the cell, it can have essential or harmful effect. Indeed, while in normal conditions, the stimuli triggered by $H_2O_2$ are vital, when at too high a concentration, $H_2O_2$ may react non-specifically causing oxidative stress and cell damage. Helmut Sies defined the two conditions as eustress and distress. The beauty of this antinomy is that stress occupies a central role. Over the last decades, biology is diverging from trade unions and

popular media in reconsidering stress as an essential element of life. Too much is not bad, but no stress equals death. Likewise, if its concentration becomes too low, $H_2O_2$ may prevent redox signalling also being harmful. Thus, it is essential for cells to maintain an equilibrium by controlling $H_2O_2$ concentration in all its sub-compartments (Sies, 2017).

To achieve this level of regulation, cells relay on the compartmentalization of $H_2O_2$ producers. Indeed, $H_2O_2$ is almost always produced in compartments which are membrane separated from its cytosolic targets, including the extracellular environment, mitochondria, and the ER (Sies & Jones, 2020; Nordzieke & Medraño-Fernandez, 2018).

The main sources that generate $H_2O_2$ toward the extracellular space are enzymes called NADPH oxidases (NOX1-5) and dual oxidase (DUOX1-2), that can be found at the plasma membrane. In mitochondria, the main sources of $H_2O_2$ are thought to be the complex I and III of the Electron Transport Chain (ETC), even if other enzymes in the mitochondrial matrix and inner mitochondrial membrane can contribute (Holmström & Finkel, 2014). Both at the plasma membrane and mitochondria, in most cases, superoxide anion ($O_2^-$) is produced which is then rapidly converted into $H_2O_2$ by superoxide dismutase (SOD1-3).

Another important source of $H_2O_2$ within the cell is the ER. In here, one of the sources is NOX4, an enzyme that can directly produce $H_2O_2$. Unlike other members of the NOX family, which are activated following a stimulus, NOX4 is thought to be constitutively active at the ER membrane (Laurindo *et al*, 2014) (see Figure 9). Another important source of $H_2O_2$ in the ER lumen is the process of oxidative folding by which disulfide bonds are formed in newly synthetized proteins. Indeed, for each disulfide formed, one molecule of $H_2O_2$ is released as a byproduct of Protein Disulfide Isomerase (PDI) reoxidation by ER oxidoreductin 1a (Ero1a) (see Figure 9) (Tu & Weissman, 2002, 2004), making the ER-lumen the most oxidized compartment within the cell. Finally, other less characterized sources of $H_2O_2$ in the ER are cytochromes belonging to the P450 family (Nordzieke & Medraño-Fernandez, 2018; Sies & Jones, 2020). To counteract the potential toxicity of excess $H_2O_2$ production, the ER harbours enzymes that act as powerful $H_2O_2$ scavengers, including peroxiredoxin 4 (PRX4) and glutathione peroxidases (GPX7 and GPX8). In these enzymes, an active cysteine becomes sulfenylated upon reaction with $H_2O_2$ (Konno *et al*, 2021). The -SOH group can react with a second cysteine to form an inter- or intramolecular disulfide which is then used to

oxidize reduced PDI (see Figure 9). This elegant mechanism allows cells to use a dangerous byproduct to sustain a fundamental function of the ER, protein folding and quality control.

Hence, the accumulation of $H_2O_2$ behind the membranes of different organelles creates the gradients needed for the generation and controlled propagation of key redox signalling (oxidative eustress in the Sies' classification), and here, peroxiporins are the fundamental players that make this possible, allowing the diffusion of $H_2O_2$ through lipid bilayers along a concentration gradient (Sies & Jones, 2020; Nordzieke & Medraño-Fernandez, 2018).

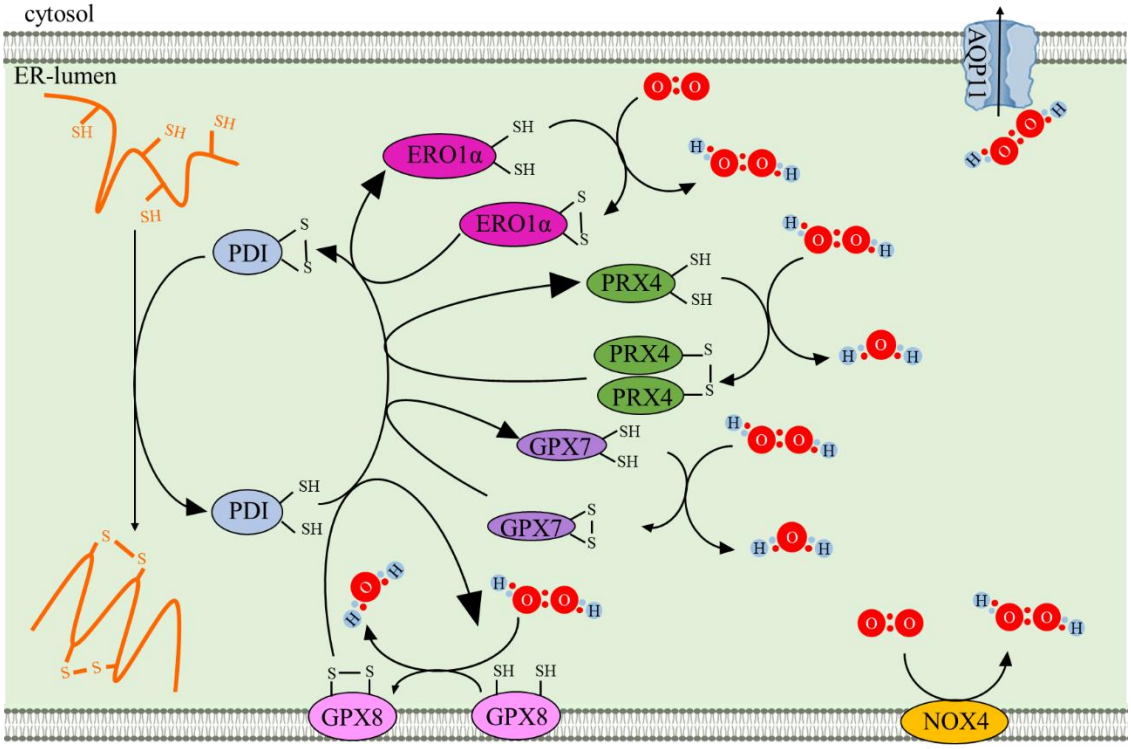



***Figure 9: Regulation of $H_2O_2$ homeostasis in the ER***
*Adapted from Konno et al., Intracellular sources of ROS/$H_2O_2$ in health and neurodegeneration: spotlight on endoplasmic reticulum, Cells, 2021.*

## 1.3 Physiological consequences of AQP11 mutations

### *1.3.1 AQPs and human kidney disorders*

The kidney is a central organ in controlling water homeostasis and urine concentration. Not surprisingly, therefore, AQPs exert a fundamental function in urine reabsorption. In the human kidney, nine AQPs (AQP1-8 and AQP11) were found differently expressed along the nephron. In all cases, disfunctions in those AQPs is associated with water balance disorders and kidney diseases (He & Yang; Su *et al*, 2020). Most relevant, mutations in AQP2 are associated with Nephrogenic Diabetes Insipidus (NDI) (Bockenhauer & Bichet, 2015), while disfunctions in AQP1-3 to increased susceptibility to Acute Kidney Injury (AKI) (Hussein *et al*; Asvapromtada *et al*, 2018). Mutations in human AQP11 are instead less characterized. A single nucleotide variant of AQP11 (rs2276415) was found to be a genetic factor that increases kidney susceptibility to AKI and Chronic Kidney Disease (CKD) progression (Choma *et al*, 2016; Han *et al*, 2019). Also, a case of congenital bilateral PKD was recently described in an infant with compound heterozygous variants in *AQP11* (Price *et al*, 2023) (see Figure 10). Hence, when I joined the host laboratory for my PhD program, I sought to understand whether and how *AQP11* mutations are linked with kidney disease.

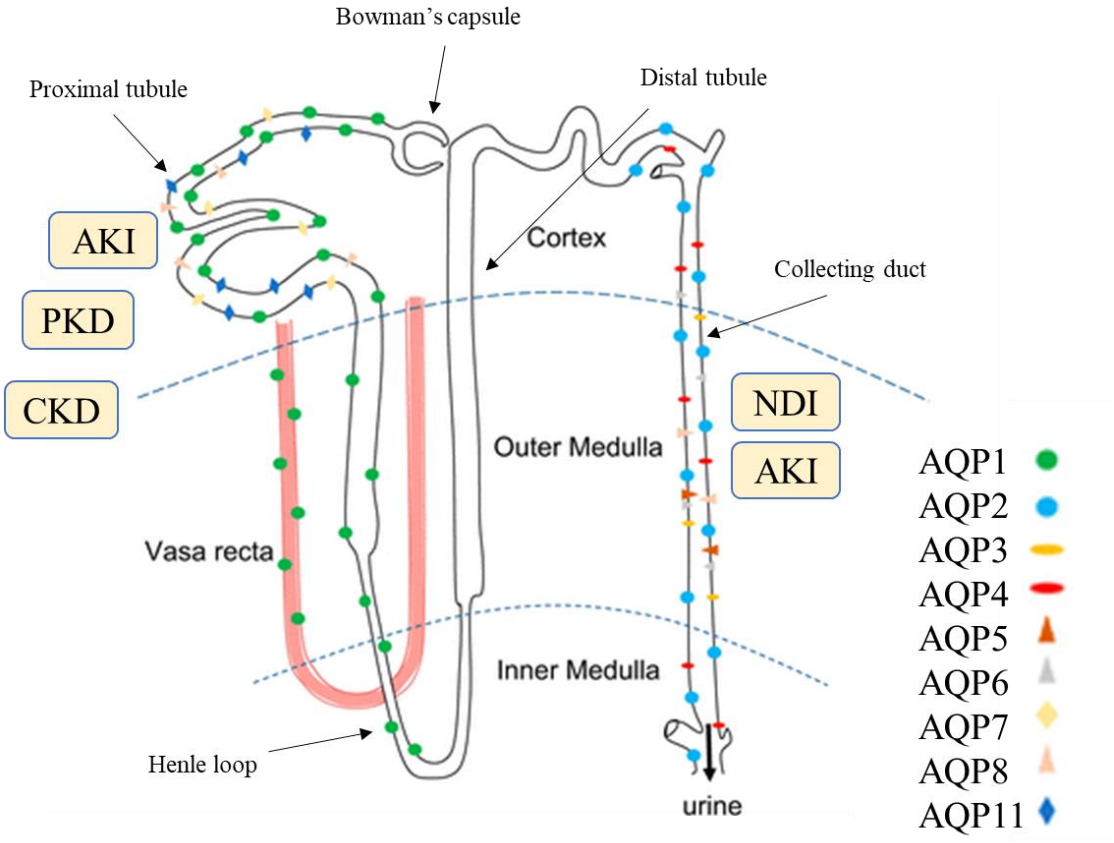



***Figure 10: Different expression of AQPs in the nephron segments and associated diseases***
*Adapted from Su et al., Aquaporins in the kidney: physiology and pathophysiology, American journal of renal physiology, 2020.*

### *1.3.2 Characterization of Aqp11$^{-/-}$ mouse model*

While only few cases of human *AQP11* mutations are reported in the literature, relevant pathophysiological information came from the study of *Aqp11*$^{-/-}$ mice. These animals are born normal, but they die before weaning (≈3 weeks after birth) due to renal failure. *Aqp11*$^{-/-}$ mice develop very early bilateral cysts in the proximal tubule (PT) of the kidney, the segment of the nephron where AQP11 is predominantly expressed (Morishita *et al*, 2005). Further analyses revealed that, in *Aqp11*$^{-/-}$ mice, the fatal PKD is preceded by vacuolization of the ER and increased expression of genes related to ER-stress (Okada *et al*, 2008; Tanaka *et al*) and oxidative stress (Hoshino *et al*, 2019). Moreover, AQP11 downregulation in epithelial PT cell line was found to increase levels of ROS (Atochina-Vasserman *et al*, 2013), consistently with the role that AQP11 exerts as $H_2O_2$ transporter in the ER (Bestetti *et al*, 2020). Importantly, post-natal inactivation of *Aqp11* at different

times revealed that the major effect on cysts formation was obtained when the gene is lost between day 2 and day 8 after birth, while no major defects were observed in the kidney of mice in which *Aqp11* was inactivated 12 days after birth (Rützler *et al*, 2017). This result suggests that AQP11 exerts an important function in the kidney in the first few weeks of life, while it may have a minor influence during adulthood. While the phenotypic characterization of *Aqp11* mutant mice was widely studied, more difficult was to understand the molecular mechanism that leads to PKD insurgence when AQP11 is missing. Inoue and collaborators suggested that the pathophysiology behind PKD in *Aqp11*$^{-/-}$ is linked to the impaired maturation of PC-1, whose gene (*PKD1*) is the most frequently mutated in ADPKD. In particular, they found that in kidney from *Aqp11*$^{-/-}$ mice, PC-1 accumulated in the ER with immature *N*-glycan processing. ER retention prevented its normal traffic to the plasma membrane (see Figure 11), likely being an important determinant of cystogenesis. Finally, they also showed that the *Pkd1*$^{+/-}$ background increases the severity of the cystic phenotype in *Aqp11*$^{-/-}$ mice, confirming that PC-1 is involved in the mechanism of cystogenesis (Inoue *et al*, 2014). Generally, ER retention is associated with proteins that struggle to reach their native conformation (Araki & Nagata 2011). Thus, we tested the possibility that the accumulation of $(H_2O_2)_{ER}$ that results by loss of AQP11 may impair PC-1 folding. This is relevant to better characterize a complex protein like PC-1and to identify the pathogenesis behind *AQP11* mutations.

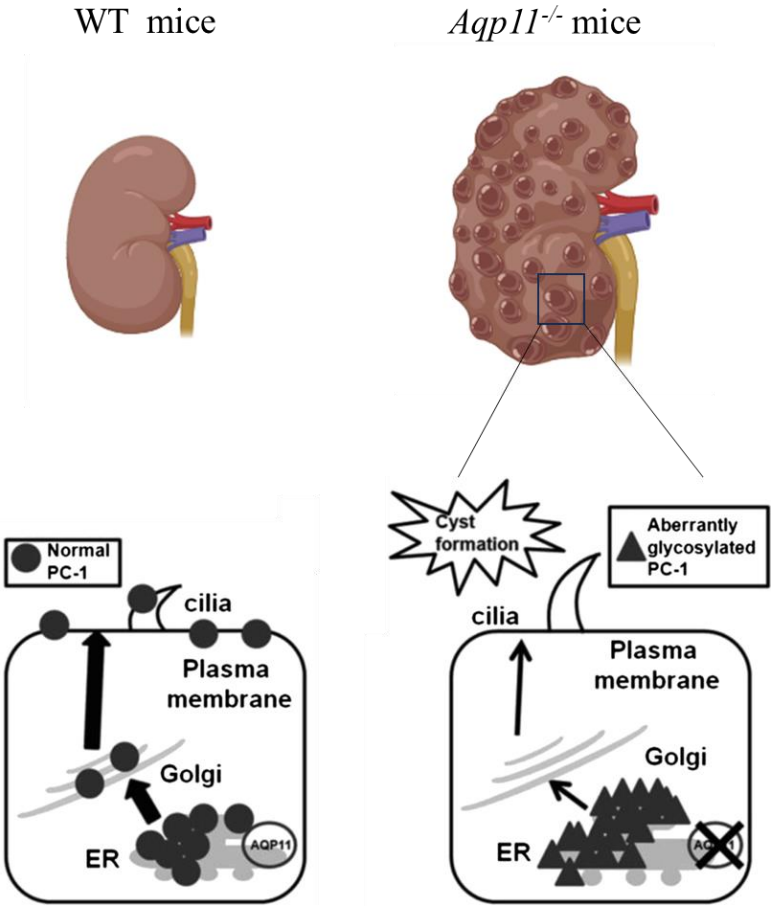



***Figure 11: Aqp11$^{-/-}$ mice develop Polycystic Kidney due to impaired maturation of PC-1***
*Adapted from Inoue et al., Aberrant glycosylation and localization of polycystic-1 cause polycystic kidney in an AQP11 knockout model, JANS, 2014.*

## 2 Aim

I started from the notion that *Aqp11*$^{-/-}$ mice develop a Polycystic Kidney Disease and die precociously of renal failure. The pathogenesis was linked to the impaired maturation and trafficking of PC-1, the product of *PKD1*, the most frequently mutated gene in Autosomal Dominant Polycystic Kidney Disease. The characterization of AQP11 as a $H_2O_2$ transporter in the ER made us curious to better understand how loss of AQP11 impacts on PC-1. In particular, we reasoned that the increase in $(H_2O_2)_{ER}$ that results from AQP11 downregulation could alter the redox homeostasis inside the lumen of this organelle, possibly interfering with proper protein folding and quality control. In this scenario, PC-1would be one of the most affected proteins.

With this purpose in mind, we tried to address the following questions:

I. Which is the effect of AQP11 knockdown on endogenous or over-expressed PC-1 or PC-2 proteins?
II. If a defect raises, is this dependent by accumulation of $H_2O_2$ in the ER?
III. If so, which is the mechanism by which $H_2O_2$ affects those proteins?

My results clearly show that PC-1 processing is highly sensitive to changes in $(H_2O_2)_{ER}$.

# 3 Results

**For clarity, I will start by explaining the sense with which I will use some words hereafter:**

**Biogenesis, maturation, and processing** are used as synonyms to indicate every step PC-1 goes through during its journey from the ER to the plasma membrane, including post translational modifications (disulfide bonds, *N*-glycosylation), folding, assembly into complex, cleavage, and trafficking.

**PC-1 cleaved forms** refer to every isoform generated upon cleavage of a portion of PC-1, including NTF, CTF, p100 and CTT.

**PC-1 autoproteolysis, GPS cleavage** refers to the *cis*-autocatalytic reaction that results in the scission between the NTF and the CTF.

**$(H_2O_2)_{ER/cytosol}$** refers to the amount of $H_2O_2$ that is measured by HyperProbe targeted to each specific compartment.

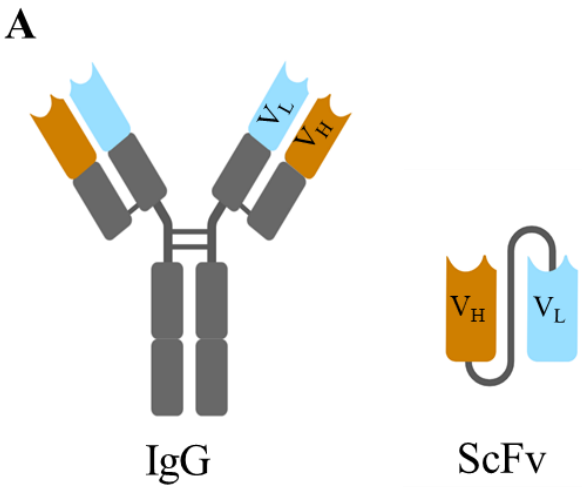
***N*-glycan processing and sugar processing** are used as synonyms to indicate every step of addition/removal of oligosaccharide moieties to the asparagine residue of the non-mature glycoprotein.

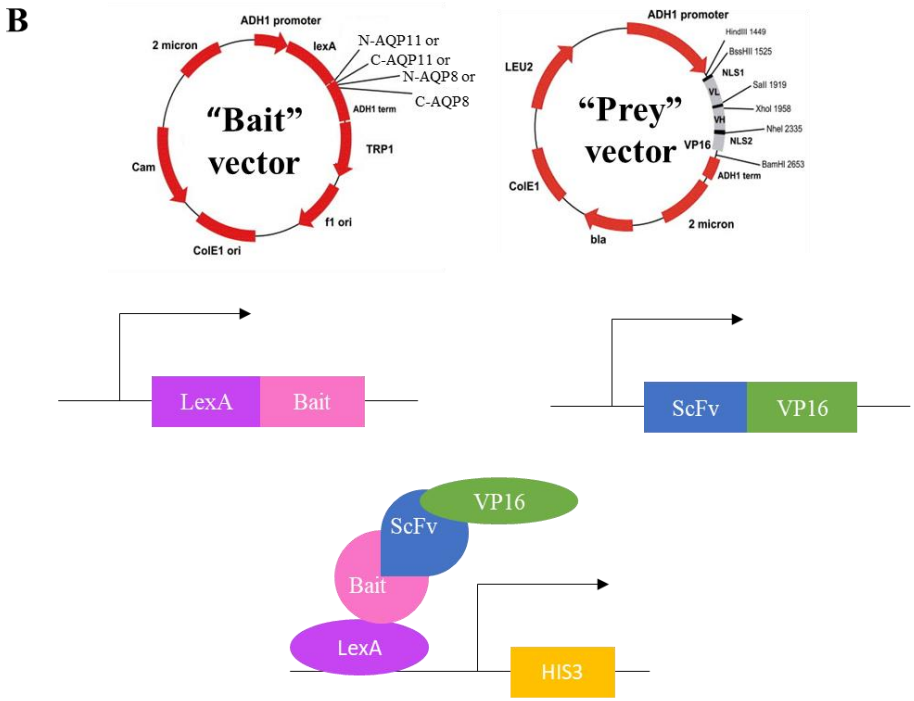
## 3.1 Screening for intracellular antibodies against AQP11µ

During my PhD, I spent some time trying to generate tools to use in my studies. Indeed, a critical obstacle was the absence of good antibodies to study AQP11. Thus, I was hosted by Antonino Cattaneo in his laboratory (Scuola Normale Superiore di Pisa) trying to generate intracellular antibodies (intrabodies) specific for AQP11 or AQP8, another AQP well characterized in our lab. The technique developed by Cattaneo and collaborators is called Intracellular Antibodies Capture Technology (IACT) (Visintin *et al*, 2002, 2004), an *in vivo* two-hybrid based screening that allows the selection of antibodies under conditions of intracellular expression. The library used for the screening is composed by human-derived Single Chain Fragment Variable (ScFv), that comprises the variable portion of Immunoglobulin (Ig) heavy (µ) and light (λ) chains connected by a linker sequence (Figure 12A). ScFvs retain the binding specificity of the full-length Ig and has the advantage of being smaller. Thus, they can be expressed in yeast for the screening. The ScFv library was tested against the cytosolic N- or C-terminal portion of either AQP11 or AQP8. We performed the screening using as antigens these two portions of AQPs since the ScFv will be expressed in the cytosol, thus recognising only cytosolic portions of the proteins. Moreover, we preferred cytosolic tails because they may acquire a more linear conformation compared with the cytosolic loops, reducing the chance of selecting conformational ScFv. Nevertheless, these epitopes are very short (between 15-30 amino acids) and a specific interaction between them and a ScFv would be hard to find. The sequences of N- or C-terminus of AQP8 or AQP11 were cloned in a "bait" plasmid in frame with the LexA DNA binding domain sequence under the control of the ADH1 promoter that allow expression in yeast. The bait plasmid also contains the TRP1 gene for tryptophan biosynthesis, that allows survival of the cells expressing it in medium deprived from tryptophan ($^{-}$W). The sequence of each ScFv of the library is instead cloned in a "prey" plasmid in frame with the VP16 transcriptional activator domain under the ADH1 promoter. The prey plasmid also contains the LEU2 gene for leucine biosynthesis that allows survival of cells in medium deprived from leucine ($^{-}$L) (Figure 12B). The two plasmids were used to transform a the L40 yeast strain that lacks the TRP1 and LEU2. In addition, L40 strain has the HIS3 gene for histidine biosynthesis under the control of the LexA promoter. Upon co-transformation with the bait and prey plasmids, L40 strain was plated in a medium deprived form tryptophan and leucine ($^{-}$WL) or deprived form

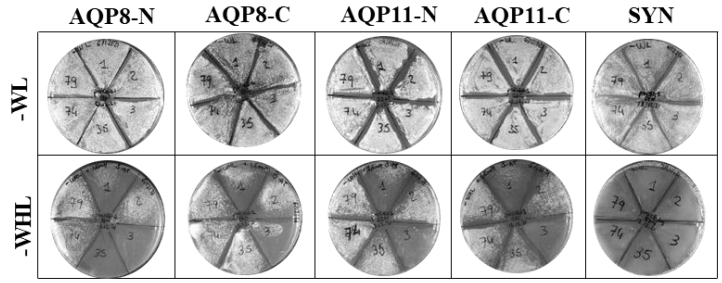
tryptophan, leucine, and histidine (-WHL). Only those cells that express both the bait and prey plasmids can grow on -WL medium. In addition, if the bait and the prey interact, the LexA DNA binding domain associated to the antigen, will bind the promoter upstream to the HIS3 gene, while the VP16 domain associated to the ScFv will activate HIS3 transcription (Figure 12C), allowing cells survival in -WHL medium.

For our screening, I used a library composed by $10^7$ different ScFv and I identified 8 of them as positive interactors. Nevertheless, the interaction was not specific for only one of the four baits we tested (N- or C- terminus or AQP8 or AQP11) but it was positive against all of them (Figure 12D), possibly interacting with a common linker sequence of 6 amino acids. With this first attempt, we did not obtain intrabodies to detect specifically AQP8 or AQP11. Due to this, during my studies, I could check levels of AQP11 upon silencing only looking at the transcript by Real Time quantitative PCR (RT qPCR). More time would be needed to repeat the screening against a different portion of the two proteins. Moreover, since the four baits share a common linker region between the LexA domain and the first amino acid of the antigen, it would be interesting to confirm the specificity of our 8 positive ScFv interactors against this common region (EFAAAM) that, in principle, could be used as new protein tag.






C




| growth on -WHL | AQP8-N | AQP8-C | AQP11-N | AQP11-C | SYN |
|---|---|---|---|---|---|
| ScFv 1 | + | + | + | + | - |
| ScFv 2 | + | + | + | + | - |
| ScFv 3 | - | + | + | - | - |
| ScFv 35 | - | + | + | + | - |
| ScFv 74 | + | + | + | + | - |
| ScFv 79 | + | + | + | + | - |

***Figure 12: Intracellular Antibodies Capture Technology screening***

*A) Schematic representation of a ScFv.*

*B) Schematic representation of the prey and the bait plasmids and co-expression in L40 yeast strain. Adapted from "The intracellular antibody capture technology: towards the high-throughput selection of functional intracellular antibodies for target validation" Visintin, Quondam and Cattaneo 2004.*

*C) Example of ScFv growth on -WL or -WHL medium: ScFv were tested against N- or C-terminus of AQP8 and AQP11. Bait-prey co-transformed yeast were plated on -WL to verify the plasmids co-expression or -WHL to test the interaction between the antigen (bait) and each ScFv (prey). Each ScFv were also tested against an unrelated protein (SYN) as a control. In the example above, we are showing only those ScFv that grew on -WHL medium (+) in the last step of the screening. None of them showed specificity only for AQP8 or AQP11.*

## 3.2 Studying the effect of AQP11$^{KD}$ on PC-1 or PC-2 maturation

*Aqp11*$^{-/-}$ mice develop a lethal polycystic kidney disease (Morishita *et al*, 2005; Tanaka *et al*; Okada *et al*, 2008; Tchekneva *et al*, 2008; Hoshino *et al*, 2019; Rützler *et al*, 2017). The proposed pathogenic mechanism behind this is the impaired maturation of PC-1 (Inoue *et al*, 2014), the most frequently mutated gene in ADPKD (ADPKD Variant Database: https://pkdb.mayo.edu/variants). However, the role that AQP11 plays in PC-1 maturation remains obscure. First, we tested the capacity of our antibodies to detect the different fragments of overexpressed PC-1 in Western Blot (WB). To determine whether and how PC-1 maturation is perturbed in cells lacking AQP11, we silenced the ER resident peroxiporin in HeLa cells (Bestetti *et al*, 2020; Sorrentino *et al*, 2022), transiently expressing a human PC-1 variant tagged at its C-terminus with a Myc epitope (PC-1-Myc). Anti-Myc antibodies decorated numerous bands in the lysates of PC-1-Myc transfectants but not in untransfected controls, confirming that the bands depend on PC-1 and are not purely aspecific. Of these, three could be identified as the expected PC-1 forms: full-length PC-1 (FL) and its proteolytic C-terminal fragment (CTF) and p100 (Fig. 13A). Their structure is schematized on the left panel. The three faster migrating bands (A, B and C highlighted in the blot) are shorter fragments that retain the C-terminal Myc-tag. As expected, anti-LRR antibodies, which recognize epitopes in the N-terminal fragment (NTF), decorated only two bands, corresponding to FL and NTF (Figure 13B).

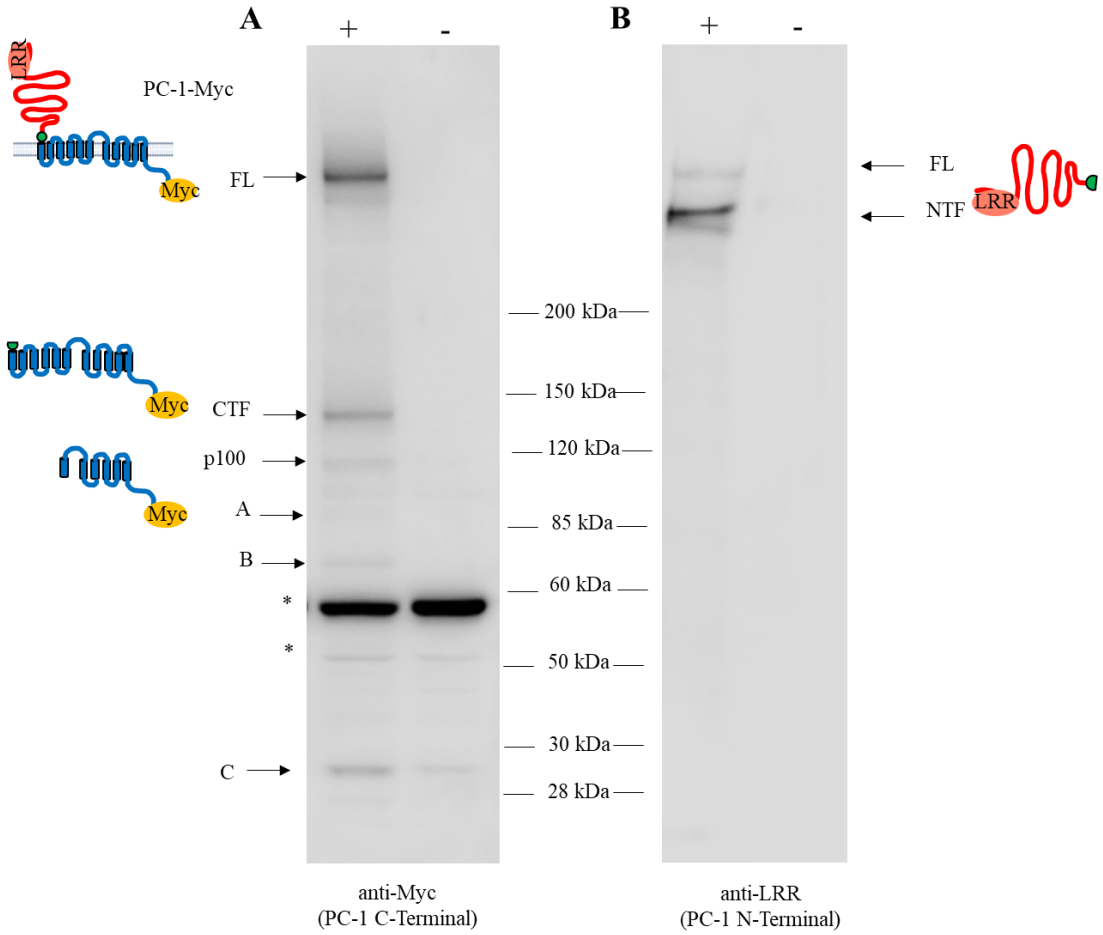



***Figure 13: Validation of the detection system from PC-1-Myc transiently transfected HeLa cells***

*A) Proteolytic processing of PC-1 yields several fragments carrying the C-terminal tag. Anti-Myc antibody detects FL, CTF, p100 and other not identified C-terminal derived forms (A, B and C) which are indicated by the arrows. The asterisk (*) points to aspecific bands which are detected also in untransfected cells.*

*B) Anti-LRR antibody detects FL and NTF fragment.*

A comparison of the PC-1 patterns revealed that less CTF and p100 accumulated in the lysates of AQP11$^{KD}$ than of control HeLa cells (Figure 14A left). Less pronounced but still significant was instead the decrease in intracellular NTF (Figure 14A right). To normalize the decrease of each cleaved form on the variability derived from transient over-expression, I quantified the defect as the ratio between the cleaved form (NTF, CTF or p100) over the sum between cleaved and FL (e.g. NTF/(NTF+FL). The results are shown in Figure 14B. For simplicity, from now on I will quantify the decrease in PC-1's cleaved forms looking at the CTF/(CTF+FL) ratio, since this isoform is more affected by AQP11$^{KD}$ compared to NTF and it is more abundant and easily detectable than p100.

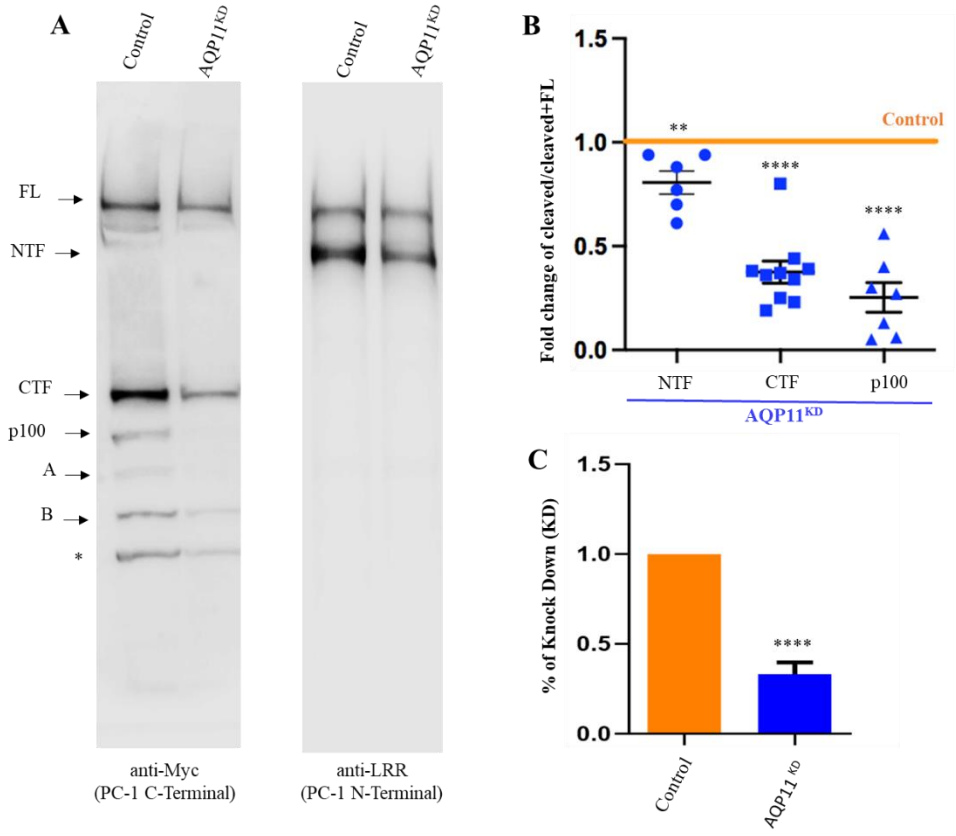



***Figure 14: PC-1's cleaved form are decreased upon AQP11 downregulation***

*A) Proteolytic fragments derived from transfected PC-1-Myc are decreased in AQP11$^{KD}$ HeLa cells. As expected, anti-Myc antibodies recognize full length (FL) PC-1 and its C-terminal fragment (CTF) and p100. Anti-LRR antibodies recognize instead the FL protein and its N-terminal fragment (NTF).*

*B) Densitometric analyses of numerous gels like the one shown in A allowed to calculate the abundance of the PC-1 fragments in silenced cells relative to controls. The graph shows the fold ratio between the indicated cleaved forms (NTF, CTF, p100) and the total protein (cleaved + FL) measured as mean-grey value intensity by ImageJ, comparing AQP11$^{KD}$ with control HeLa cells. Each dot corresponds to one individual experiment. The mean with standard error (SEM) from six (NTF), ten (CTF) and seven (p100) independent experiments was calculated. Unpaired t-test was performed comparing AQP11$^{KD}$ with control condition.*

*C) Residual transcript expression level quantified by RT-qPCR.*

The effect of AQP11 silencing was assessed also in other cell types: Human Embryonic Kidney 293T (HEK293T) cells transfected with human PC-1-Myc (Figure 15A, left panel) and Mouse Embryonic Fibroblasts (MEF) expressing endogenous PC-1 HA-tagged (Figure 15A, right panel). Like in HeLa cells, the CTF/(CTF+FL) ratio is decreased in those cell lines, albeit at lower degrees (Figure 15B). This result suggests that the phenotype linked to the absence of AQP11 in not specie-specific or cell type-specific.

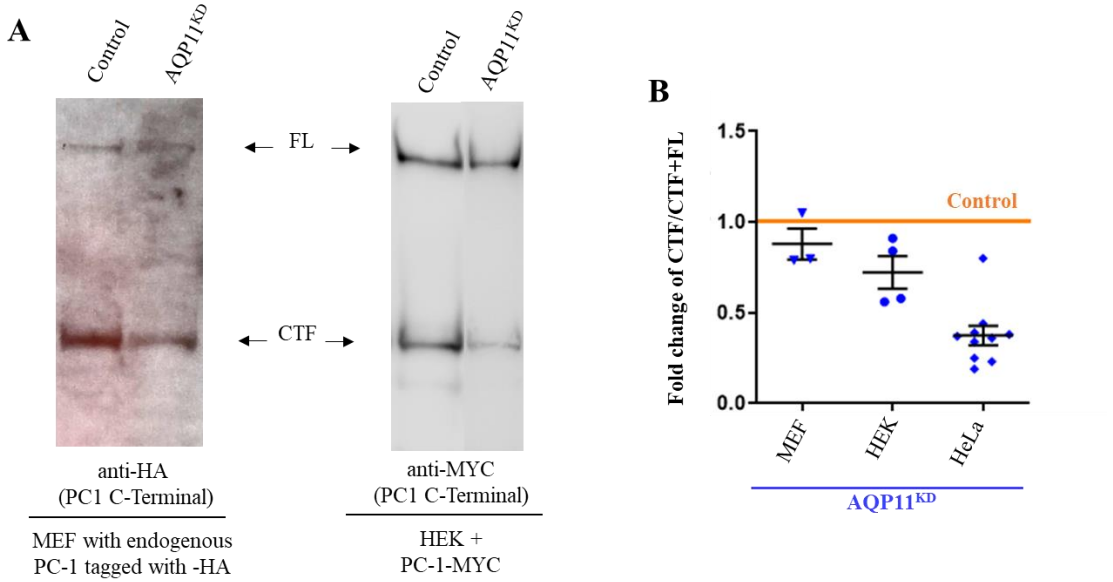



***Figure 15: Validation of the phenotype in other cell types***

*A) AQP11$^{KD}$ inhibits CTF accumulation also in MEF and HEK293T cells, albeit at different extents (see quantifications in panel B).*

*B) The graph shows the CTF/(CTF+FL) fold ratio measured as mean-grey value intensity by ImageJ, comparing AQP11$^{KD}$ with control MEF, HEK293T or HeLa cells. Each dot corresponds to one individual experiment. The mean with standard error (SEM) from three (MEF), four (HEK293) and ten (HeLa) independent experiments was calculated. Unpaired t-test was performed comparing AQP11$^{KD}$ with control condition.*

The second gene most frequently mutated in ADPKD is PKD2, encoding PC-2. The assembly between PC-1 and PC-2 in the ER is important for proper PC-1 maturation, cleavage, and transport to the plasma membrane (Chapin *et al*, 2010; Gainullin *et al*, 2015). One possible mechanism by which AQP11 depletion affects PC-1 maturation could be *via* PC-2. To investigate this possibility, we tested the effect of AQP11$^{KD}$ on endogenous PC-2 or HeLa transfectants transiently expressing a tagged version (PC-2-Myc). The first result of this experiment was that, unlike PC-1, neither the expression of endogenous PC-2 (Figure 16A) nor its capability of oligomerizing (Figure 16A-B) were affected by AQP11 silencing. Second, I reasoned that if PC-2 were affected by loss of AQP11, its downregulation should result in a phenotype similar to the one observed in AQP11$^{KD}$ cells. However, further reduction of the PC-2 pools by silencing (PC-2$^{KD}$) did not affect the PC-1 CTF/(CTF+FL) ratio, as instead clearly did AQP11$^{KD}$ (Figure 16C-E). These results suggested that the defect does not depend on PC-2.

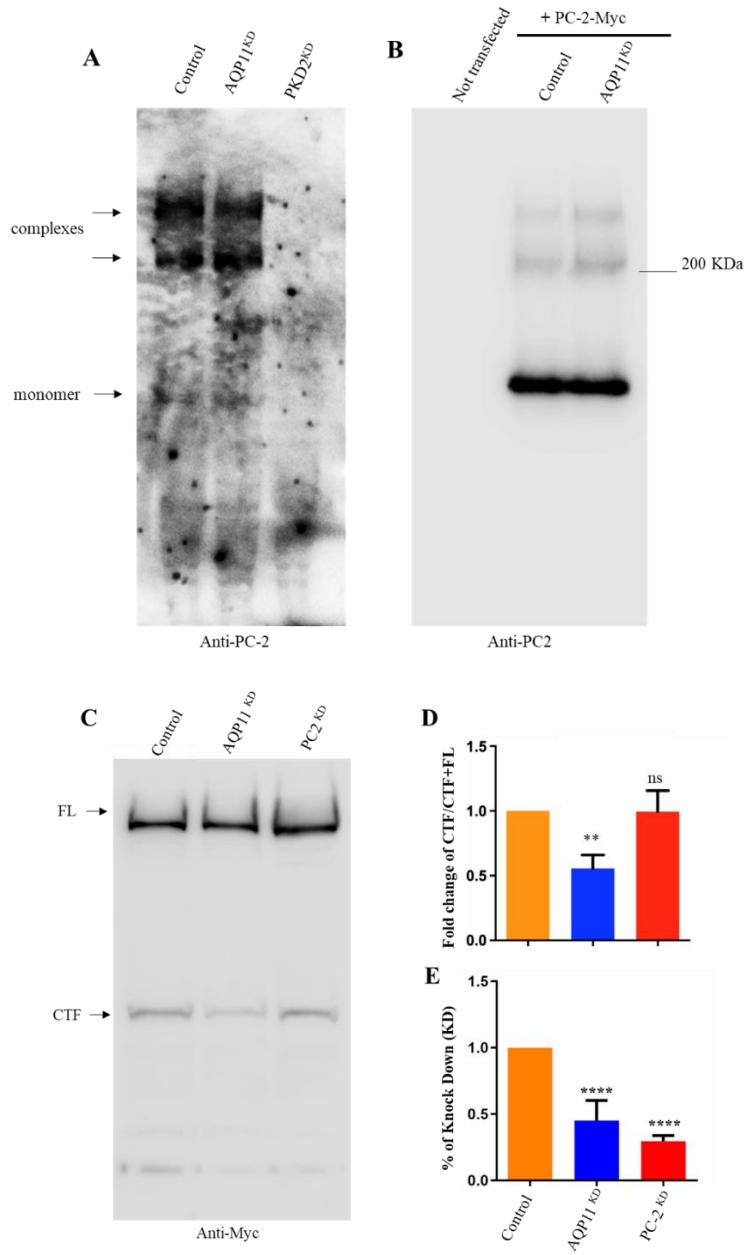



***Figure 16. Test whether AQP11KD impacts PC-1 maturation via PC-2***

*Unlike PC-1, endogenous (A) or over expressed PC-2 (B) is not significantly altered by AQP11$^{KD}$.*

- *A) Differently from AQP11$^{KD}$, PC-2 silencing does not decrease CTF/(CTF+FL) ratio.*
- *B) The graph shows the CTF/(CTF+FL) fold ratio measured as mean-grey value intensity, comparing AQP11$^{KD}$ with control HeLa cells. The mean with standard error (SEM) from five independent experiments was calculated. The decrease in CTF accumulation was calculated comparing only the experiments in which both AQP11 and PC-2 were silenced in parallel. Unpaired t-test was performed comparing AQP11$^{KD}$ or PC-2$^{KD}$ with control condition.*
- *C) Residual transcript expression level quantified by RT-qPCR.*

However, reasoning that PC-2 molecules could become limiting in cells overexpressing PC-1, I hypothesized that an unbalanced stoichiometry between PC-1 and PC-2 could have an impact when the folding and transport systems of the secretory apparatus are further overwhelmed by AQP11 depletion. Thus, I co-transfected the two differently tagged polypeptides in HeLa for testing this hypothesis. Clearly, increasing the levels of Myc-tagged PC-2 dramatically favoured the accumulation of PC-1-HA isoforms (Figure 17A-B). Despite the increased of CTF molecules, however, the different CTF/(CTF+FL) ratio between $AQP11^{KD}$ and control cells was conserved upon PC-2 overexpression, although it could be ameliorated (Figure 17B). Taken together, these results indicated that AQP11 downregulation affects PC-1 lowering the accumulation of its cleaved forms, in particular the CTF fragment. This process seems to be independent by PC-2. Nevertheless PC-2 overexpression could be of help in sustaining the demanding processing of PC-1 under adverse conditions.

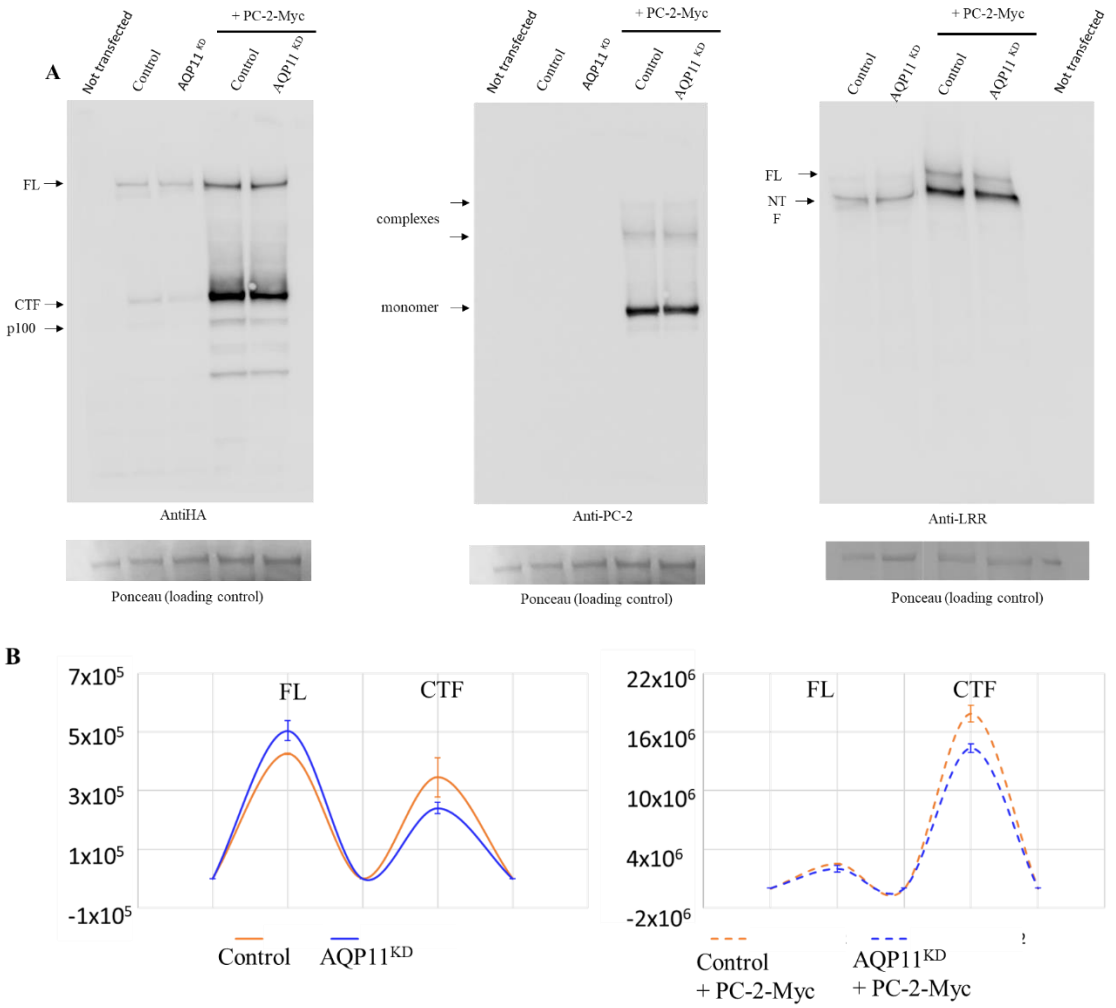



***Figure 17. Association with PC-2 stabilizes PC-1 but does not abolish the requirement for AQP11***

*HeLa cells were transiently transfected and/or silenced as indicated. Aliquots of their lysates were resolved electrophoretically, and blots decorated with anti-HA, anti-LRR or anti-PC-2 antibodies.*

*A) Co-expression of PC-2-Myc stabilizes PC-1-HA derived isoforms but does not completely rescue impaired CTF accumulation in AQP11$^{KD}$ cells (see panel B for quantifications).*

*B) Quantification relative to the mean-grey value of FL or CTF bands in AQP11$^{KD}$ and control cells with (right panel) or without (left panel) simultaneous co-expression of PC-2-Myc. The mean with standard error (SEM) from two independent experiments was calculated.*

### 3.3 CTF decrease depends on accumulation of $(H_2O_2)_{ER}$

Impaired CTF accumulation could be caused by the absence of AQP11 or by the physiological consequences of its absence. Indeed, AQP11 associates with NOX4 molecules in the ER membrane (Medraño-Fernandez, Sorrentino and Sitia, unpublished results) and it could serve additional functions beside $H_2O_2$ transport. We have shown previously that $AQP11^{KD}$ cells have higher concentration of $H_2O_2$ in their ER lumen (Bestetti *et al*, 2020). To determine whether impaired PC-1 processing was due to altered redox conditions, we sought means to manipulate $(H_2O_2)_{ER}$. In parallel experiments, we found that -like $AQP11^{KD}$- also silencing Cystathione β-synthase ($CBS^{KD}$), an enzyme involved in the transsulfuration pathway and, also in the closure mechanism of AQP8 (Bestetti *et al*, 2018), caused a similar increase in $(H_2O_2)_{ER}$ (Sorrentino, Medraño-Fernandez and Sitia, unpublished), although the mechanism is still not understood. Thus, in a first set of experiments, I silenced either AQP11 or CBS in PC-1 expressing HeLa, measuring $(H_2O_2)_{ER}$ using the $H_2O_2$-sensitive HyPer probe (Belousov *et al*, 2006) and CTF/(CTF+FL) ratios. So, we performed spinning-disk confocal imaging of our Hela cells that stably express HyPer probe in the ER (Bestetti *et al*, 2020) and we assessed the level of $H_2O_2$ in this compartment. This experiment confirmed our previous data that the absence of $AQP11^{KD}$ increase the level of $H_2O_2$ in the ER (Bestetti *et al*, 2020). The same happened when I silenced CBS compared to control. Importantly, the strong increase of $(H_2O_2)_{ER}$ in $AQP11^{KD}$ and $CBS^{KD}$ compared to control was maintained also upon PC-1-Myc expression (Figure 18A-B). Moreover, looking at same conditions by WB, $CBS^{KD}$ caused a decrease in the CTF/(CTF+FL) ratio that was like $AQP11^{KD}$ (Figure 18C-D). Taken together, these results strongly suggest that the increasing oxidative condition of the ER impacts on CTF processing, causing its decrease.

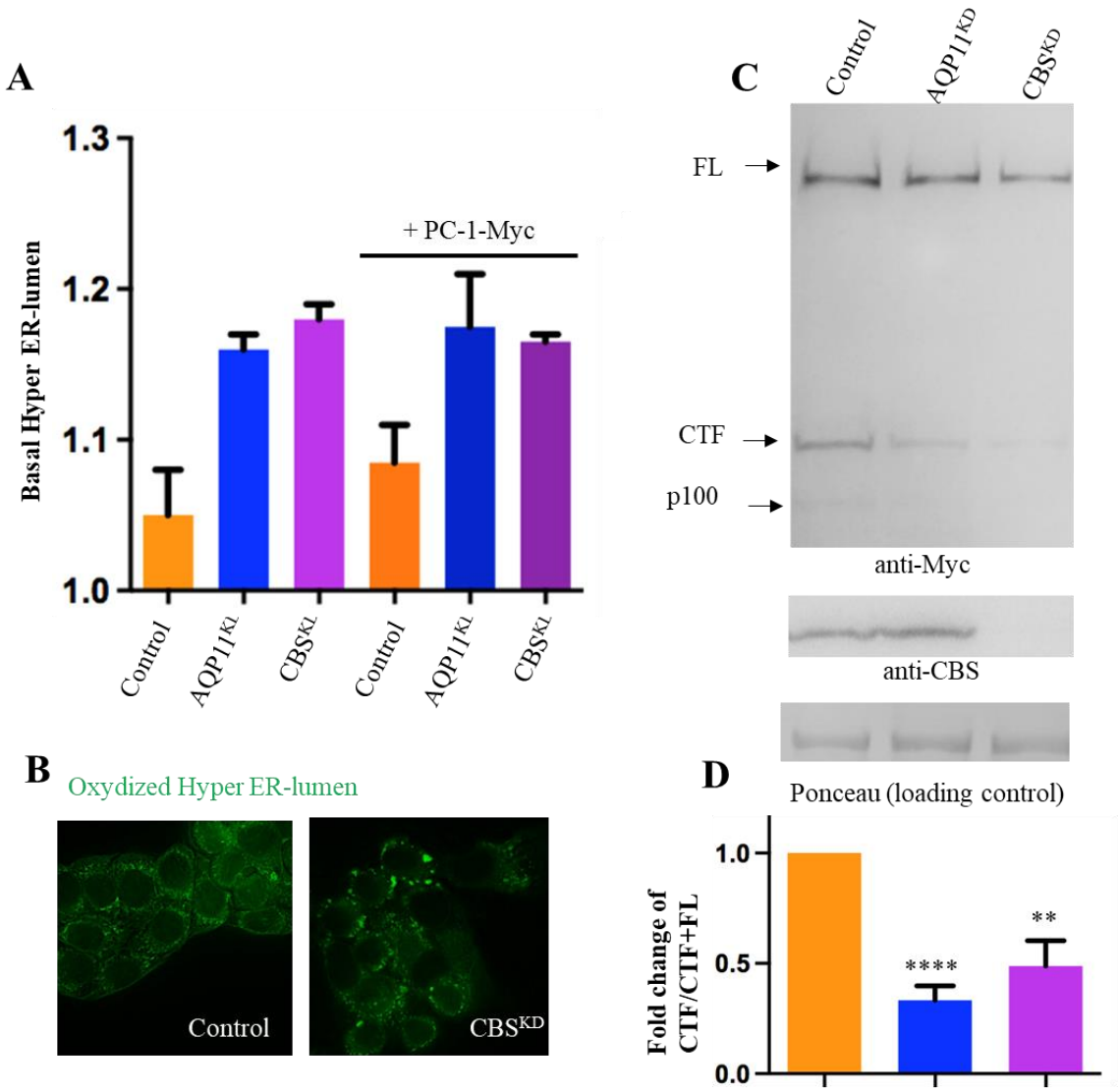



***Figure 18. CBS silencing causes an increase in $(H_2O_2)_{ER}$ and a decrease in CTF accumulation resembling the absence of AQP11 phenotype.***

*Stable HeLa transfectants expressing HyPer in the ER were silenced and transfected as indicated.*

*A) $(H_2O_2)_{ER}$ was quantified (top panel) as described previously (Bestetti et al., 2020; Sorrentino et al., 2022). The graph shows that the downregulation of AQP11 and CBS increases similar changes in the basal level of $(H_2O_2)_{ER}$ measured by Hyper ER-Lumen. The mean with standard error (SEM) from two independent experiments was calculated.*

*B) Representative image of HeLa cells stably expressing Hyper ER-lumen treated as indicated.*

*C) Like $AQP11^{KD}$, $CBS^{KD}$ reduces CTF/(CTF+FL) ratio compared to control cells.*

*D) The graph shows the CTF/(CTF+FL) fold ratio measured as mean-grey value intensity measured by ImageJ, comparing $AQP11^{KD}$ or $CBS^{KD}$ with control HeLa cells. The mean with standard error (SEM) from ten (AQP11KD) or four ($CBS^{KD}$) independent experiments was calculated. Unpaired t-test was performed comparing $AQP11^{KD}$ or $CBS^{KD}$ with control condition.*

To confirm the hypothesis that the level of $(H_2O_2)_{ER}$ influences the amount of CTF produced, I reasoned in the other way around: that if we could rescue $(H_2O_2)_{ER}$ that results from AQP11 silencing, I should also correct the defects in PC-1 processing. Thus, I decided to express an ER-targeted Catalase (ER-CAT), a powerful $H_2O_2$ scavenging enzyme (Konno et al., 2015). As previously described (Sorrentino *et al*, 2022), this enzyme restored normal $(H_2O_2)_{ER}$ levels following AQP11 silencing (Figure 19A). Excitingly, ER-CAT expression restored CTF accumulation (Figure 19B), confirming the central role of $(H_2O_2)_{ER}$ in controlling the biogenesis of polycystin complexes. In conclusion, these results strongly suggested that CTF processing is influenced by $(H_2O_2)_{ER}$ levels.

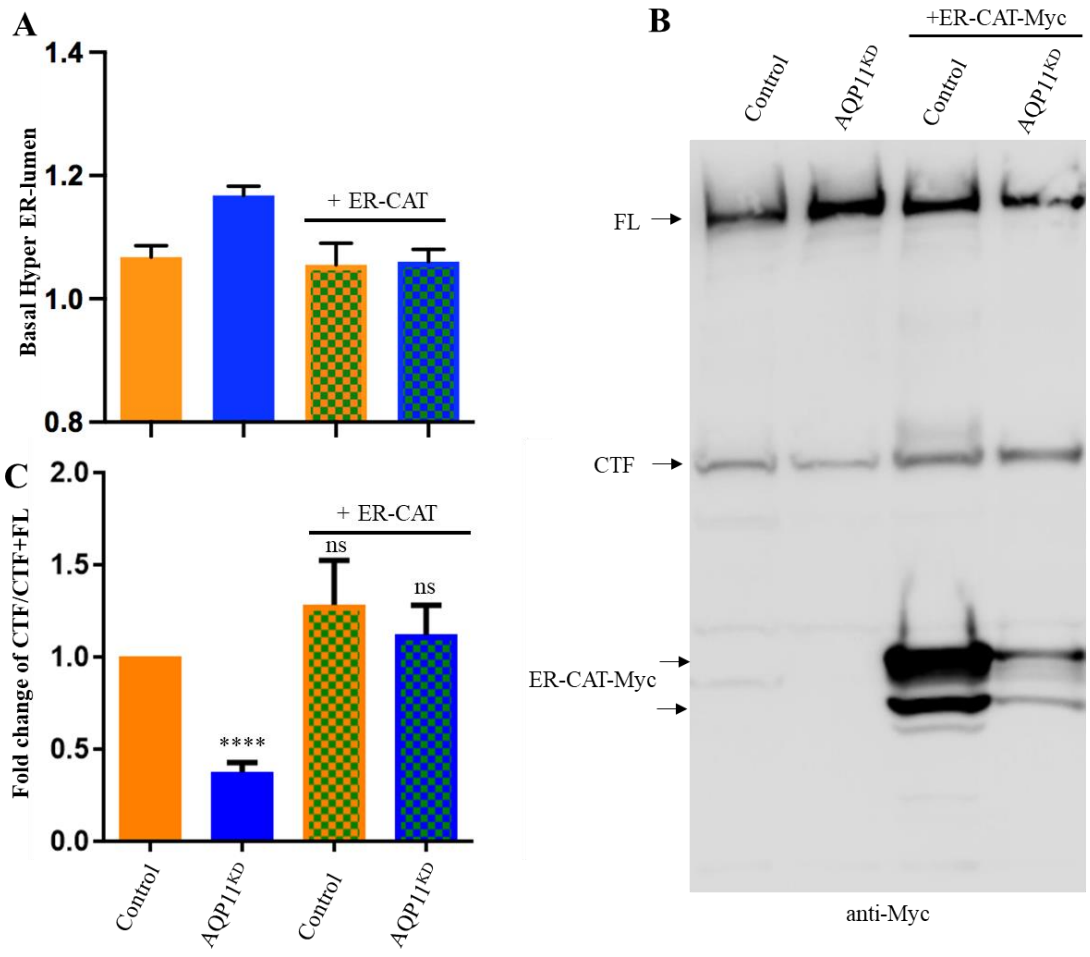



***Figure 19. Expression of ER-CAT-Myc reduces $(H_2O_2)_{ER}$ and rescues CTF/(CTF+FL) ratio in AQP11$^{KD}$ cells.***

*Stable HeLa transfectants expressing HyPer in the ER were silenced and transfected as indicated.*

*A) Imaging analyses of the expression of catalase in the ER counteracts the increase in $(H_2O_2)_{ER}$ induced by AQP11$^{KD}$ measured by Hyper ER-Lumen sensor. The mean with standard error (SEM) from two independent experiments was calculated.*

*B) The blot clearly shows that the characteristic decrease of CTF is no longer evident in cells that express ER-CAT-Myc. Thus, lowering $(H_2O_2)_{ER}$ rescues CTF accumulation in AQP11$^{KD}$ cells.*

*C) The graph shows the CTF/(CTF+FL) fold ratio measured as mean-gray value intensity measured by ImageJ, comparing AQP11$^{KD}$ with control HeLa cells, with/without ER-CAT-Myc co-expression. The mean with standard error (SEM) from three (Control+ER-CAT-Myc) and eight (AQP11$^{KD}$+ ER-CAT-Myc) independent experiments was calculated. Unpaired t-test was performed comparing each condition with untrasfected control.*

### 3.4 Non-native disulfides are not detected in our system following AQP11$^{KD}$

$H_2O_2$ is known to react with cysteine residues of target proteins by sulfenylation of thiol groups (SH→SOH). This modification makes cysteines more prone to form disulfide bonds (S-S). Disulfides are often used in cells to regulate proteins activity and stability through conformational changes (Holmström & Finkel, 2014). Thus, I speculated that the excess of $H_2O_2$ derived from loss of AQP11 could promote sulfenylation of cysteines and oxidation of methionines that normally are not direct target of $H_2O_2$. Therefore, an increased $(H_2O_2)_{ER}$ could promote the formation of non-native intra- or inter-chain disulfides that could alter the conformation of cysteine rich proteins and so disturb their correct folding and their localization. Moreover, when sulfenic acid further reacts with $H_2O_2$ before the target cysteine forms a disulfide, this results in sulfinylation and finally an irreversible sulfonylation (SOH→$SO_2H$→$SO_3H$) (Sies & Jones, 2020). Thus, cysteine sulfonylation could prevent the formation of native disulfides and, as a result, proper protein folding. Considering that PC-1 counts 95 total cysteines and 39 methionines, I tested whether the excess of $(H_2O_2)_{ER}$ -resulting from AQP11$^{KD}$- could interfere with its oxidative folding. To assess this idea, I used polyacrylamide gels, and I loaded the sample in non-reducing conditions to compare the migration of PC-1 extracted from control or AQP11$^{KD}$ cells. The logic behind this experiment is that formation of interchain bonds would likely decrease PC-1 mobility. In contrast, intrachain bonds -particularly if linking distant cysteines in the primary sequence- might increase the electrophoretic mobility reducing the hydrodynamic volume of the molecule. A similar difference allows to distinguish circular or linear plasmids. Looking at the FL isoform with anti-Myc antibodies in non-reducing samples, I did not observe easily detectable shifts in gel mobility running height that would indicate aberrant disulfide linkages in cells with higher $(H_2O_2)_{ER}$ (Figure 20 upper panel). The same was true for the NTF fragments detected by the anti-LRR antibody (Figure 20 middle panel). In addition, comparing the same sample in reducing and non-reducing condition, I noticed that neither FL nor NTF show any intermediate of folding. On the contrary, CTF and p100 migrate as a doublet under non-reducing conditions, indicating that a folding intermediate is formed (Figure 20 upper panel). Nevertheless, both bands are present similarly in control and AQP11$^{KD}$ cells and both are decreased when AQP11 is silenced (Figure 20 upper and middle panels) indicating that there is not a form which is evidently favoured between the

two conditions. Even if by this experiment I was not able to detect any gross difference in disulfide bonding, it should be noted that the large size of the proteins analysed precludes the detection of subtle changes in their structure which would require more sensitive assays.

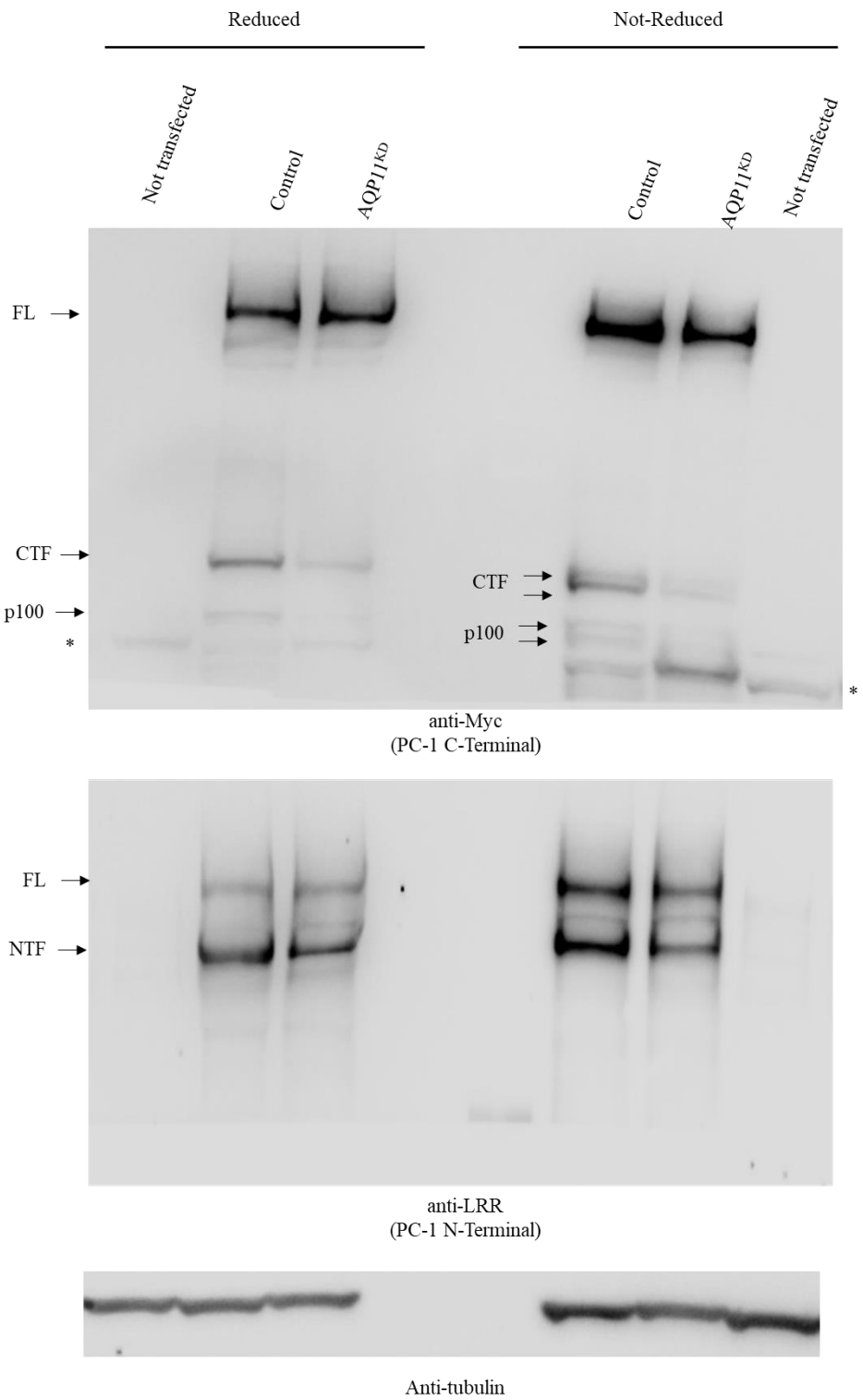



***Figure 20. Comparing PC-1-Myc samples with (reduced) or without (non-reduced) addition of DTT in control and AQP11$^{KD}$ cells:***

*WB developed with anti-Myc antibody revealed no differences in molecular mass or redox intermediate formation of C-terminal derived forms comparing non-reduced control and AQP11$^{KD}$ cells (upper panel), nor in the N-terminal derived forms (middle panel).*

### 3.5 AQP11$^{KD}$ does not slow down PC-1 autoproteolysis

To further explore the mechanism by which $(H_2O_2)_{ER}$ affect PC-1, we reasoned that possibly the autoproteolysis of the protein may be impaired, resulting in less production of cleaved forms. Indeed, many pathogenic mutations linked to ADPKD affect PC-1 autoproteolysis disrupting its GPS site (Qian et al, 2002). In addition, the timing of cysts development in mice expressing an uncleavable form of PC-1 (*Pkd1*$^{V/V}$) is similar to the one in *Aqp11*$^{-/-}$ mice (Yu *et al*, 2007; Inoue *et al*, 2014). For *cis*-autoproteolysis to begin, the amino acids involved (His$^{3047}$, Leu$^{3048}$ and Thr$^{3049}$) need to be kept in a strained conformation (Wei *et al*, 2007). Among the structural elements that maintain this strained conformation there is a disulfide bond formed between Cys$^{3015}$ and Cys$^{3043}$ (Trudel et al., 2015). Hence, I hypothesized that this disulfide$^{3015\text{-}3043}$ could be target of increased $(H_2O_2)_{ER}$ *via* cysteine modification causing defective PC-1 autoproteolysis. Thus, I performed pulse-chase experiments -that permit us to assayed only the protein of new synthesis- for testing the velocity of PC-1 cleavage. In this setup, newly synthetized proteins were labelled with radioactive $^{35}$S-labelled cysteines and methionines and chased in the presence of excess unlabelled amino acids. I chose a 20 min pulse reasoning that at the velocity of about 5 amino acids per second, human ribosomes would complete the first FL PC-1 in about 900 seconds. After the pulse, cells were washed, and cultured for different time points. PC-1 was then immunoprecipitated with a mixture of anti-Myc and anti-LRR antibodies and resolved by SDS-PAGE. Gels were blotted to nitrocellulose and first developed to detect the radioactive signal (Figure 21A upper membrane). The filter was then decorated with anti-LRR or anti-Myc antibodies to compare the entire protein pools (Figure 21A middle and lower membrane). A representative gel of three experiment is shown. The total signal increased during the first 20 minutes of chase, likely due to the completion of nascent polypeptides. As expected, the FL band decreases progressively during further chase points, reflecting its cleavage. In the gel shown, FL processing seemed even faster, an NTF band being detectable already at the end of the 20 minutes pulse. Quantification of the three experiments showed similar processing rate of the FL (Figure 21B upper panel). In contrast, radioactive NTF fragments disappeared slightly faster in AQP11$^{KD}$ cells, consistent with the lower NTF/(NTF+FL) ratio evident when total proteins are analysed (Fig. 21B lower panel). The lower NTF levels in AQP11$^{KD}$ cells might reflect faster degradation. Unfortunately, therefore, newly made CTF was not

detected by our radioactive assays due to its lower content in cysteines and methionines and the high background of our IP system in the 150-80 molecular weight range.

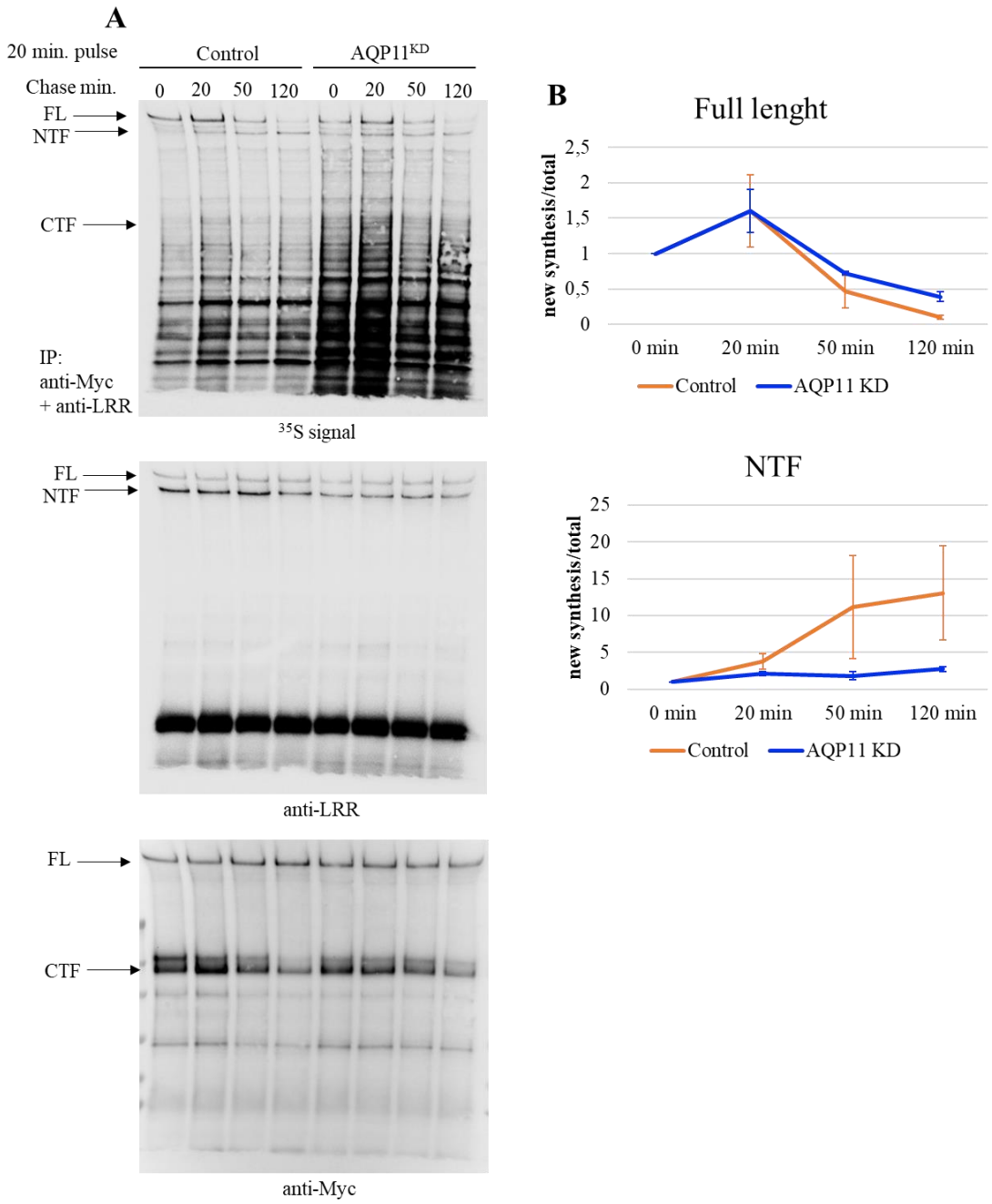



***Figure 21. AQP11$^{KD}$ does not inhibit PC-1 autoproteolysis***

*A) HEK293T cells expressing PC-1-Myc w/wo previous AQP11 silencing were labelled for 20 minutes with radioactive amino acids, and their lysates immunoprecipitated with a mix of anti-Myc and anti-LRR antibodies. The gel was transferred to nitrocellulose and the membrane first developed for autoradiography to detect newly synthetized, radioactive proteins (up). The same membrane was then decorated with anti-LRR (middle) and anti-Myc (low) antibodies to detect the total protein. The dark 55 kDa band decorated by anti-LLR likely consists of the heavy chain of the mouse antibody used for immunoprecipitation.*

*B) The graphs show the mean with standard error (SEM) from three independent experiments where the ratio between the signal from the newly synthetized and the total FL or NTF was calculated.*

## 3.6 AQP11$^{KD}$ affects CTF stability via $(H_2O_2)_{ER}$ but does not promote CTF degradation

We found that PC-1-Myc autoproteolysis is not affected by AQP11$^{KD}$ in HeLa cells. Nevertheless, the newly formed NTF in not accumulated (Figure 21A-B). Thus, we hypothesized that the stability of the cleaved forms can be reduced by AQP11 silencing. To further investigate the stability of PC-1 isoforms, we blocked protein synthesis with cycloheximide (CHX) -a drug that exerts its effect by interfering with the exit of tRNA from ribosome- treating HeLa cells for different times and compared the rate of disappearance of PC-1 fragments in control or AQP11$^{KD}$ in presence or absence of the ER-CAT-Myc. The reasoning behind this was that, blocking the synthesis of the FL, we can prevent the formation of new NTF or CTF and study their half-life at different extents of $(H_2O_2)_{ER}$. These experiments revealed that the FL bands disappear at similar rates in all the three conditions (Fig. 22A-B left panel), confirming that its cleavage/degradation are not modulated by $(H_2O_2)_{ER}$. In contrast, in AQP11$^{KD}$ cells CTF starts to disappear faster after the second hour of CHX treatment, but it is stabilized upon ER-CAT-Myc co-expression (Figure 22A-B right panel). Unlike CTF, NTF was very stable also upon 4 hours of CHX treatment (Figure 22C). The fate of this isoform could not be compared owing to the toxicity of CHX. Altogether, these data indicate that $(H_2O_2)_{ER}$ influences the stability of CTF.

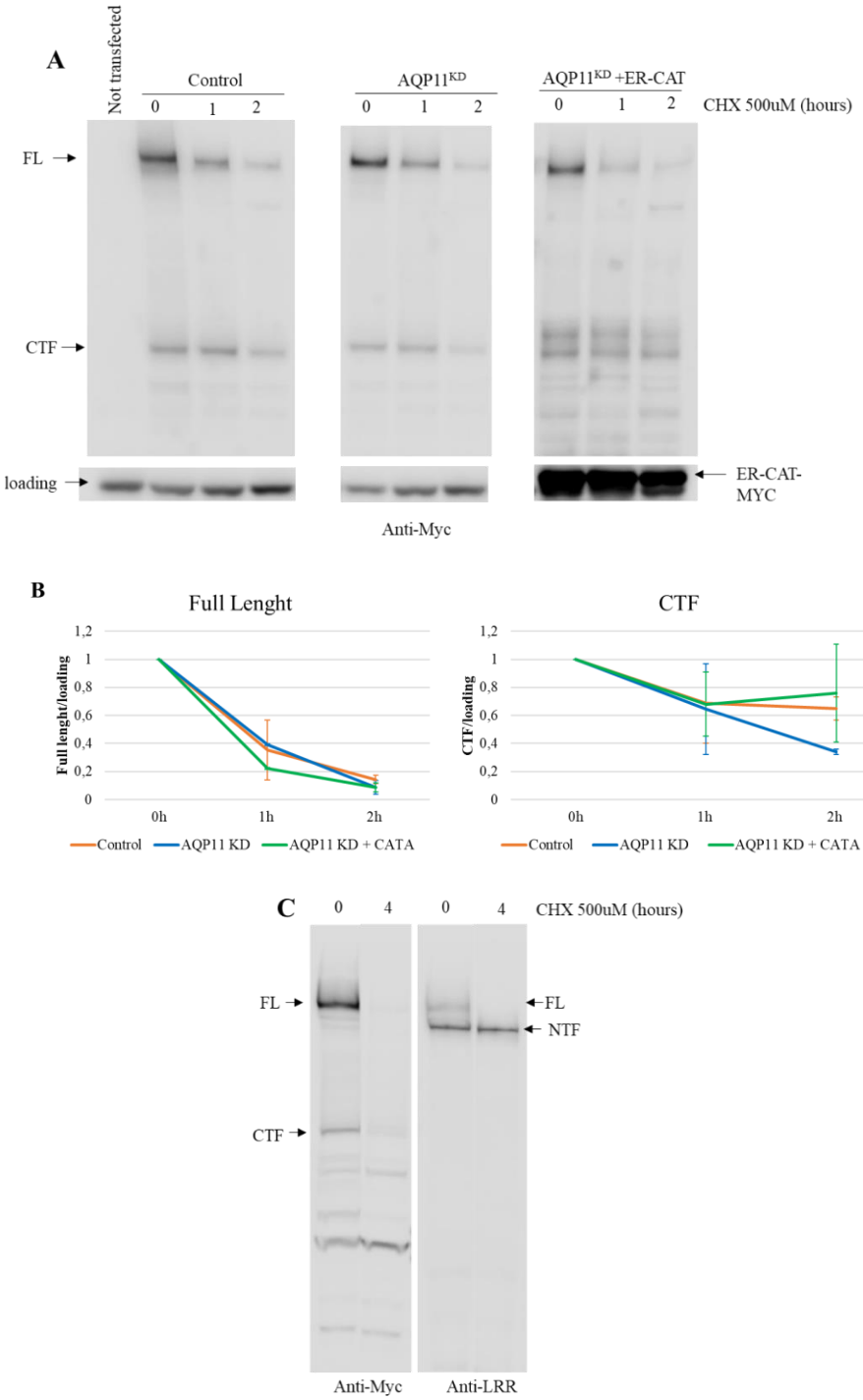



***Figure 22. CTF stability is influenced by $(H_2O_2)_{ER}$***

*HeLa cells transfected and silenced as indicated were cultured in the presence of CHX to block protein synthesis.*

*A) Aliquots of their cell lysates were resolved by SDS-PAGE and blots decorated with anti Myc. Note that the decreased CTF stability in $AQP11^{KD}$ cells is rescued by ER-CAT-Myc.*

*B) The graphs show the mean with standard error (SEM) from three independent experiments where the ratio between FL or CTF and the loading control was calculated.*

*C) HeLa transfectants expressing PC-1 were cultured for 4 hours with or without cycloheximide (CHX). Note the higher stability of NTF: CTF is almost entirely degraded, while NTF shows longer half-life.*

To understand if increased $(H_2O_2)_{ER}$ accelerated CTF degradation, we tested whether blocking either autophagy or proteasomal activity rescues its accumulation. To this end, we treated HeLa cells with CHX alone or in combination with bafilomycin A -that inhibits lysosomal acidification and lysosome-autophagosome fusion- or MG132 – a proteasome inhibitor- to block autophagy and ERAD respectively. The results indicated that preventing proteasomal but not autophagic degradation rescues CTF, although partially (Figure 23A). Indeed, MG132 restored the levels of CTF molecules present before CHX addition (0h) (Figure 23A). However, the newly processed CTF molecules generated by FL autoproteolysis after protein synthesis blockade did not accumulate in the presence of proteasome inhibitors. Also, the FL band was not recovered upon MG132 treatment (Figure 23A). Thus, proteasomal degradation was not the sole cause for CTF decrease. Moreover, partial rescue of CTF was observed both in control and $AQP11^{KD}$ cells, suggesting that CTF degradation by the proteasome is not specifically promoted by $AQP11^{KD}$ (Figure 23A-B).

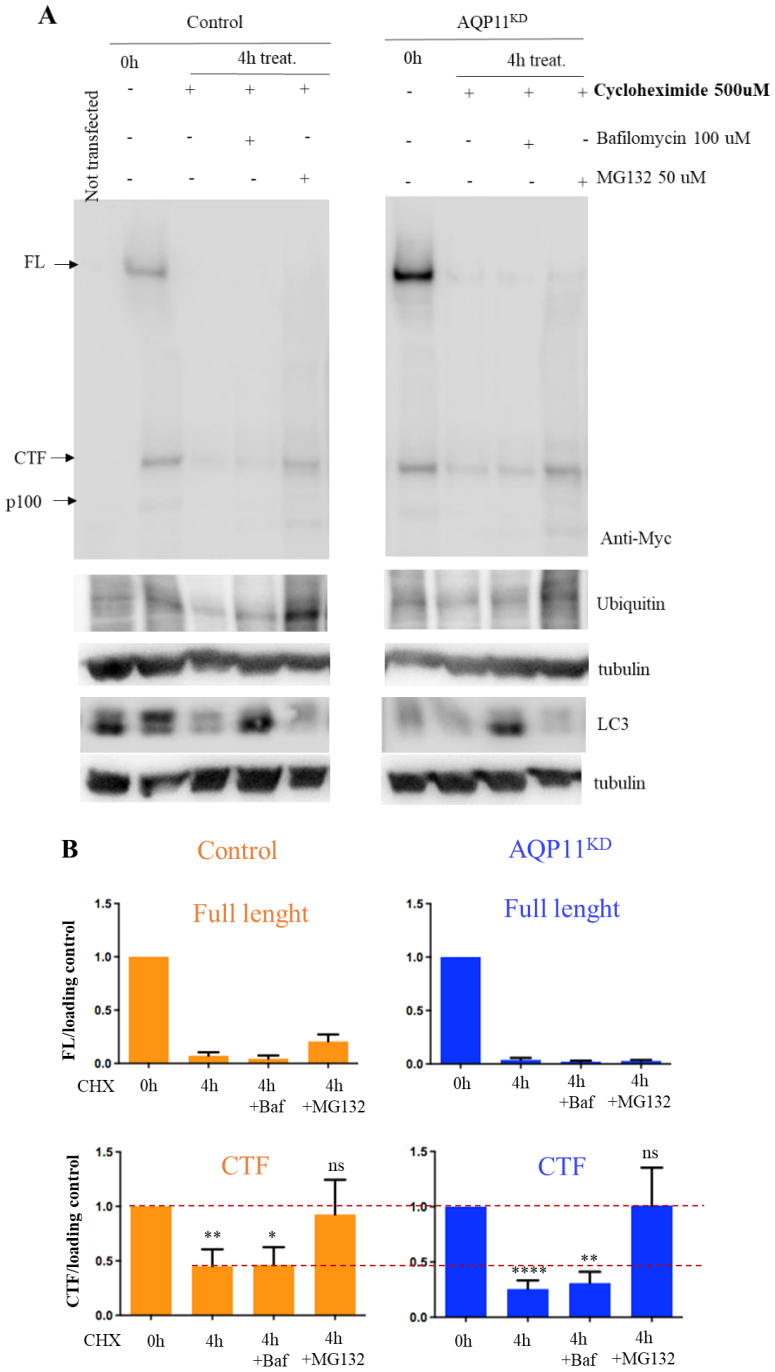



***Figure 23: Test Increased degradation of CTF upon AQP11$^{KD}$.***

*HeLa transfectants expressing PC-1-Myc and silenced as indicated were treated with CHX for 4 hours with or without inhibitors of lysosomal (bafilomycin) or proteasomal (MG132) degradation.*

*A) Aliquots of the lysates were immunoblotted with the indicated antibodies. Accumulation of ubiquitinated proteins or LC3 was used as control for the proper work of the MG132 and bafilomycin respectively.*

*B) The graph shows the CTF/(CTF+FL) fold ratio measured as mean-grey value intensity by ImageJ, comparing AQP11$^{KD}$ with control HeLa cells. The mean with standard error (SEM) from three independent experiments was calculated. Unpaired t-test was performed comparing each condition with its correspondent untreated control.*

### 3.7 AQP11$^{KD}$ does not promote CTF insolubility or accumulation of smaller CT-derived forms:

Since blocking the proteasome rescued only partially CTF accumulation, we wondered whether the missing molecules could aggregate and become detergent insoluble. Indeed, misfolded proteins undergo reduction of disulfide bonds, especially of interchain ones, prior to retrotranslocation to the cytosol and subsequent degradation (Fagioli et al, 2001). Hence, to allow enzymatic disulfides oxidation, isomerization and reduction within the same compartment, the maintenance of ER redox-homeostasis is essential (Fassio & Sitia, 2002). Either failure in misfolded proteins dislocation or degradation could result in formation of Russell Bodies (RS) or cytosolic aggresomes respectively (Kopito & Sitia, 2000). Hence, I reasoned that, the excess of $(H_2O_2)_{ER}$ could prevent PC-1 molecules retrotranslocation by the formation of intra-chain disulfides resulting in aberrant interaction and even aggregation of the protein. Alternatively, misfolded PC-1 could reach the cytosol aggregating instead of being degraded. Thus, to test if the missing fraction of CTF in AQP11$^{KD}$ cells aggregates, we looked for it in the cell pellet upon lysis. First, we lysed cells in 1% CHAPS. Upon centrifugation, we collected both the supernatant containing soluble proteins and the pellet that was solubilized in 2% SDS and sonicated to get rid of DNA. Comparing the two fractions of proteins, we did not find major differences in the CTF/(CTF+FL) ratio (Figure 24A-B), indicating that condensation into detergent insoluble forms was not the main cause of CTF reduction in AQP11$^{KD}$ cells.

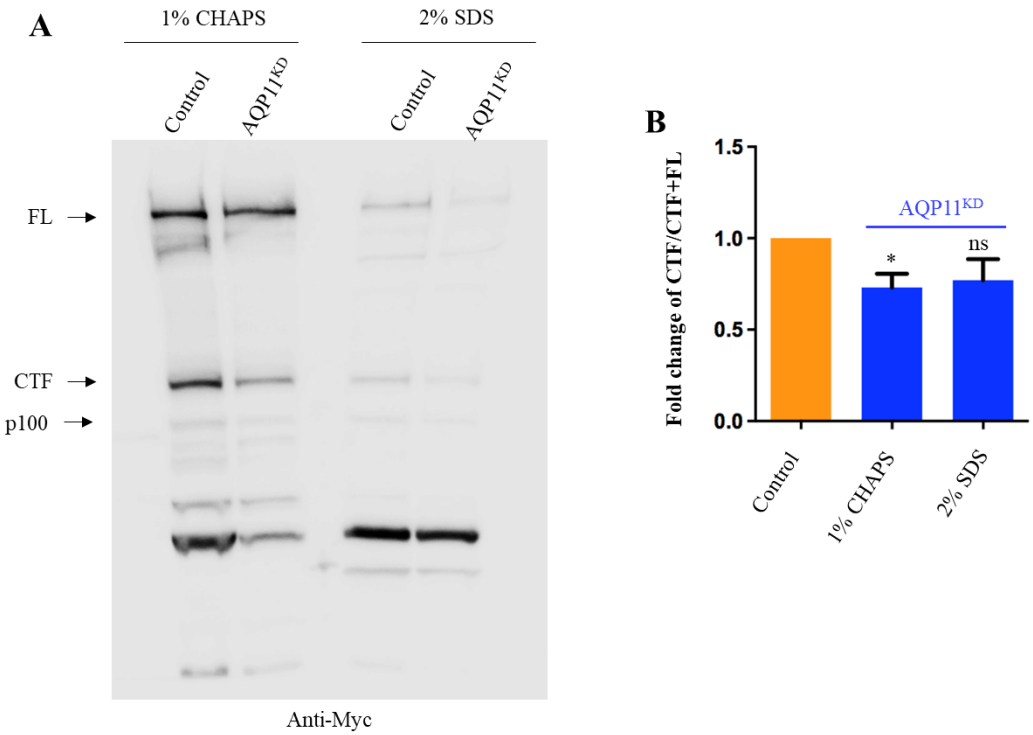



***Figure 24. AQP11$^{KD}$ does not significantly increase PC-1 detergent insolubility***

*A) HeLa transfectants expressing PC-1-Myc were silenced as indicated and lysed in two steps. First, post nuclear supernatants were obtained by centrifugation after 1% CHAPS solubilization. Then, the pellet was resuspended in 2% SDS to solubilize insoluble proteins.*

*B) The graph shows the CTF/(CTF+FL) fold ratio measured as mean-grey value intensity by ImageJ, comparing AQP11$^{KD}$ with control HeLa cells. The mean with standard error (SEM) from three independent experiments was calculated. Unpaired t-test was performed comparing AQP11$^{KD}$ with control condition.*

Yet another possibility to explain CTF reduction in AQP11$^{KD}$ cells is its further processing into p100 and/or C-terminal Tail (CTT) (Woodward et al, 2010; Lal et al; Onuchic et al, 2021; Lin et al., 2018; Merrick et al 2012). After the potential involvement of γ-secretase in CTT production (Merrick et al., 2012) neither the site nor the mechanism of these cleavages have been studied in depth. As shown in Figure 14, p100 accumulation was more severely affected than CTF and NTF upon AQP11$^{KD}$. Thus, we decided to check other smaller C-terminal PC-1 fragments exploiting higher density polyacrylamide gels. This allowed us to visualize a ≈30 kDa band that could correspond to CTT (Merrick *et al*; Onuchic *et al*, 2021). This fragment was very stable and did not decrease upon 4 hours of protein synthesis blockade (Fig. 25A). Also, when compared with other C-terminus derived forms, CTT is the one on which AQP11$^{KD}$ has the smaller impact. Despite this, CTT does not show accumulation in AQP11$^{KD}$, and it does not further

accumulate upon proteasome blockade (Fig. 24A-B). Overall, neither detergent insolubility nor further cleavage of CTF can fully justify its decreased in condition of increased $(H_2O_2)_{ER}$, leaving an open question on the mechanism behind.

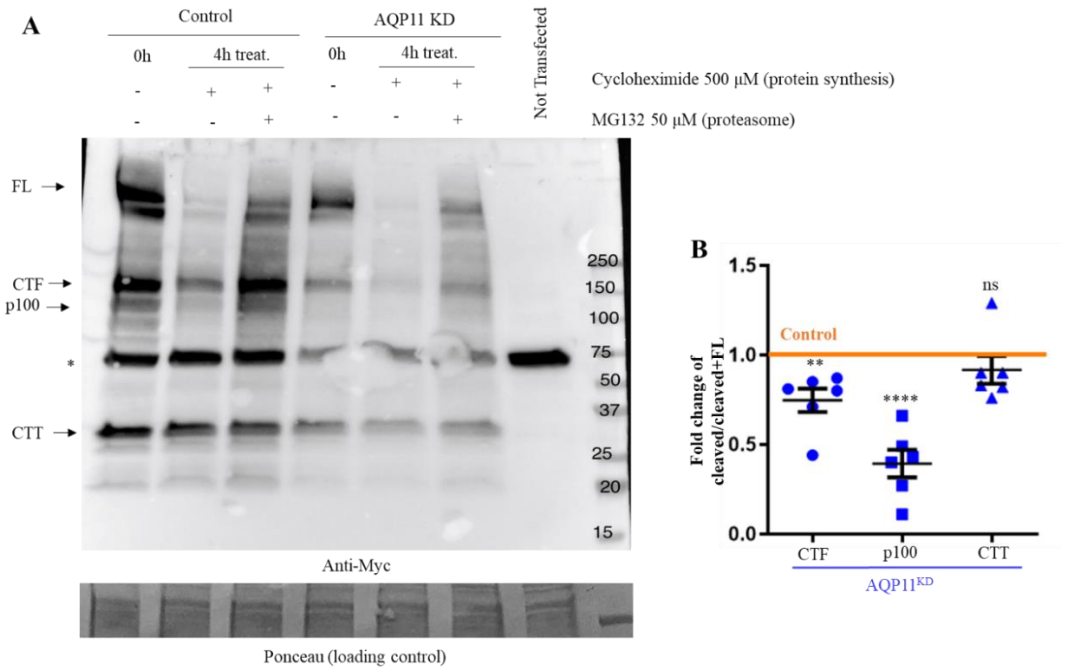



***Figure 25: Stability of a 30 kDa C-terminal fragment of PC-1 (CTT?).***

*A) HeLa transfectants expressing PC-1-Myc were treated as indicated. To identify also smaller proteolytic fragments aliquots from the cell lysates were resolved by 4-12% polyacrylamide gels.*

*B) The graph shows the cleaved/(cleaved+FL) fold ratio for each indicated fragment (CTF, p100, CTT) measured as mean-grey value intensity by ImageJ, comparing AQP11$^{KD}$ with control HeLa cells. Each dot corresponds to one individual experiment. Only experiments where we could detect in parallel the three isoforms were analysed. The mean with standard error (SEM) from six independent experiments was calculated. The amount of CTF, p100 or CTT was analysed in parallel on the same membrane. Unpaired t-test was performed comparing AQP11$^{KD}$ with control.*

## 3.8 AQP11$^{KD}$ impairs a late step of sugar processing

Based on their studies, Inoue and colleagues surmised that the development of a fatal polycystic kidney disease in *Aqp11*$^{-/-}$ mice was due to impaired PC-1 *N*-glycan processing and reduced trafficking at the plasma membrane. In particular, endogenous PC-1 from *Aqp11*$^{-/-}$ mouse kidney showed higher molecular weight compared to PC-1 molecules isolated from WT animals, remained almost entirely Endo-H sensitive, and accumulated in the ER fraction upon organellar fractionation (Inoue *et al*, 2014). To test whether also in our cell model PC-1 shows defective trafficking and/or sugar processing, we evaluated its sensitivity to endoglycosidases Endo-H or PNGase-F treatment, comparing AQP11$^{KD}$ with control HeLa cells. Indeed, Endo-H is an enzyme able to remove only simple *N*-glycans. Sensitivity is lost when the oligosaccharide moiety is modified by enzymes localized in the medial Golgi. Thus, increased sensitivity to Endo-H could indicate impaired *N*-glycan processing due to ER-retention. On the other hand, PNGase-F also cuts *N*-glycans upon their processing in the Golgi apparatus, providing a positive control for our assay. As we previously observed, when samples are not treated with endoglycosidases, PC-1 does not show different electrophoretic mobility on SDS-PAGE that could point to diverse *N*-glycan processing with neither anti-Myc (left panel) nor anti-LRR (right panel) antibodies. In my hands, treatment with endoglycosidases did not reveal major differences between silenced and control cells, suggesting that *N*-glycans are similarly processed in the two conditions. Importantly, all the isoforms remain entirely Endo-H sensitive in HeLa cells (Figure 26A), indicating that in those cells over-expressed PC-1-Myc mostly remains ER localized and the pool that arrives to the plasma membrane undergoing *N*-glycans processing is limited. Indeed, this result was further confirmed by a colocalization imaging analysis between the ER-marker calnexin and over-expressed PC-1-Myc (Figure 26B). We did not test the Endo-H sensitivity of the protein in other cell types; thus, we cannot conclude if its major localization in the ER is specific for HeLa cells or if it depends by the fact that PC-2 molecules become limited in a context in which we are only overexpressing PC-1 (Gainullin *et al*, 2015).

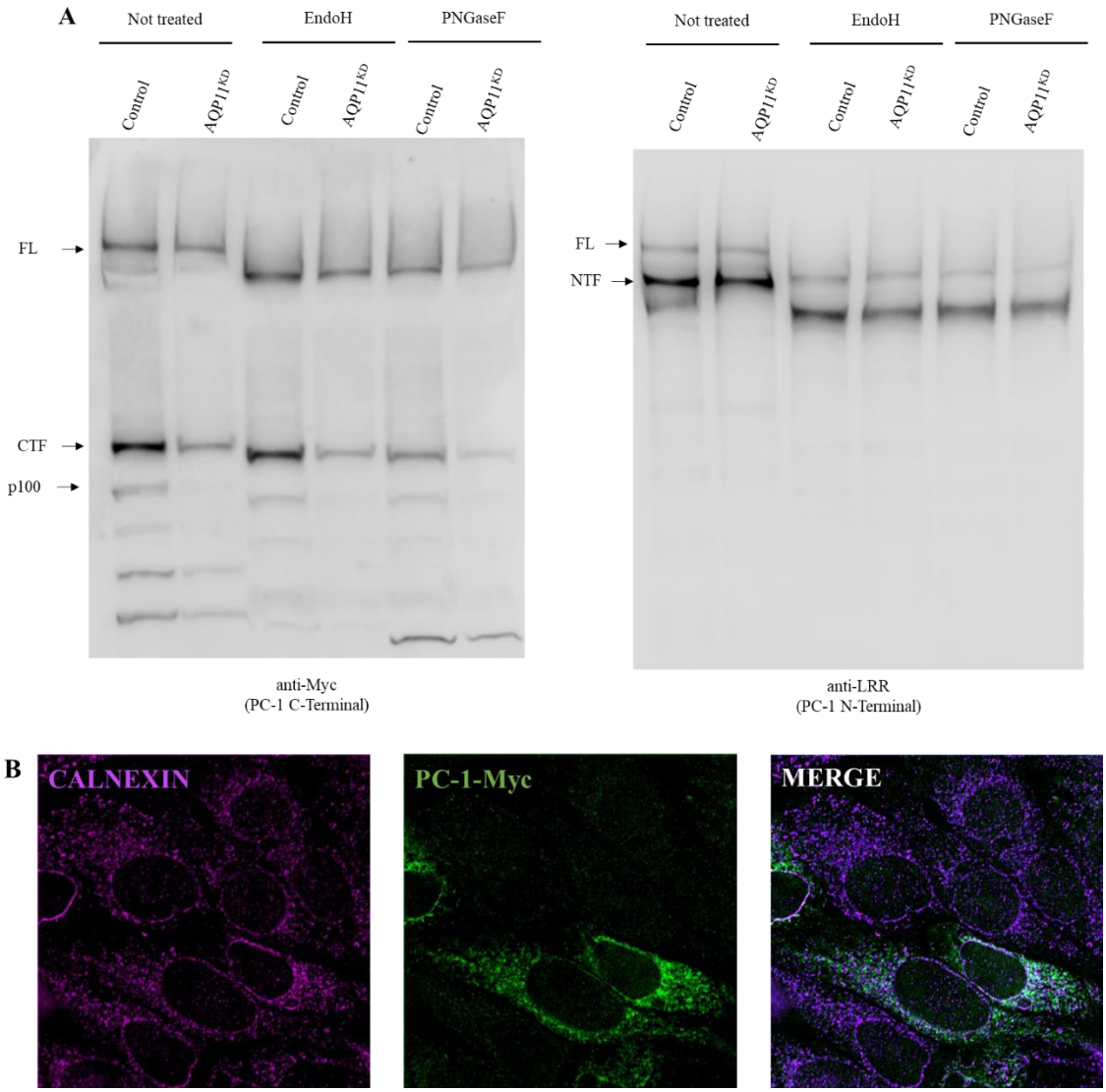



***Figure 26. Endoglycosidases treatment of overexpressed PC-1-Myc in HeLa cells***

*A) Treatment with endoglycosidases Endo-H and PNGase-F revealed that in HeLa cells overexpressed PC-1-Myc remains Endo-H sensitive both in control and AQP11$^{KD}$ cells, indicating that it is ER-retained. No major differences were found between the two conditions.*

*B) ER-colocalization is confirmed by the calnexin co-staining.*

## 3.9 AQP11$^{KD}$ generally affects sugar processing

Since overexpressed PC-1-Myc mostly remains in the ER when expressed in HeLa cells, we decided to check for possible problems in PC-1 glycosylation taking advantage of the QIF16 mutant (Qian lab). This mutant only retains the NTF and the GPS autoproteolytic site of PC-1, while the entire transmembrane CTF is substituted by a human IgG Fc-Tag (Figure 27A).

The use of this mutant has several advantages:

I. the NTF is the most glycosylated part of PC-1 (around 50 out of 60 of the total *N*-glycosylation sites are located in it)

II. not having transmembrane regions, this mutant can be secreted. Thus, looking at the secreted pool of the protein we can be sure that we are looking at proteins that underwent through every step of sugar processing along the secretory pathway. Indeed, when overexpressed in HeLa cells, the secreted pool of QIF16 became Endo-H resistant (Figure 27B), indicating that its sugars can undergo further processing in the Golgi apparatus.

III. we can compare the amount of secreted QIF16 in AQP11$^{KD}$ or control cells to evaluate if its secretion is affected.

IV. retaining the GPS site, the mutant can still undergo autoproteolysis resulting in the dissociation between NTF and Fc. Thus, we can have a further readout to study PC-1 cleavage under AQP11 silencing conditions.

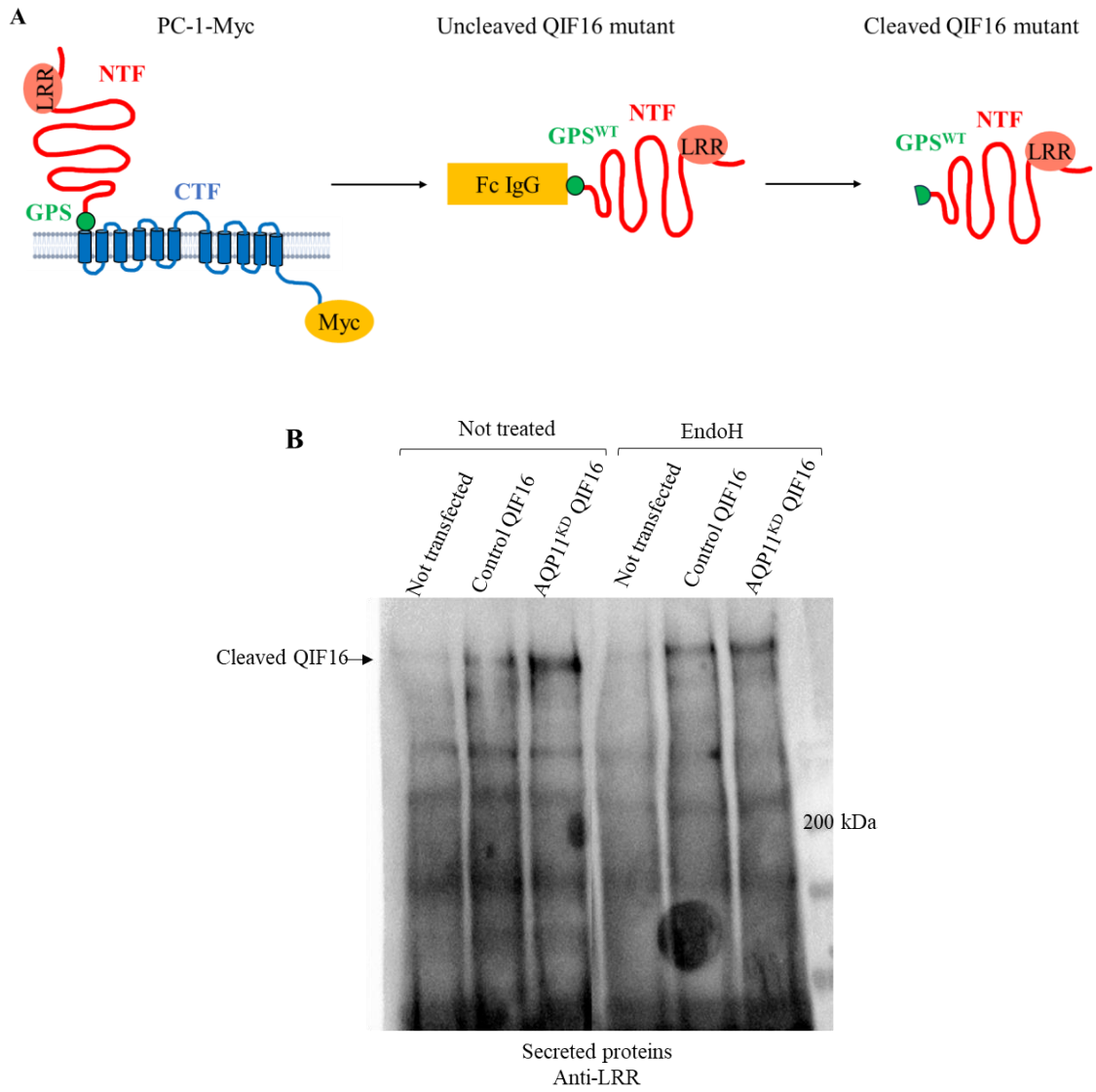



***Figure 27. Schematic representation of the QIF16 mutant and Endo-H treatment***

*A) Schematic representation of PC-1-Myc and QIF16 mutant before and after GPS autoproteolysis. QIF16 mutant retains the NTF and can undergo autoproteolysis by GPS, while CTF is substituted by a human IgG Fc-tag.*

*B) Secreted QIF16 mutant overexpressed in HeLa cells is Endo-H resistant.*

The HEK/Flp cell line, inducible to express the QIF16 mutant was kindly provided by Prof. Feng Qian. Thus, we decided to take advantage from these cells to investigate the effects of AQP11$^{KD}$ on the glycosylation, transport, and cleavage of the NTF fragment, independently from upstream events. Looking at proteins present in total cell lysates by the anti-LRR antibody, the QIF16 mutant migrates as a doublet: the upper band corresponds to the mutant before autoproteolysis, the lower one to the fragment obtained upon cleavage of the Fc-tag. No major differences could be observed between controls and AQP11$^{KD}$ cells comparing the amount of cleaved protein, as a further confirmation that PC-1 autoproteolysis is not severely affected by AQP11 silencing (Figures 21 and 22). In addition, no shift in the molecular weight of the QIF16 mutant were observed intracellularly (Figure 28A left), suggesting that *N*-glycans are normally processed. Interestingly, however, a small but reproducible mobility shift could be detected on the secreted fraction of cleaved QIF16 mutant in AQP11$^{KD}$ cells compared to untreated controls (Figure 28A middle). To test whether this shift was due to a different processing of sugars, we treated samples with endoglycosidase PNGase-F. Our results showed that PNGase-F treatment abolished the molecular mass shift between control and AQP11$^{KD}$, indicating that it was due to a different processing of *N*-glycans (Figure 28A right). In addition, only secreted proteins displayed aberrant glycosylation. This observation points at a difference that become evident in a post-ER compartment.

To test if QIF16 trafficking was impaired in AQP11$^{KD}$ cells, we quantified the amount of secreted cleaved QIF16 mutant as a function of total intracellular molecules. This analysis revealed that in AQP11$^{KD}$ HEK/Flp cells, cleaved QIF16 was less secreted compared to control (Figure 28B). Thus, cells harbouring reduced amounts of AQP11 seem to experience reduced QIF16 secretion. Collectively, we found that upon AQP11$^{KD}$, the glycans of an NTF fragment derived from the QIF16 mutant are not properly processed and their secretion is reduced. These data are in line with the findings in *Aqp11*$^{-/-}$ mice (Inoue *et al*, 2014). As anticipated above, glycans differ only in secreted molecules, suggesting that one or more processing enzymes may be misregulated in cells with low AQP11.

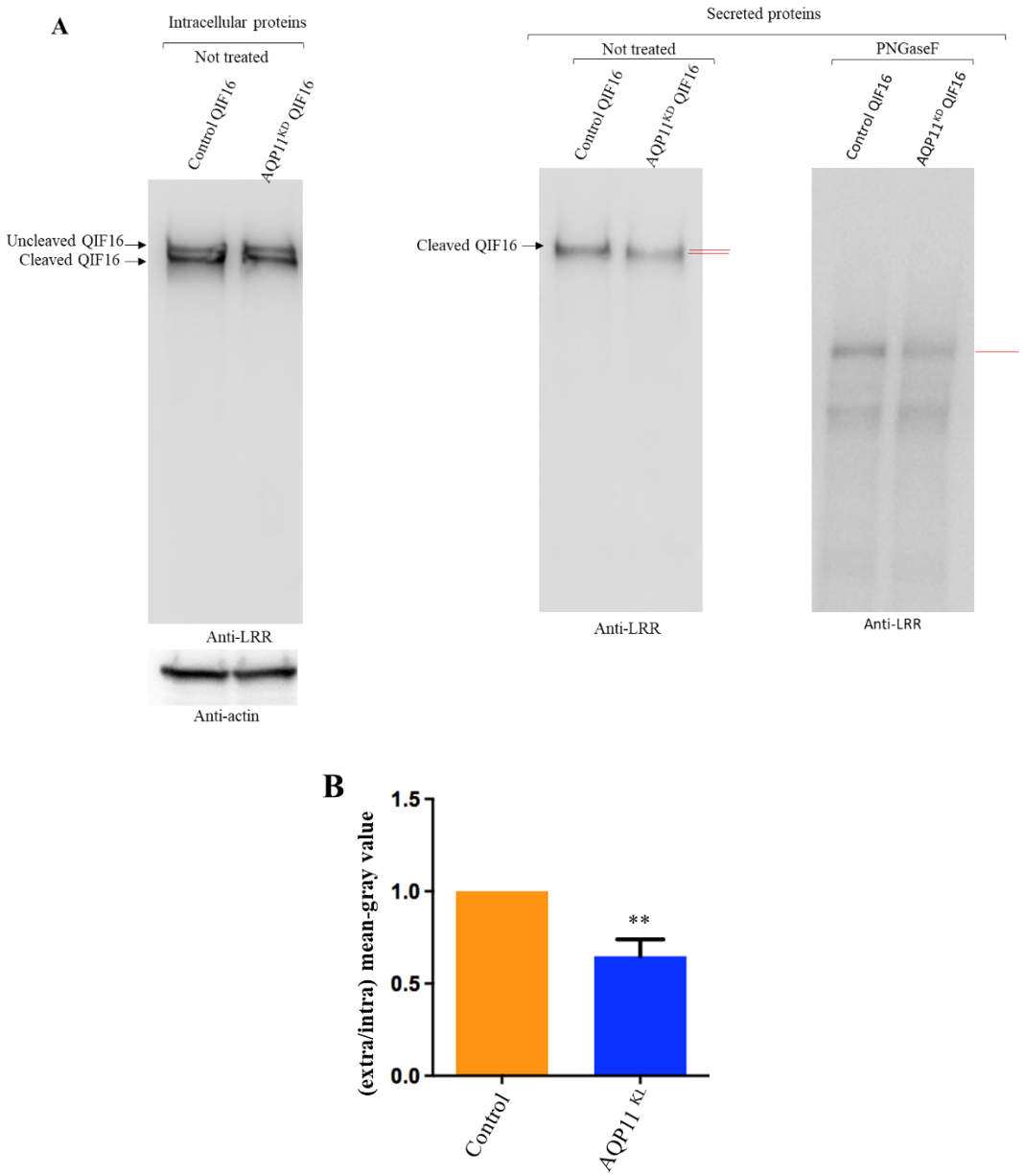



***Figure 28. Secreted QIF16 mutant shows a different N-glycan processing and slower secretion in AQP11$^{KD}$ cells***

*A) QIF16 mutant does not show major differences intracellularly while it displays a smaller molecular weight when secreted in AQP11$^{KD}$. This difference is abolished upon PNGase-F treatment.*

*B) QIF16 mutant is less secreted in AQP11$^{KD}$compared with control. Quantification of the secretion was done by the ratio between the mean-grey value intensity value of the extracellular and the intracellular signal. The mean with standard error (SEM) from three independent experiments was calculated. Unpaired t-test was performed comparing AQP11$^{KD}$ with control.*

To understand whether the defective *N*-glycan processing and secretion that we observed for the QIF16 mutant upon AQP11 downregulation reflected a general problem or rather a specific feature of PC-1 derived molecules, I decided to test another secreted glycoprotein under similar conditions. To this end, I made use of HeLa cells that can be induced to express μ and λ chains that assemble to form secretory IgM ($HeLa_{\mu s\lambda}$) (Bakunts *et al*, 2017). Electrophoretic analyses under non-reducing conditions showed that $AQP11^{KD}$ does not significantly affect intracellular IgM polymerization, indeed no major differences in size or abundance of the various assembly intermediates were found comparing controls untreated and $AQP11^{KD}$ cells (Figure 29A left). Interestingly, however, IgM molecules found in the medium conditioned by AQP11 silenced cells displayed lower molecular mass than in control cells (Figure 29A middle). The difference is barely seen in polymers or in the few $\mu_2\lambda_2$ subunits that avoid quality control (Anelli & Sitia, 2008). It becomes easily detectable when the migration of Ig-μ chains is compared after DTT reduction. Again, the difference is cancelled when samples are treated with endoglycosidase PNGase-F (Figure 29A right), pointing at a different processing of the sugars. We also quantified the amount of secreted IgM in the two samples by ELISA assay founding out that it is only mildly reduced in $AQP11^{KD}$ compared to controls (Figure 29B). To resume, these data reveal that silencing of AQP11 affects post-ER processing of certain *N*-glycans, while the biogenesis of PC-1 is more severely affected than that of IgM.

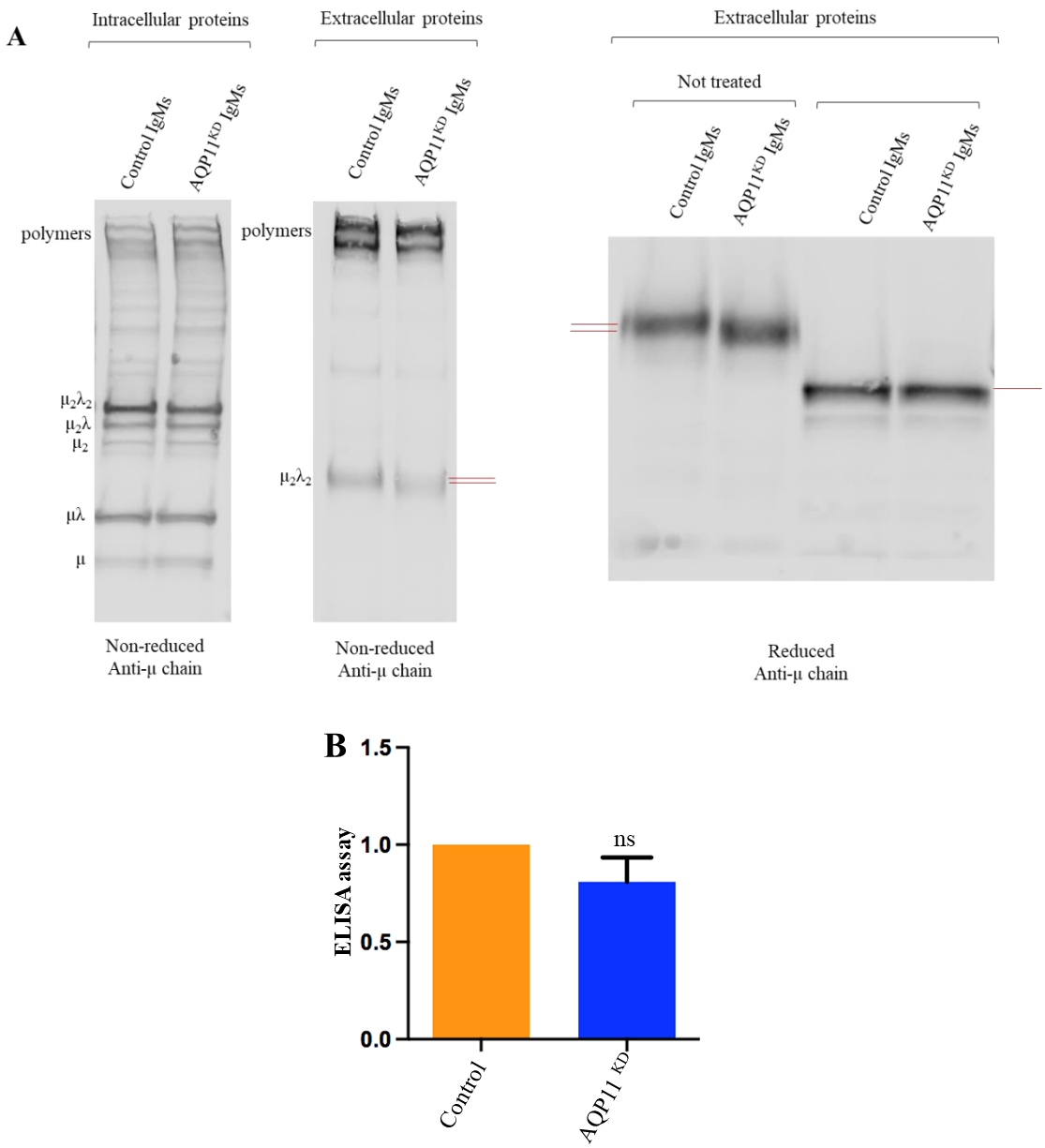



***Figure 29. Secreted IgM show defective N-glycans processing in AQP11$^{KD}$ cells***

*A) Intracellular IgM are not affected by AQP11 silencing, while secreted IgM display a smaller molecular weight. This difference is abolished upon PNGase-F treatment.*

*B) Quantification by ELISA assay revealed no major differences in secreted IgM amount comparing AQP11$^{KD}$ with control. The mean with standard error (SEM) from three independent experiments was calculated. Unpaired t-test was performed comparing AQP11$^{KD}$ with control.*

To better investigate the mechanism that leads to defective *N*-glycan processing in AQP11$^{KD}$ cells, we decided to look at the phenotype on IgM since they are easier handle compared to the QIF16 mutant. In particular, we wondered whether this defect was linked to the excess of $(H_2O_2)_{ER}$ that results upon AQP11$^{KD}$. With this aim, I tried to rescue aberrant glycosylation restoring normal levels of $(H_2O_2)_{ER}$ by ER-CAT-Myc overexpression. Interestingly, ER-CAT-Myc expression does not rescue glycans processing in AQP11$^{KD}$ cells (Figure 30). This suggests that increased $(H_2O_2)_{ER}$ is not the main cause of this defect. Nevertheless, we are in a system in which all the cells are stably expressing IgM, while a limited fraction of them is transiently expressing ER-CAT-Myc. Thus, low number of cells expressing catalase could be not sufficient to see a rescue on the total cells by WB and further analysis are needed. Alternatively, this defect is not indeed due to excessive $(H_2O_2)_{ER}$ but more likely due to the lowering of $(H_2O_2)_{cytosol}$ that also results from AQP11 downregulation (Bestetti *et al*, 2020) and that may result in the lack of a cytosolic redox signalling. A third possibility is that the defect may be not linked at all to the function that AQP11 exerts as $H_2O_2$ transporter. Further analyses are needed to clarify this point.

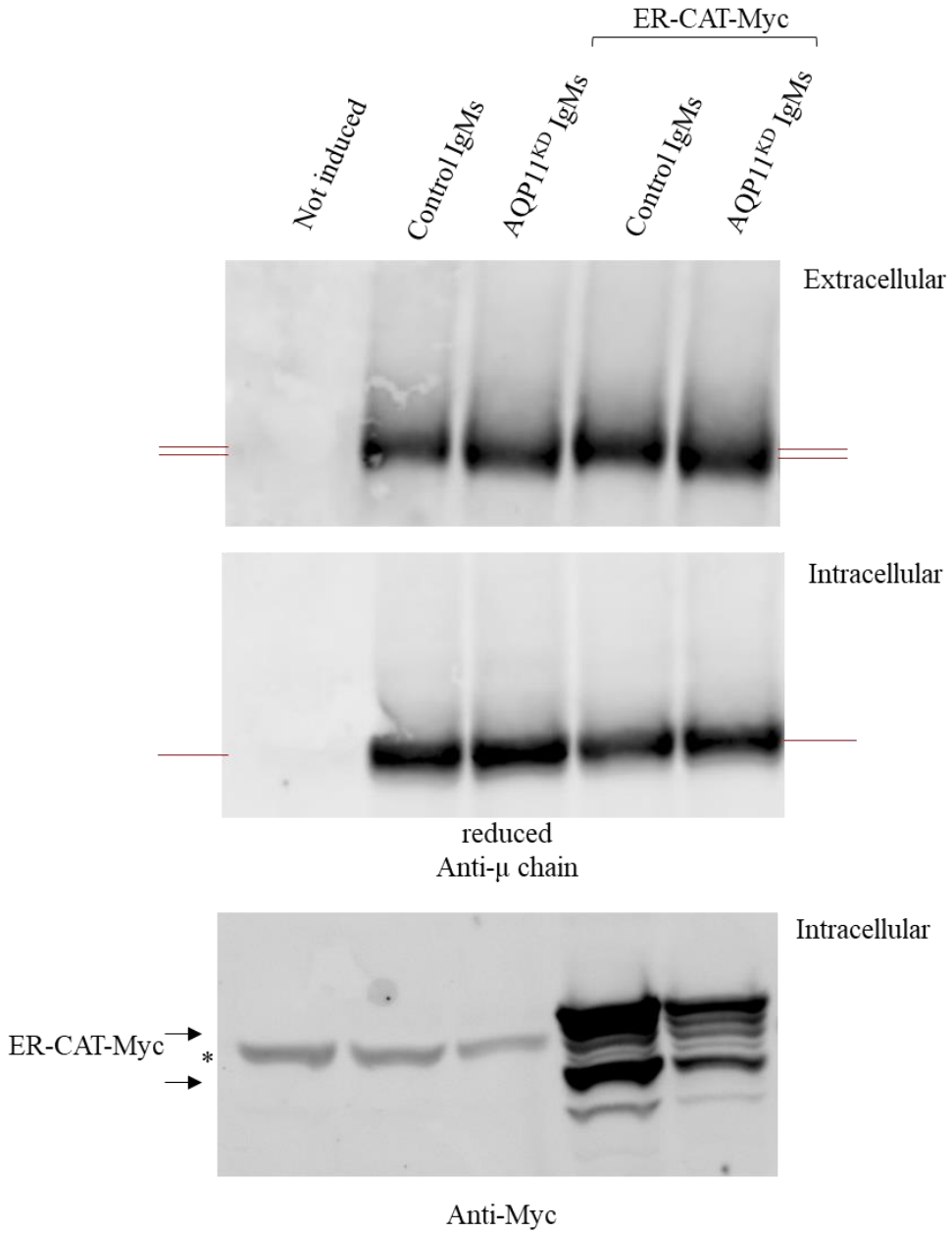



***Figure 30. Expression of ER-CAT-Myc in AQP11$^{KD}$ HeLa$_{\mu s\lambda}$ cells***
*Restoring normal levels of $(H_2O_2)_{ER}$ by ER-CAT-Myc overexpression in AQP11$^{KD}$ HeLa$_{\mu s\lambda}$ does not rescue aberrant N-glycan processing of μ chain.*

# 4 Discussion

## 4.1 Loss of AQP11 leads to atypical Polycystic Kidney Disease

Aquaporins (AQPs) are channels that facilitate membrane diffusion principally of water. Not surprisingly, considering the central role of the kidney in water homeostasis, frequent are the mutations in the genes encoding AQPs that are associated with this organ disfunction (He & Yang; Su *et al*, 2020). In addition, some AQPs, can also transport other small uncharged molecules beside water, such as glycerol -aquaglyceroporins- or $H_2O_2$ -peroxiporins- (Bienert *et al*, 2006; Verkman, 2011). Among known peroxiporins, AQP11 is uniquely stably localized in the ER and its deficiency leads to Polycystic Kindey Disease (PKD) (Inoue *et al*, 2014; Price *et al*, 2023). Hence, the central question that I tried to solve in my thesis is: how could the absence of this ER-localized peroxiporin cause PKD?

A detailed analysis of *Aqp11*$^{-/-}$ mice suggested that kidney cystogenesis implies impaired maturation of PC-1 (Inoue *et al*, 2014). In my studies, I found that AQP11$^{KD}$ in cells decreases overexpressed PC-1's cleaved forms (Figure 14). This defect is due to the absence of AQP11 and the resulting accumulation of $H_2O_2$ which is trapped in the ER (Figure 18 and 19). Defective PC-1 maturation is a feature which is shared with other ADPKD-related genes (Harris *et al*, 2002). Nevertheless, many are the differences between *Aqp11*$^{-/-}$ mice and other murine models of ADPKD or patients. One of these differences is the timing of cysts development. Indeed, both in mouse and human, ADPKD usually has a late onset, with end-stage disease starting around age 50-60 in human. Differently, in *Aqp11*$^{-/-}$ mice cysts development starts at 1 week after birth arriving at end-stage in 3-weeks old mice.

The early disease onset in *Aqp11*$^{-/-}$ mice resembles more Autosomal Recessive Polycystic Kidney Disease (ARPKD), a rarer form of PKD affecting 1:10.000 live birth (Bergmann, 2019). ARPKD is principally associated with mutations in the Polycystic Kidney Hepatic Disease 1 (*PKHD1*) gene, encoding fibrocystin (Onuchic *et al*, 2002; Bergmann *et al*, 2004) or DAZ-Interactin Protein 1-like (*DZIP1L*), encoding DZIP1L (Lu *et al*, 2017), two proteins involved in primary cilia biogenesis. Likewise, a case of bilateral cystic dysplasia associated with compound heterozygous variants in human *AQP11* described by Price and colleagues, was diagnosed in utero (Price *et al*, 2023).

Altogether, these findings suggest that in a background with healthy PC-1, heterozygous mutations in *AQP11* may not be sufficient to reduce PC-1 functionality under the critical level to start cystogenesis (Hopp *et al*, 2012; Fedeles *et al*, 2014). Thus, homozygous or combined heterozygous mutations in *AQP11* and/or *PKD1* genes seem to be needed to see an effect *in vivo*. These data may also explain why very few cases of human *AQP11* mutations are reported in literature, since genetic diagnosis in utero is not a common practice. If loss of function mutations in *AQP11* are needed for PC-1 to be compromised, incomplete silencing in our experiments where there is around a 20-40% of residual mRNAs, may underestimate the effect on PC-1. Unfortunately, we failed in generating $AQP11^{KO}$ cells but likely with 100% depletion the phenotype of PC-1 could be even stronger. Moreover, precocious cystogenesis found in $Aqp11^{-/-}$ and in the case described by Price (Price *et al*, 2023), suggests that AQP11 might exert an important role during kidney development, which also corresponds to the time of maximal *PKD1* expression in both mice and humans (Padovano et al., 2020). Another hint of this comes from an interesting observation done by Rutzler and colleagues, who studied the effects of inactivating murine *Aqp11* postnatally at different time points. By this method, they found that the later was the gene inactivated after birth, the milder was the phenotype. No major defects were found when the inactivation started from day 12 after birth. This result is reminiscent of a study in which inactivating *Pkd1* in a mouse model after post-natal day 13 leads to a less severe disease (Piontek *et al*, 2007; Leonhard *et al*, 2016). All together, these studies suggest that *AQP11* may be important to assist a key role of PC-1 during development and in the first weeks of life.

Beside the timing, also the place in which cysts develop is different between $Aqp11^{-/-}$ and ADPKD murine models and patients. In human and mouse kidney, AQP11 is principally expressed in proximal tubules: accordingly, mice lacking this peroxiporin undergo cystogenesis specifically in this segment of the nephron, differently from ADPKD patients and corresponding mouse models who present cysts in all nephron segments (Bergmann, 2019). It is worth to notice that, during development, PC-1 is majorly expressed in tubular epithelia in mice (Geng *et al*, 1997) and proximal tubules in human (Chauvet *et al*, 2002), again pointing at a stronger interplay between these two proteins during nephrogenesis. Importantly, inactivation of murine *Pkd1* at post-natal day 10, revealed that the outer medulla tissue is the most severely affected region of the

kidney (Leonhard *et al*, 2016), which also corresponds to the medullary stripe where proximal straight tubules are located (Zhuo & Li 2014). The high demand of PC-1 during kidney formation as well as the expression of AQP11 in an area particularly sensitive to loss of PC-1 may explain the time and location of cysts development in *Aqp11*$^{-/-}$ mice.

If evolution selected animals in which a given protein accumulates in a tissue, we can assume that that protein plays a particularly important function there. So, what is the role that AQP11 exerts in PT cell? At present, I can offer only speculative conjectures. Interestingly, proximal and distal tubule cells show different metabolic profiles. The former indeed relies more on fatty acid oxidation (FAO) for ATP production, while the second have a glycolytic metabolism. Many studies in the literature link ADPKD with altered mitochondrial functions and metabolism, which is switched from FAO to glycolysis, leading to the so-called Warburg effect typical of tumors. Of notice, PC-1 is found to be enriched at MAMs, where it is important for the exchange of $Ca^{2+}$ between ER and mitochondria. The localization and channel activity of Polycystins at MAMs depends by intracellular $O_2$ level. In normoxic conditions, Polycystins-mediated $Ca^{2+}$ release at MAMs was proposed to stimulate oxidative metabolism by activating key enzymes involved in this process. Accordingly, dysregulated uptake of $Ca^{2+}$ by mitochondria could be the cause of the metabolic reprogramming in ADPKD (Padovano et al, 2017; Podrini et al, 2020, 2018). Importantly, many proteins involved in oxidative folding in the ER are also enriched at MAMs, including some chaperones such as ERp57 and ERp44, but also the oxidoreductase Ero1a. The interplay existing between $Ca^{2+}$ and redox in the ER is also well established. Indeed, while Erp57 is known to inhibit the SERCA pump and ER-$Ca^{2+}$ replenishment under oxidizing conditions, ERp44 inhibits the IP3R and $Ca^{2+}$ efflux from the ER under reducing conditions. Also, IP3R oxidation by Ero1a interferes with its association with ERp44, thus increasing $Ca^{2+}$ release (Li & Camacho, 2004; Higo *et al*, 2005; Simmen *et al*, 2010; Anelli *et al*, 2012). In this contest, an altered redox homeostasis in the ER could also dysregulate the inter-organellar exchange of $Ca^{2+}$ and, consequently, metabolism.

Taking together these observations, we can speculate that the higher expression of the $H_2O_2$ transporter AQP11 in PT cells might be a strategy to better regulate ER-redox homeostasis in a tissue in which a switch from FAO to glycolysis could be more

detrimental compared to distal tubule cells where glycolysis is already the main fuel for energy production.

## 4.2 PC-1 is sensitive to changes in $(H_2O_2)_{ER}$ level

The main conclusion that can be drawn from my studies is that the levels of $H_2O_2$ in the ER dramatically affect polycystin biogenesis. Indeed, we published that the absence of AQP11 in the ER membrane increases the $H_2O_2$ level in this compartment (Bestetti *et al*, 2020), possibly altering its redox-homeostasis. To further confirm the correlation between the increase level of $H_2O_2$ and the defects in PC-1 processing, I silenced Cystathionine β-Synthase (CBS), another experimental setup that allows us to increase the $H_2O_2$ in the ER (Figure 18A). Surprisingly, the results show that $CBS^{KD}$ affects PC-1 with a similar phenotype of $AQP11^{KD}$ (Figure 18B). For what concern CBS, the mechanism that leads to peroxide accumulation, after this protein downregulation, remains to be clarified. Since CBS is a cytosolic enzyme that has nothing to do with water transport, it is the peroxiporin function of AQP11 that possibly becomes limiting upon $CBS^{KD}$. Indeed, we previously published that CBS is important for the closure mechanism of AQP8, another peroxiporin that resides at the plasma membrane (Bestetti *et al*, 2018). This process implies first the $H_2O_2$-mediated sulfenylation of $Cys^{53}$ located in the channel pore. Secondly, $Cys^{53}$ is persulfidated by $H_sS$ produced by CBS (-SH→-SOH→-SSH), resulting in the channel closure. Thus, downregulation of CBS impairs AQP8 closure. Currently, whether and how AQP11 opening and closure mechanism could be similarly regulated is not known. However, the observation that AQP11 and CBS downregulation result in a similar increase in $(H_2O_2)_{ER}$ may suggests that CBS could be important to maintain this channel in an opened state, which would be the opposite then what described for AQP8. In addition, even if mutations in CBS are seldom directly linked to cystic kidney disease (Sacharow *et al*, 2004), the hyper homocystinuria (hHcys) that results from the lack of this enzyme was previously associated with oxidative stress due to NOXs hyperactivation in glomeruli (Yi *et al*, 2009).

Compelling evidence of the link between PC-1 maturation and $(H_2O_2)_{ER}$ comes from the experiments in which I expressed active catalase in the ER. As previously shown, expression of ER-CAT restored the levels of $(H_2O_2)_{ER}$ in $AQP11^{KD}$ to those observed in

control cells (Figure 19A). Most importantly, ER-CAT expression rescued the typical PC-1 phenotype observed upon $AQP11^{KD}$ (Figure 19B-C). Taken together, these findings indicated that it is the excess of $(H_2O_2)_{ER}$ caused by AQP11 depletion that disturbs PC-1 maturation. Of notice, ER-CAT expression in control conditions accumulates more CTF compared to the counterpart with AQP11 silencing (Figure 19C, compare orange plaid with blue plaid bars). This can be correlated with the higher expression of ER-CAT in control compared to silenced cells (Figure 19B), that could improve CTF stability even more. However, I never measured catalase enzymatic activity in the two conditions. In addition, differently from previously published results (Sorrentino *et al*, 2022), ER-CAT expression did not decrease $(H_2O_2)_{ER}$ to a greater extent in control cells compared to untransfected controls (Figure 19A, compare orange bar with orange plaid bar). This can be explained taking into consideration that, when I measure HyperProbe oxidation, I cannot select cells expressing ER-CAT-Myc since the construct is not fluorescent. Thus, in my analysis I selected randomly cells without considering ER-CAT expression. This may underestimate the differences between the two cell populations. Augmenting the number of experiments would possibly reveal this difference. In addition, a pool of HyPer probe may remain partially oxidized even in the presence of catalase, because its disulfide bond can be formed *via* the PDI- Ero1α paths (Konno et al., 2015). Importantly, it seems that ER-CAT expression *per se* stabilizes CTF even more than in the control non-transfected counterpart (Figure 19C, compare orange bar with orange plaid bar). If this correlates with a more reduced environment in the ER (Sorrentino et al., 2022), strategies aimed at decreasing $(H_2O_2)_{ER}$ may be used with therapeutic purposes in those ADPKD cases in which mutations affect stability of otherwise functional PC-1.

Another approach that I tried to manipulate $(H_2O_2)_{ER}$, was the expression of D-amino acid oxidase (DAAO), an enzyme that catalyses the conversion of D-amino acids to D-immino acids forming $H_2O_2$ as byproduct (Mozzarelli *et al*, 2018). DAAO was previously used as a tool to induce production of $H_2O_2$ in different subcellular compartments where the enzyme was targeted, such as the cytosol and the nucleus (Soheil *et al*, 2020). Until now, however, nobody targeted the protein to the ER-lumen. I managed to express a Halo-tagged version of the enzyme in the ER by the addition of a leader sequence at the N-terminus of the protein and a KDEL sequence for ER-retention at its C-terminus (Figure 31). Unfortunately, when I added exogenously D-amino acids to HeLa cells expressing

HyperER-lumen I did not detect any change in Hyper oxidation (data not shown), possibly due to the lack of functional D-amino acids transporters on the ER membrane.

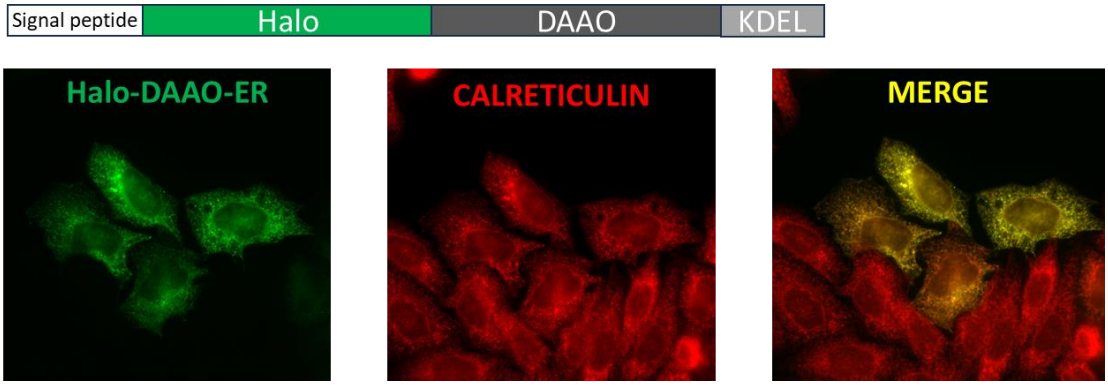



***Figure 31: Halo-DAAO-ER expression in HeLa cells***
*Co-localization with the ER-marker calreticulin shows that the enzyme is properly targeted to the ER-lumen.*

## 4.3 How $(H_2O_2)_{ER}$ could influence PC-1 biogenesis?

The Endoplasmic Reticulum is the organelle with the highest concentration of $H_2O_2$ within the cell. Indeed, the ER-lumen is the place where many oxidizing enzymes are located, and oxidative protein folding occurs. This process entails the formation of one $H_2O_2$ molecule for each disulfide catalysed by the PDI-Ero1α axis (Tu *et al*, 2000; Tu & Weissman, 2004). Although redox reactions in the ER are mainly channelled *via* enzymatic relays, the ability of $H_2O_2$ to sustain protein folding directly by promoting formation of disulphide bonds (Karala et al, 2009), or indirectly *via* PRX4 (Zito *et al*, 2010; Tavender *et al*, 2010) is also well established. In normal conditions, which Helmut Sies would define conditions of oxidative eustress, $H_2O_2$ is likely to react only with target cysteine residues. To achieve this, redox oxidation of target cysteines is spatio-temporally controlled, meaning that this molecule needs to be more concentrated in the time and place where the reaction takes place. A tight spatio-temporal control of $H_2O_2$ fluxes is important to prevent non-specific reactions (Sies & Jones, 2020; Nordzieke & Medraño-Fernandez, 2018). Thus, excess $H_2O_2$ may result in distress and jeopardize the specificity of the redox pathways at work. In this scenario, also cysteines that normally are not target for $H_2O_2$ may be oxidized, possibly impairing the target protein to reach its native conformation.

PC-1 has 95 cysteines in its sequence and missense mutations in ~21% of them are pathogenic (ADPKD variant database, https://pkdb.mayo.edu) (Figure 32). Among total cysteines, 82 are exposed to the luminal side of the ER (of which 76 located in the NTF and 6 in the CTF). These residues can be in principle exposed to changes in $(H_2O_2)_{ER.}$

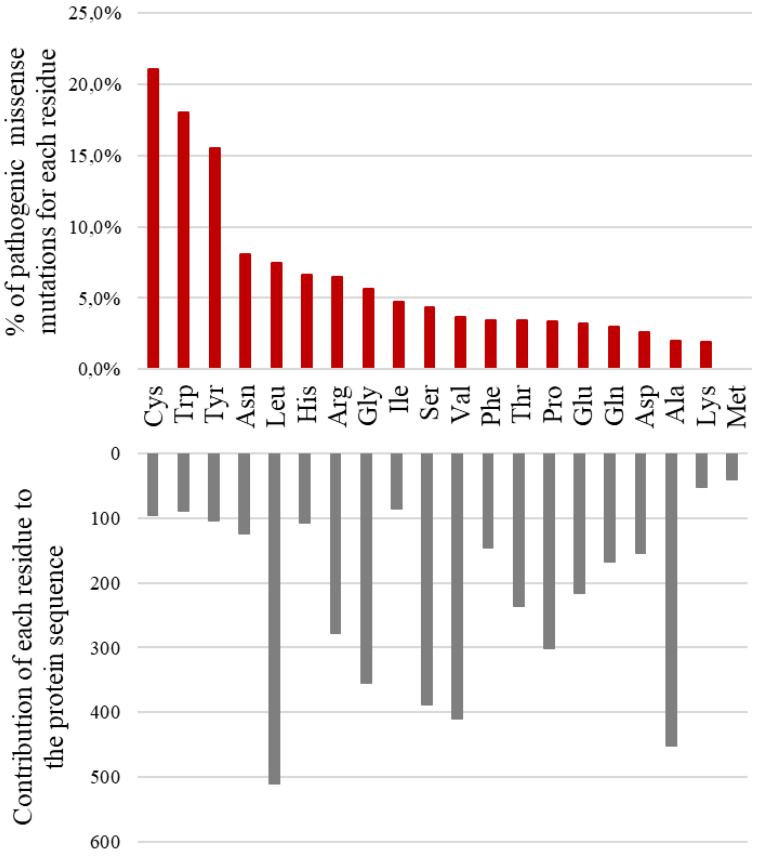



***Figure 32. Analysis of PC-1 pathogenic mutations***
*Here is shown for each amino acid its numeric contribution within human PC-1's sequence (bottom graph) and the % of them which missense mutation is categorized as «pathogenic or likely pathogenic». ADPKD variant (https://pkdb.mayo.edu/variants). 20 over 95 total Cys (21,1%) are pathogenic or likely pathogenic if mutated, being the amino acid that majorly contributes to pathogenicity.*

Curiously, in PC-1's sequence are also found 7 CxxC motifs which are reminiscent of the active site of PDI protein family. These motifs can facilitate the formation of disulfides in client proteins. When in a favoured aminoacidic environment, the two cysteines of the CxxC are prone to form a disulfide which can be disrupted by a nucleophilic attack from the reactive thiolate ($-S^-$) in a client protein, resulting in the formation of an intermediate "mixed" disulfide. Then, the mixed disulfide is transferred

to another cysteine of the client protein resulting in the formation of a native disulfide. Interestingly, some of those CxxC motifs in PC-1 sequence are evolutionary conserved from fish, suggesting that they may exert a functional role (see Table 2). In addition, 6 of them are on the portion of the protein exposed to the lumen of the ER, thus in principle they may be used as isomerase-like domains. Indeed, one speculation for the role of those CxxC motifs is that, since PC-1 folding is so demanding, the presence of those domains may facilitate the formation of its own disulfides thorough the formation of folding intermediates. Unfortunately, it would be difficult to assess whether those CxxC motifs are in an environment favourable for them to be reactive, since NTF 3D structure is not resolved (Su *et al*, 2018).

In addition, part of PC-1's sequence is predicted to be intrinsically disordered with many pathogenic missense mutations found to occur within these Intrinsically Disordered Regions (IDRs) (Hardy & Tsiokas 2020, calculated by ELM online tool http://elm.eu.org/). IDRs properties can depend on various conditions, including environmental factors such as redox potential (Reichmann & Jakob, 2013). I performed a similar analysis using the IUPred2A online tool (Abor et al, 2018; http://iupred2a.elte.hu) to make a prediction of IDRs on PC-1 as well as the regions within the protein which conformation is predicted to be redox-sensitive. IUPred2A uses the energy estimation approach (Dosztányi *et al*, 2005) to assign an energy value (score) to each residue of the protein, based on the amino acid type and the composition of its sequential neighbourhood. The higher the final score, the higher the probability of disorder. The range of the score goes from 0 which is assigned to structured regions, to 1 which is assigned to disordered regions. The cutoff is set by default by the software to 0.5. If the score is $\leq 0.5$ that region is likely to be structured, if it is $\geq 0.5$ that region is likely to be unstructured. This analysis confirmed that some of PC-1 regions are likely disordered, in both the NTF and CTF (Figure 32A). Interestingly, some regions of the protein are predicted to transit from a more ordered to a disordered state with a redox-sensitive mechanism (Figure 32B). Those redox-sensitive disordered regions cover different domains of the NTF and approximately the 11% of their amino acidic sequence is composed by cysteines, which may explain their predicted redox sensitivity. Putative redox-conditional IDRs contain one of the CxxC motifs (1*, see Table 2), while other

three (4*, 5* and 6*, see Table 2) are found in the vicinity, possibly suffering from redox changes.

To sum up, one possible mechanism by which increased $(H_2O_2)_{ER}$ that results from $AQP11^{KD}$ interferes with PC-1 maturation is through the non-specific oxidation of one or more cysteines exposed to the ER-lumen. Nevertheless, we were not able to notice any evident difference in folding intermediates formation looking at PC-1-Myc in non-reducing SDS-PAGE comparing control and $AQP11^{KD}$ cells (Figure 20), but this could be due to the limited resolution of our system. Redoxomic analyses are necessary to address this issue further. Alternatively, PC-1 may be indirectly affected by $H_2O_2$ *via* one of those enzymes previously identified to be fundamental for its maturation. The inhibition of one of those enzymes through a redox modification would not only affect PC-1 but more likely protein folding in general. Nevertheless, IgM polymerization is not majorly affected by $AQP11^{KD}$, arguing against a general perturbation of the oxidative folding machineries. Again, being PC-1 so frail to perturbation in the folding machinery, together with the major involvement of PC-1 in proximal tubules formation and the preferential localization of AQP11 in that segment of the nephron, makes this protein the perfect victim.

| **CxxC motifs position in PC-1 sequence** | **Human** | **Mouse** | **Japanese rice fish** |
|---|---|---|---|
| 1* N-terminal Cys rich domain flanking LRR1 | CGPC | CGPC | CGPC |
| 2* PKD2 domain | CPAC | | |
| 3* PKD11 domain | CDRC | CDRC | CDHC |
| 4* REJ domain | CVSC | CVSC | CVSC |
| 5* REJ domain | CLNC | CHNC | CSNC |
| 6* REJ domain | CRSC | CRSC | CEEC |
| 7* TM1 | CAVC | CVSC | |

***Table 2: List of CxxC motifs***
*in human, mouse and Japanese rice fish PC-1 sequence. The underlined residues are the ones that change in evolution.*

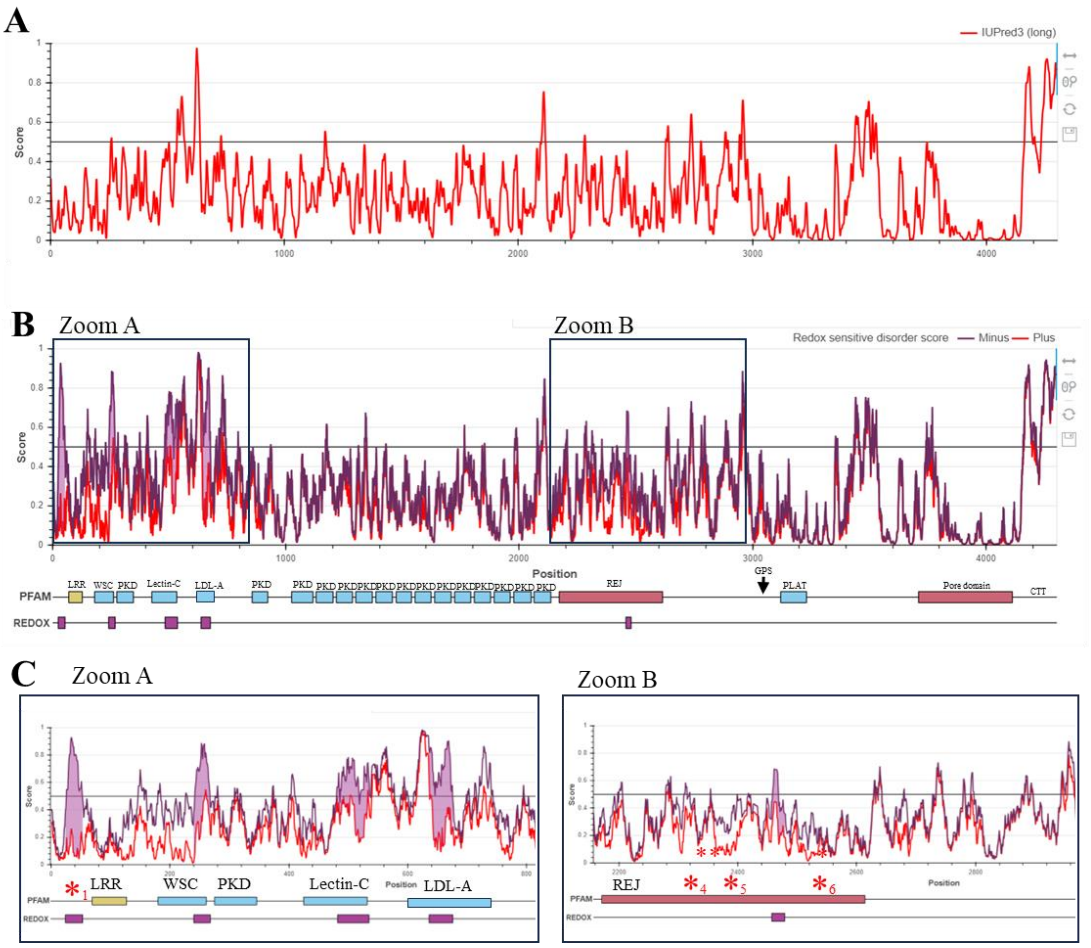



***Figure 33: Analysis of predicted IDRs and redox-conditional IDRs in human PC-1 protein sequence***

*IPUred2A is a probabilistic prediction of disorder within a protein sequence. PC-1 regions with score ≥0.5 are likely to de disordered. PC-1 predicted IDRs are represented by the red line (A) and predicted redox-sensitive conditional IDRs are represented by the purple line (B). In (C) is presented e zoom of the putative redox-sensitive IDRs. Red asterisks correspond to CxxC motifs.*

## 4.4 AQP11$^{KD}$ decreases PC-1 cleaved forms

Whilst the redox dependency of PC-1 processing is clearly established, the mechanism(s) remain far from being understood. The lower cleaved forms levels found in AQP11$^{KD}$ cells could be due to defective autoproteolysis, an event that requires proper arrangement of two vicinal cysteine residues (Trudel et al., 2016). Much to our surprise, however, autoproteolysis was not affected (Figure 21 and 22). So, NTF and CTF fragments are generated at similar rates, yet their accumulation is impaired. Particularly severe is the loss of p100 (Figure 14), whilst normal were the levels of CTT (Figure 25), a fragment that plays a key role in the pathogenesis of PKD (Onuchic *et al*, 2021). The different extent by which each isoform is reduced could be due to their different stability, as we observed comparing NTF, CTF and CTT upon treatment with CHX (Fig. 22C and 25A). Another variable could be the different subcellular localization of those fragments. For instance, the p100 is known to localize and act prevalently in the ER (Woodward et al, 2010) where AQP11 resides.

Also, we assessed different sensitivity of PC-1 in different cell types (Figures 15). A possible explanation to this may be the different expression of factors helping PC-1 maturation, including PC-2. The analysis of the expression level of those factors in the different cell types that we used in our work can clarify this point. Nevertheless, co-expression of PC-2 stabilizes PC-1 but did not abolish the defect in CTF accumulation (Figure 17A-B). This experiment brings fuel to the notion that PC-1 is a protein requiring complete attention of the folding machinery. Variation in the expression level of one of its assistants may be of help to a sickly protein like PC-1. Of interest, would be to assess whether co-expression of PC-2 also promote membrane trafficking of PC-1 in HeLa cells, where the protein remains mostly ER-localized (Figure 26).

If autoproteolysis is normal, where do p100, CTF and NTF end up, in order of disappearance? Degradation by proteasomes explains only in part the defective accumulation (Figure 23), and so do conformational changes that determine detergent insolubility (Figure 24). Proteolytic cleavage of the C-terminal HA and Myc epitopes could be promoted in cells lacking AQP11. However, it is hard to envisage how increased $(H_2O_2)_{ER}$ could impact an event occurring in the cytosolic face of the ER membrane. In fact, the phenotype was rescued by expressing catalase in the ER. Moreover, AQP11$^{KD}$ had little if any effect on a Myc positive 30 kDa band, which might correspond to CTT

(Figure 25), a proteolytic fragment shown to accumulate in the mitochondrial matrix and in the nucleus (Lin *et al*; Chauvet *et al*, 2004; Podrini *et al*, 2019; Merrick *et al*). At the moment, a piece of the puzzle is missing to understand which is the fate of the isoforms that we found reduced upon $AQP11^{KD}$. Future research is needed to dissect this crucial mechanism that possibly implies the involvement of more then one of the processes analysed in this study. Interestingly, a recent work shows that increasing intracellular level of ROS, including by addition of exogenous $H_2O_2$, can stabilize PC-1's CTT when overexpressed in Madin-Darbin Canine Kidney (MDCK) cells. In addition, they found that ROS regulate the localization of CTT in a dose-dependent manner. Low ROS level targets CTT to mitochondria, while high ROS level to the nucleus (Pellegrini et al, 2023). This observation opens the possibility that, in our setting with increased $(H_2O_2)_{ER}$, not only CTT cleavage could be promoted reducing CTF, but also this isoform could be target to the nucleus. To investigate this hypothesis, it would be useful to check whether, upon AQP11 downregulation, CTT accumulates in the post-lysis pellet together with nuclei.
In addition, the recent discovery of the beneficial role of CTT in kidney cells lacking PC-1 (Onuchic *et al*, 2021) tells us that there is much to be learned about the pathophysiology of polycystins.

## 4.5 $AQP11^{KD}$ affects N-linked glycan processing

Addition and trimming of oligosaccharide moieties to the Asn residue of ER-newly synthetized proteins have been found to play a crucial role in quality control. Indeed, removal of glucose moieties by Glucosidases I and II allow unfolded proteins to enter the CNX/CRT cycle to fold. Also, Glucosidase II remove the third glucose to allow exit from the CNX/CRT cycle. If the protein is properly folded it will be sent to the Golgi apparatus. Alternatively, the glucose can be re-added by UDP-glucose enzyme to allow misfolded proteins to enter again the cycle (Ellgaard *et al*, 1999). Finally, the removal of one mannose moiety by Mannosidase I is used to distinguish between newly synthetized unfolded proteins and old misfolded proteins that need to be targeted to degradation (Fagioli & Sitia, 2001) (see Figure 11). Mutations in *ALG5, ALG8, ALG9, GANAB* and *PRKCSH* genes, encoding for enzymes involved in the assembly of *N*-glycan precursors

in the ER (see Table 1), were previously found to have a major effect on PC-1 glycosylation (Porath *et al*, 2016; Besse *et al*, 2018, 2019; Lemoine *et al*, 2022; Li *et al*, 2003; Besse *et al*, 2017b; Fedeles *et al*, 2011; Huynh *et al*, 2020), indicating how much this protein could be sensitive to failure in the *N*-glycosylation process. PC-1's *N*-glycans processing was found to be affected in *Aqp11*$^{-/-}$ mice (Inoue *et al*, 2014). Also, in our hands silencing AQP11 results in aberrant sugar processing, but in a way differing from what observed by Inoue. Indeed, we noticed that two secreted products, the QIF16 mutant and Ig-μ chains showed reduced molecular weight due to defective *N*-glycan processing following AQP11$^{KD}$ (Figs. 28A and 29A). No differences in electrophoretic mobility were detectable in the intracellular precursors of the two molecules. These results suggest that such a defect is not protein-specific and involves other glycoproteins in transit through the late secretory pathway. This may depend by the fact that the problem occurs at the Golgi level, or it may be due to a problem in the ER which prevent further processing immediately prior to secretion. Furthermore, preliminary data indicate that co-expression of ER-CAT does to rescue the aberrant *N*-glycans processing that we observe upon AQP11$^{KD}$ (Figure 30). If this will be confirmed, $(H_2O_2)_{ER}$ would be exonerated from being the cause. A possible explanation to this is that decreased cytosolic $H_2O_2$ that also results from AQP11$^{KD}$ (Bestetti *et al*, 2020) may be the reason. In this scenario, the activity of transmembrane Golgi glycosyltransferases or glycosidases might be modulated by redox modifications from the cytosolic side. Alternatively, the lack of a cytosolic signal might interfere with the activity of a transcription factor involved in regulating the expression of one of those enzymes. A further possibility is that AQP11 might travel between ER and Golgi by vesicular transport and its depletion may also dysregulate the redox-state inside the lumen of the Golgi. In this connection, it was recently showed that the absence of QSOX, an enzyme thought to produce $H_2O_2$ while inserting disulfides into its client proteins, impacted O-glycosyl transferases in the late Golgi stacks (Ilani *et al*, 2023). However, whether AQP11$^{KD}$ alter $(H_2O_2)_{Golgi}$ is not known yet. To assess this, it would be nice to target the HyperProbe to the distal stations of the secretory compartment to address whether an $H_2O_2$ gradient exists, akin to the pH and zinc gradients, that cargoes encounter during their travel to the extracellular space (Watanabe et al., 2019).

Beside glycosylation, also the amount of secreted QIF16 or IgM were quantified in AQP11$^{KD}$ cells and compared to controls. Our data revealed that lowering the AQP11 pool in HeLa cells inhibited overall secretion to a very small degree. In AQP11$^{KD}$ cells, QIF16 was more affected than IgM (Figures 28B and 29B). However, secretion of QIF16 was assessed only by WB. More sensitive assay, such as the ELISA used to quantified secreted IgM, are needed before we venture into speculations regarding an exaggerated sensitivity of QIF16 trafficking. It remains to be seen whether it is the anterograde trafficking from ER to Golgi or subsequent transport to the plasma membrane that is affected. Whatever the underlying cause, we did not observe major intracellular accumulation of the QIF16 mutant, pointing at the possibility that the fraction which is not secreted might be degraded. Importantly, even if these data are in accordance with previous ones on *Aqp11*$^{-/-}$ mice (Inoue *et al*, 2014), we should consider that the transport of a mutant that does not include the CTF may differ from the one of the wild type protein.

## 4.6 Concluding remarks

The phenotypic characterization of *Aqp11*$^{-/-}$ mice precedes the identification of this channel as peroxiporin. Thus, how mutations in *Aqp11* leads to impaired maturation of PC-1 was not clarified. With my cell culture model, I confirmed that AQP11 is an important factor for PC-1 biogenesis and I found out the accumulation of $(H_2O_2)_{ER}$ resulting from AQP11$^{KD}$ is the cause. Nevertheless, why PC-1 is so sensitive to redox changes in the ER, as well as which is the fate of decreased PC-1's cleaved forms upon AQP11$^{KD}$ are still open questions. Also, PC-1 was previously found to be aberrantly glycosylated in kidney from *Aqp11*$^{-/-}$ mice. In here, I confirmed this result in my cell model, and I added the observation that the impaired step occurs late in the secretory pathway, since it is visible only on the secreted proteins. Of interest, downregulation of AQP11 not only affects PC-1, but also IgM and a recombinant PC-1 fragment that can be secreted. These findings point at AQP11 as a hub controlling *N*-glycan processing, which may be redox regulated.

# 5 Materials and methods

## 5.1 Cells culture and methods

All the cell lines used were cultured in Dulbecco's modified Eagle's medium (DMED) high glucose (Gibco, ThermoFisher) with the supplementation of 10% Fetal Bovine Serum (FBS, EuroClone), 1% L-Glutamine (Gibco, ThermoFisher) and 1% Penicillin-Streptomycin (EuroClone). For HEK Flp QIF16 (PKD Research Resourse Consortium), also 100 μg/mL of Hygromycin and 10 μg/mL of Blasticidine were added to the medium.

| Cell line | Origin |
|---|---|
| **HeLa** | commercial |
| **HEK293T** | commercial |
| **HeLa Hyper ER-lumen** | R. Sitia lab. Universita' Vita-Salute San Raffaele, Milan. (Bestetti et al., 2020) |
| **HeLa$_{\mu s\lambda}$** | E. Van Ankeen lab. Universita' Vita-Salute San Raffaele, Milan. (Vitale et al., 2019) |
| **HEK Flp QIF16** | F. Qian lab. University of Maryland School of Medicine, Baltimore (PKD Research Resource Consortium) |
| **MEF PC-1-HA** | A. Boletta lab. Universita' San Raffaele Hospital, Milan. (Nigro et al., 2019) |

***Table 3 List of the cell lines used in this work***

For simplicity, I schematized below the specific experimental time-line that was used to treat each different cell line. Details about the protocol are clarified below.

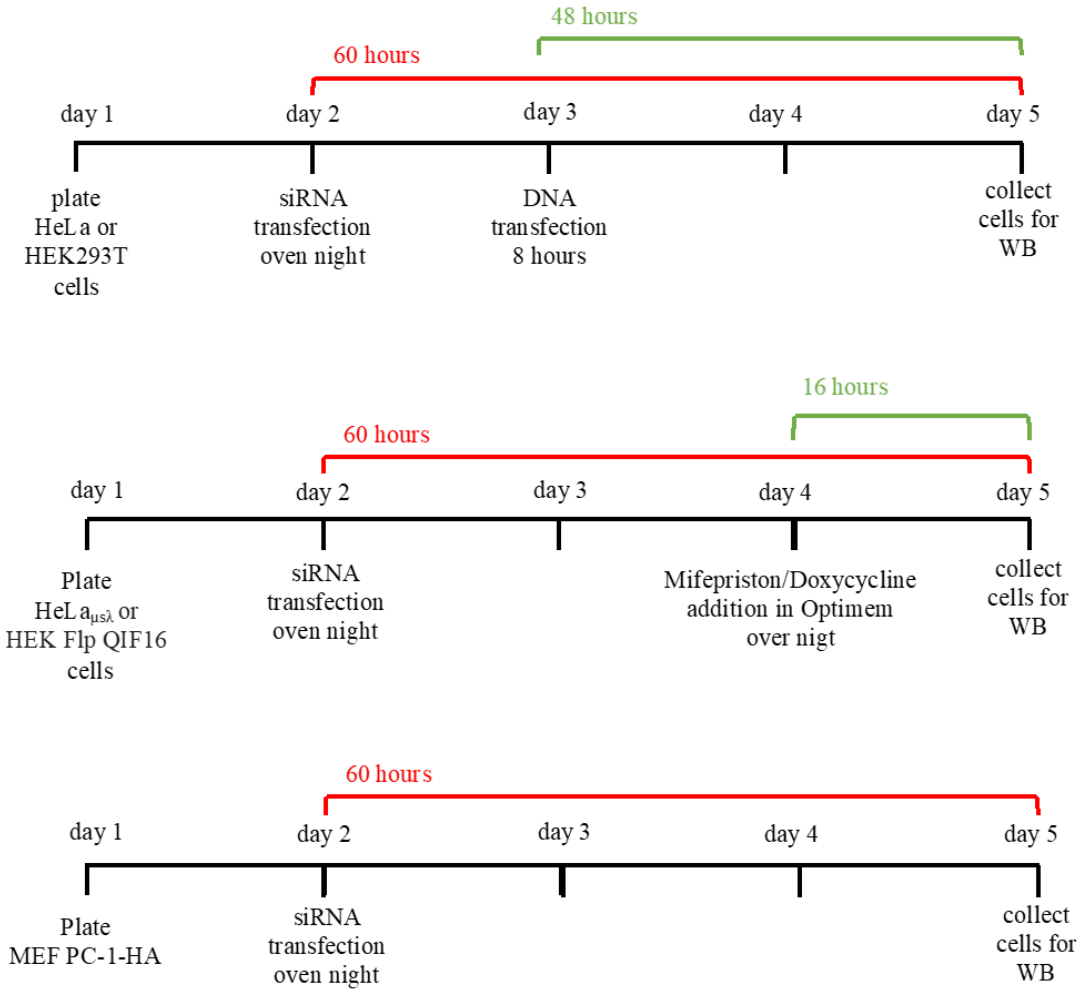



***Figure 34: Experimental time-line for each cell line***
*Each cell line was treated as indicated and finally cells were collected, lysed and samples analysed by SDS-PAGE and subsequent immunoblot (WB).*

| Number of cells to plate for each cell line | 6-well plate | 6-cm plate | 10-cm plate |
|---|---|---|---|
| **HeLa, HeLa $_{\mu s\lambda}$** | $1.5X10^5$ | $2.5X10^5$ | $5X10^5$ |
| **HEK 293T, HEK Flp QIF16** | $2.5X10^5$ | $5X10^5$ | $1X10^6$ |
| **MEF PC-1-HA** | | $2.5X10^5$ | |

***Table 4: number of cells plated for each cell line***

## 5.2 Small interfering RNAs, plasmids and transfection procedures

For small interfering RNA (siRNA) transfection I used RNAi MAX reagent (Invitrogen 13778075).

The day after plating (~60% cells confluency), prepare two mixes as follows:

A) (250 μL Optimem + 3 μL siRNA 20 μL) x 6-well plate

B) (250 μL Optimem + 4 μL RNAi MAX) x 6-well plate

Incubate the two mixes separately 5 minutes at room temperature (RT).

Mix B in A and incubate 20 minutes at RT.

Add drop by drop 500 μL of the mix to each well in which were previously added 500 μL of fresh medium (final concentration 60 nM siRNA for each well). Leave over-night and replace with fresh medium the following day.

| Gene | siRNA sense sequence 5'→3' |
|---|---|
| ***AQP11* (human)** | GAGCUUCGCUUGCAAGAAUTT |
| ***AQP11* (mouse)** | GCCUGAGUCUGACCAAGUATT |
| ***PKD2* (human)** | GACGCCGTGATCGTGAAGCTAGAGA |
| ***CBS* (human)** | CTCACATCCTAGACCAGTA |
| ***siRNA Universal negative control*** | REF: SIC001, Sigma |

***Table 5: List of siRNA sequences used in this work***

For plasmids transfection we used Jet Pei reagent (Polyplus PP10110N).

Prepare two mixes as follows:

A) (42μL of NaCl 150 mM + X μg DNA) x 6-well plate

B) (42 μL of NaCl 150 mM + 2X μL JetPei) x 6-well plate

Incubate separately for 5 minutes at RT.

Mix B in A and incubate 20 minutes at RT.

Add drop by drop 84 μL of the mix to each well in which was previously added 1 mL of fresh medium. Leave over day (~ 8 hours) and then replace with fresh medium.

| Plasmid | DNA transfected (x 6-well plate) | Origine |
|---|---|---|
| **PC-1-Myc/HA** | 1 μg | A. Boletta lab., San Raffaele Hospital, Milan. |
| **PC-2-Myc (QF2-3N)** | 0,5 μg | F. Qian, PKD Research Resource Consortium |
| **ER-CAT-Myc** | 1 μg | E. Avezov lab., University of Cambridge, UK |

***Table 6: List of plasmids used in this work***

To induce IgM expression in HeLa $_{\mu s\lambda}$ cells, 0.5 nM mifepristone was added to the medium over-night and cells were collected the following day.

To induce QIF16 mutant expression in HEK Flp QIF16 cells, 1 μg/mL doxycycline was added to the medium over-night and cells were collected the following day.

## 5.3 SDS-PAGE and immunoblot

After treatments, cells were lysed with a Lysis Buffer (LB) containing 1% CHAPS, 150 mM NaCl, 20mM Tris-HCl ph 7.5 and 5mM EDTA in water. LB was supplemented with a cocktail of protease inhibitor (04693132001, Roche) and N-etilmaleimide (E3876, Sigma Aldric) to prevent disulphides formation upon lysis. For lysis, cells were kept 30 minutes on ice and then centrifuged at 14.000xg for 20 minutes. Following, the supernatant was collected for further analysis. For the experiments in which we tested possible precipitation of CTF with cell's membranes, upon centrifugation the pellet was resuspended in LB supplemented with 2% SDS and sonicated at 100W for 10 minutes to get rid of DNA.

Protein from total lysate were quantified through Bicinchonic acid assay (BCA) assay and protein samples were prepared by adding Sample Buffer 5x (10% SDS, 250 mM Tris HCl pH 6.8, Glycerol 50%, Bromophenol Blue) with/without 750 mM DTT to a 1x final dilution (SB5x + DTT). After, samples were heated at 65°C for 10 minutes and spun. Finally, protein samples were loaded and run on a 3-8% or 4-12% precast gel (EA0378BOX, NP0335BOX, Biorad). Upon SDS-PAGE, proteins were transferred in

wet on a nitrocellulose membrane (0.2 μm) for 2 hours at 350 mA. Finally, nitrocellulose was saturated with PBS1x-0,1% Tween + 5% milk for 1 hour at RT and incubated with primary antibodies diluted in PBS1x-0,1% Tween + 3% BSA and incubated over-night at 4°C.

| Primary antibodies | Species | Dilution | Conde | Brand |
|---|---|---|---|---|
| **Anti-Myc tag** | rabbit | 1:1000 | 2272S | Cell Signalling |
| **Anti-HA tag** | rat | 1:1000 | 11867423001 | Roche |
| **Anti-LRR (PC-1)** | mouse | 1:500 | 7E12 | Santa Cruz |
| **Anti-PC-2** | mouse | 1:500 | D-3 | Santa Cruz |
| **Anti-CBS** | rabbit | 1:1000 | 140600 | Abcam |
| **Anti-μ chain Alexa 647** | goat | 1:1000 | A21238 | Invitrogen |
| **Anti-LC3B** | rabbit | 1:1000 | NB100-2220 | Novus |
| **Anti-Ubiquitin P4D1** | mouse | 1:1000 | Sc-8017 | Santa Cruz |
| **Anti-tubulin** | mouse | 1:10.000 | T6074 | Sigma |

***Table 7: List of primary antibodies used in this work for immunoblot***

HRP-conjugated secondary antibodies were diluted in PBS1x-0,1% Tween + 5% milk and incubated for 1 hour at RT and membranes were developed with ECL (GEHRPN2209, Amersham). Images were acquired by Uvitec (Eppendorf) and subsequently analysed by ImageJ software.

## 5.4 Real-Time qPCR

To address level of AQP11 or PKD2 downregulation following siRNA treatment, we performed RT-qPCR. For RNA extraction I used TriFast reagent (EMR507200, Euroclone) followed by chloroform-phenol extraction method. For retrotranscription, ImProm-II Reverse Transcriptase (A3801, Promega) protocol was used. For real-time qPCR, iTAQ Universal SYBR Green Supermix (1725121, Biorad) protocol was used on a Real time CXF Connect (Biorad).

| ***Gene*** | ***Forward qPCR primer*** | ***Reverse qPCR primer*** |
|---|---|---|
| ***Human AQP11*** | TAGCTTGCAGGAATCCCATC | CTCCTGCATAGGCCAAAAAG |
| ***Human PKD2*** | GAACAAGACTCATGGAGGAAA | GGAAGAGCTGTGACATCATC |
| ***Human GAPDH*** | TGAAGGTCGGAGTCAACGGATT | CATGTAAACCATGTAGTTGAGGT |
| ***Mouse Aqp11*** | CTTTCTCTGCACTTTCCGTG | CTGTCCTGGGACTTAGTTCG |
| ***Mouse Hprt1*** | TTATGTCCCCCGTTGACTGA | ACATTGTGGCCCTCTGTGTG |

***Table 8: List of primer sequences used in this work forRT qPCR***

## 5.5 Radioactive pulse-chase

For the radioactive pulse-chase, $5x10^5$ HEK 293T were plated in 10 cm plates the day before siRNA transfection. siRNA, were kept over-night. The day after, cells were washed out and transfected using 6 µg of plasmid DNA/plate. DNA was washed out 8 hours after. Upon 48 hours from DNA transfection, cells were detached, counted and pelleted (see time-line in Figure 34). After centrifugation, the medium was thrown away and cells were resuspended in medium deprived from cysteine and methionine (1 mL/$10^7$ cells) for starvation, and incubated 20 minutes at 37°C. After, a mix of radioactive cysteines and methionines (3 µL/$10^6$ cells) was added and cells were incubated 20 minutes at 37°C. Finally, cells were pelleted, resuspended in complete medium (1mL/$3x10^6$ cells) and divided in time points ($3x10^6$ cells/each). For time 0 minutes, an excess of cold PBS1x was added immediately after and cells were pelleted at 4°C, washed again with PBS1x, the supernatant was thrown away and cells were lysed in 500 µL of LB. For the other time points, cells were incubated at 37°C for 20, 50 and 120 minutes and finally treated as described for the time 0.

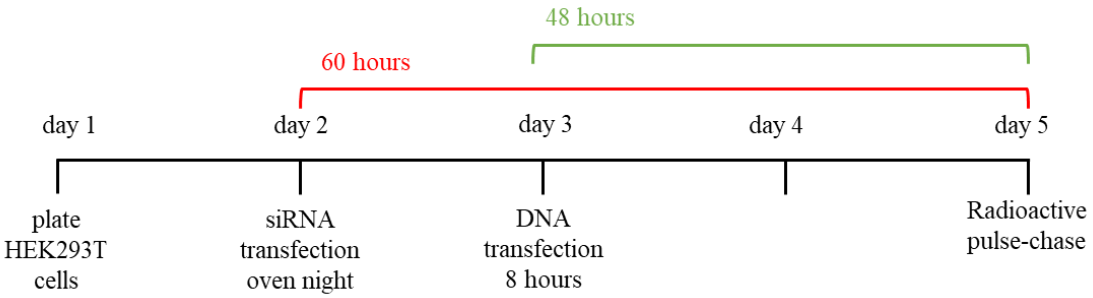



***Figure 35: Time-line for radioactive pulse-chase experiment***

For immunoprecipitation of PC-1-Myc, 25 µL of anti-Myc beads (20168, Thermo Scientific) and 1 µg of anti-PC-1 (7E12) + 25 µL of PGS beads (Neo Biotec, NB-45-00037-5) were added to the total lysate from $1,5x10^6$ cells, Then, LB was added up to 500 µL. Samples were incubated on a rotor wheel at 4°C over-night. The following day, samples were centrifuged at 3000 rpm 5 minutes at 4°C and the left over was collected. Beads were subsequently washed with three different buffers: Buffer A for the first wash (500 mM NaCl, 0.5% NP40, 0.05% SDS, 10 mM Tris-HCl pH 7.4); Buffer B for the second wash (150 mM NaCl, 0.25% NP40, 10 mM Tris-HCl pH 7.4); Buffer C for the

third was (5 mM Tris-HCl pH 7.4). Finally, beads were resuspended in SB2x + 250 mM DTT and boiled at 65°C for 10 minutes before loading them on SDS-PAGE.

## 5.6 Protein synthesis and degradation inhibition

To study PC-1 stability in different conditions, HeLa cells were treated as described in the section "cell culture and methods". At day 5, before being collected, cells were further treated by the addition of 500 μM Cycloheximide (CHX) for 0, 1, 2 or 4 hours to block protein synthesis. Only samples in which CHX was kept in culture for 4 hours were also treated with/without the addition of 100 μM Bafilomycin or 50 μM MG132 to block autophagy or the proteasome respectively. Upon treatments, cells were normally collected and processed for SDS-PAGE.

## 5.7 Deglycosylation assay

For the deglycosylation assay, total lysate or Optimem from over-night secretion were collected and supplemented with protease inhibitor and N-etilmaleimide. Then, a volume corresponding to $10^6$ cells was concentrated by addition of 10% Trichloroacetic acid (TCA) over-night at 4°C. The following day, samples were centrifuged at 17.000xg for 20 minutes at 4°C to precipitate secreted proteins, the supernatant was discarded, and the pellet washed two times: for the first wash cold 80% Acetone in water was used, for the second cold 100% Acetone was used. Finally, the protein pellet was resuspended in 20 μL of denaturing buffer (supplemented with the Endo-H and PNGase-F kit), split in three (not treated, Endo-H or PNGase-F treated samples) and further processed according with Endo-H (P0703L, New England Biolab) or PNGase-F (P0704S, New England Biolab) protocol. Finally, samples were diluted in SB5x + DTT and loaded on SDS-PAGE.

## 5.8 ELISA on secreted IgM

Samples for ELISA test were obtained from HeLa$_{\mu s\lambda}$ upon 48 hours of silencing with siRNA control or against AQP11 transcript. Successively, HeLa$_{\mu s\lambda}$ were treated with mifepristone 0.5 nM over night to induce IgM expression (Bakunts *et al*, 2017). The following day, the medium was washed and 1 ml Optimem was added for 4 hours before to collect it. The volume of medium corresponding to the secretion from $10^6$ cells was diluted 1:10 in PBS1x before to load it on the ELISA plate.

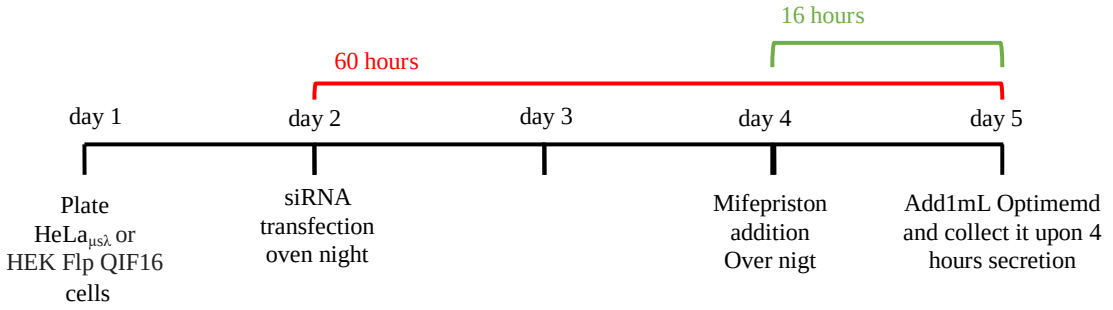



***Figure 36: Time-line for ELISA test***

ELISA 96-well plates were coated with anti-μ (61-6800, Zymed) 1:200 in PBS1x over night at 4°C (100μL/well). The following day, wells were washed three times with PBS1x and successively blocked with PBS1x + 3% milk (200 μL/well) 1 hour at 37°C. Next, wells were washed three times with PBS1x + 0.05% Tween. Samples (1:10 dilution in PBS1x) were added (100 μL/well) and incubated for 2 hours at 37°C. Upon three washes with PBS1x + 0.05% Tween, anti-μ HRP (1021-05, SouthernBiotech) 1:1000 in PBS1x was added (100 μL/well) and incubated for 1 hour at 37°C. Finally, wells were washed three times with PBS1x + 0.05% Tween and SigmaFAst OPD (P9187-50SET, Sigma) was added and incubated 15 minutes at RT before to read the plate at 450 nm. The calibration curve was prepared by using dilutions of purified mouse myeloma IgM (026800, Invitrogen) in PBS1x ph 7.4 + 0.1% azide.

## 5.9 Immunofluorescence

For Immunofluorescence (IF) experiments, $4x10^5$ HeLa cells were plated at day 1 on a 13 mm glass coverslip and subsequently treated like described in the section "cell culture and methods". At the end of the treatments, cells were fixed in 4% PFA for 10 minutes at RT. Permeabilization was done in PBS1x 0,1% Triton for 5 minutes at RT and following blocking in PBS1x + 10% FCS for 1 hour at RT. Upon blocking, cells were incubated with primary antibodies diluted in blocking solution for 1 hour at RT. Next, cells were washed three times in PBS1x and Alexa-fluorescent secondary antibodies (Invitrogen) were added diluted in blocking solution for 1 hour at RT. Finally, cells were washed three times in PBS1x and mounted on the support with mowiol.

| PRIMARY ANTIBODIES | SPECIES | DILUTION | CONDE | BRAND |
|---|---|---|---|---|
| **ANTI-MYC TAG** | mouse | 1:100 | 9E10 | in house |
| **ANTI-CALNEXIN** | rabbit | 1:500 | C5C9 | Cell signalling |
| **ANTI-CALRETICULIN** | rabbit | 1:500 | C4606 | Sigma |

***Table 9: List of primary antibodies used in this work for immunofluorescence***

## 5.10 Generation of Halo-DAAO-ER

To generate Halo-DAAO-ER, DAAO CDS was PCR amplified starting from cytosolic-DAAO expressing plasmid (supplied by Belousov laboratory, Shemyakin-Ovchinnikov Institute of Bioorganic Chemistry RAS, Moscow). The forward and reverse primers used to amplify DAAO contained NotI and KpnI restriction site respectively. In addition, a KDEL sequence for ER-retention was added to the reverse primer before the stop codon. The PCR product was subcloned in frame with Halo into the pcDNA3.1-Halo-Erp44 vector (Tempio *et al*, 2021) from which Erp44 was removed by NotI and KpnI digestion. The plasmid already contains the leader sequence of Erp44 upstream to Halo CDS. To visualize Halo-DAAO, cells were incubated over night with Halo-Tag$^{TMR}$ ligand (G299A, Sigma) diluted 1:20.000 in the cell medium and finally fixed and processed for IF.

| | |
|---|---|
| **Forward primer 5'→3'** | GGAGCGGCCGCTATGCACTCTCAGAAGCGCG TCGTTGTCCTCGGATCAGG |
| **Reverse Primer 5'→3'** | AACGGTACCCTACAGCTCGTCCTTGTCGCTCA ACTTCGACTCCCGCGCCGCGC |

***Table 10: Primer used to generate Halo-DAAO-ER***

## 5.11 Hyper Imaging

HyPer technology takes advantage of a bacterial transcription factor that senses $H_2O_2$ levels. In bacteria, the increase in intracellular $H_2O_2$ triggers the formation of a disulfide bond between two redox-sensitive cysteines in the OxyR promoting the activation of the transcription factor and the upregulation of antioxidant genes. In HyPer, the two cysteines have been separated by a modified YFP. Thus, when the probe is exposed to $H_2O_2$ the formation of the disulfide is induced, and as consequence, the rearrangement of the 3D structure changes the emission spectra of the linked YFP. The modified fluorescent domain is ratiometric. Indeed, it has two different excitation wavelengths (420nm and 480 nm), and both emit at 520nm. The ratio between the modifications of the emission spectra at 480 and 420 nm correlates with $H_2O_2$ levels (Bilan & Belousov). To perform live imaging on HeLa stably expressing HyperER-Lumen, $8x10^4$ cells were plated in a 35-mm plate on 25mm glass coverslip. The following day, cells were first silenced and then transfected. After 48 hours from silencing and 40 hours from transfection, cells were equilibrated in Ringer Buffer (140 nM NaCl, 10, mM Hepes, 10 mM Glucose, 2 mM $CaCl_2$, 1 mM $MgSO_4$, 1.5 mM $K_2HPO_4$, pH 7.4) for 10 minutes at RT before starting live imaging. Confocal images were acquired with an Ultraview confocal microscope (PerkinElmer) with a EC Plan - Neofluar 20X (NA 0.45) Dry (Carl Zeiss). Images were collected every 2 seconds for 1 minute by dual excitation with a 488-nm argon and 405-nm violet diode lasers. For calculating the value of the Basal $H_2O_2$ level, we made the ratio 488/405nm with ImageJ software of ≥25 cells/well. We represented as the average of the first 21-60sec acquisition set-points, the initial 20sec excluded to allow exposure to laser equilibration. For each condition were done two independent experiments.

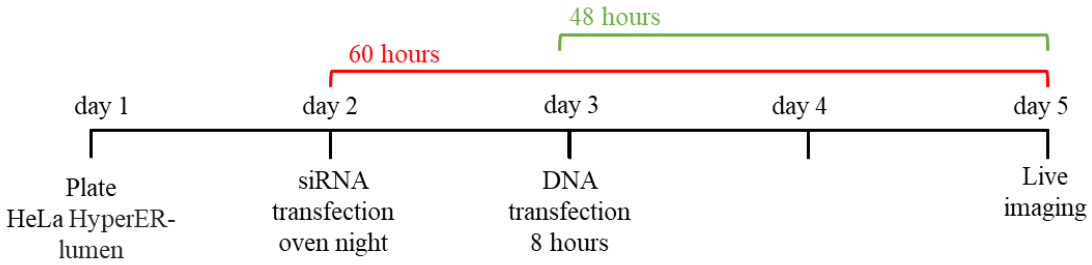



***Figure 37: Time-line for live-imaging with HyperProbe***

## 5.12 Quantification and statistical analysis

To quantify the decrease in PC-1's cleaved forms, the mean-gray value was quantified by ImageJ software for each band (FL, NTF, CTF, p100 or CTT). Next, for each individual condition, the mean-gray value of any of the PC-1's cleaved forms were divided by the sum between the cleaved form mean-gray value and the FL mean-gray $(\text{cleaved/cleaved+FL})_{\text{mean-gray value}}$.

The mean between ≥ 3 individual experiments was calculated and statistical significance between each condition vs control was assessed by unpaired t-test (GraphPad Prism software).

For qPCR quantification, the relative expression of each gene was calculated based on the Cq value. Cq corresponds to the PCR cycle number at which the sample reaction curve intersects the threshold line, which is the level of detection at which the reaction reached a fluorescent intensity above background levels. The Cq of the gene of interest in each sample was normalized on the Cq of the housekeeping gene (*GAPDH* or *Hpr1*). The formula below was applied to calculate the residual expression of the gene in Knock Down (KD) samples compared to control.

$$\Delta Cq \text{ in control} = Cq_{(GENE)} - Cq_{(house\ keeping)}$$

$$\Delta Cq \text{ in KD} = Cq_{(GENE)} - Cq_{(house\ keeping)}$$

$$\Delta\Delta Cq = \Delta Cq \text{ in KD} - \Delta Cq \text{ in control}$$

The mean residual expression between the experiments analysed in parallel by SDS-PAGE, was calculated. The significance difference between each condition vs control was assessed by unpaired t-test (GraphPad Prism software).

## 5.13 Intracellular Antibodies Capture Technology screening

N- or C-terminus of AQP8 and AQP11 were amplified starting from HaloAQP8 and HaloAQP11 plasmids respectively (Bertolotti *et al*, 2016; Bestetti *et al*, 2020) using specific primers containing EcoRI and BamHI restriction site. Next, the PCR products were digested and cloned into the pMIC-BD1 "bait" vector between EcoRI and BamHI restriction sites.

| *Baits* | *Forward primer 5'→3'* | *Reverse primer 5'→3'* |
|---|---|---|
| ***AQP8-N*** | GTGATCGAATTCGCAGCAGCAGCAATGTCTGGAGAGATAGCCATGTGTGAG | CACTAGGGATCCGGCGGCGGCC**T**ACCTGCCACCCACGCTCGGCTC |
| ***AQP8-C*** | GTGATCGAATTCGCAGCAGCAATGAAGACCCGCCTCATC | CACTAGGGATCCGGCGGCGGCTCACCGAGCCTTCAG |
| ***AQP11-N*** | GTGATCGAATTCGCAGCAGCAATGTCGCCGCTGCTGGGG | CACTAGGGATCCGGCGGCGGCCT**A**CAGCTCGGACCGGAG |
| ***AQP11-C*** | GTGATCGAATTCGCAGCAGCC**A**TGCATAACAACCATACA | CACTAGGGATCCGGCGGCGGCTTATTCCTTTTTATTAAT |

***Table 11: List of primers used to generate the "Baits"***

The resulting vectors were used to transform L40 yeast strain that was plated on -L medium.

For transformation, yeast cells were grown in 1 L of liquid culture (Yeast- Peptone-Adenine-Glucose, YPAD medium) to reach a concentration of 0,6-0,8 OD (exponential grow phase). Following, the yeast culture was pelleted by centrifugation at 3000 rpm for 5 minutes at RT. The pellet was washed two times in TE1x pH 7.5 (Tris 100 mM, EDTA 10 mM) and finally resuspended in 12 mL of TE-LiAc pH 7.5 (TE1x, Lithium Acetate 1M). Then, 250 μg of plasmid DNA and 10 mg of Salmo Testis DNA (STD) that improved transformation efficiency were added and mixed by vortexing. To facilitate yeast wall break, 140 mL of 40% PEG in TE-LiAc were added. What follows is a

conditioning step during which yeasts are grown at 30°C for 30 minutes shacking at 160 rpm. At the end, 17,6 mL of DMSO was added and the heat-shock was performed (15 minutes at 42°C, followed by cold YPA addition and kept on ice for 5 minutes). Cells were then pelleted and washed two times in YPA. Finally, the pellet was resuspended in 1 L of YPAD and recovered at 30°C for 1 hour shacking at 160 rpm. At the end of the recovery, cells were pelleted and washed two times in -L medium and finally resuspended in 5 mL of -L and plated on -L plates.

For the primary screening, we decided to test the human ScFv library against the mix of the four baits together. Here, I will resume the main steps of the primary screening:

1. We cultured a mix of the four baits together that were co-transform with 250 ug of ScFv library. Co-transformed cells were plated on -WL and -WHL plates and let grown at 30°C for 3 days.
2. After 3 days, we checked for colonies containing positive interactors that were able to grow on both -WL and -WHL plates. 360 colonies were chosen and picked to plate them separately on -WL and -WHL plates.
3. Upon regrow, a colony PCR was performed on yeast total lysates. Briefly, each colony was lysed by adding NaOH 20 mM and incubating 10 minutes at 95°C. On the lysate, a PCR was performed using primers to amplify the ScFv sequence on the prey plasmid.
4. Colony PCR were following digested by BstNI restriction enzymes that cuts a very common sequence (CCWGG) by generating different digestion patterns for each different ScFv amplified.
5. The digestion product was run on a polyacrylamide gel to visualize the "finger print" of each ScFv. In this way we could recognize the colonies in which the positive interaction was given by the same ScFv. Only one ScFv per type was subsequently testes in the secondary screening.

Each single ScFv that gave a positive interaction with the baits was extracted by MINI-preps from colonies grown on -WHL. First, cells were pelleted at 14.000 rpm for 2 minutes, resuspended in Lyticase Buffer (Sorbitol 2M, TrisHCl 1M pH 8, $CaCl_2$ 1M, 8% β-mercaptoethanol, 0,25% Lyticase in water) and incubated at 37°C for 1 hour by shacking. This step allows the break of the yeast wall. After, yeast cells were lysed using

the mini-prep extraction kit (A6814, Promega) generally used for bacterial mini-prep extraction. At the end, what is obtained for each colony is a mix between the prey and the bait plasmid. To isolate the prey from the bait plasmid, the mix of the two was following used to transform DH5α competent bacteria by electroporation at 200 V. Only one plasmid copy will transform a single bacterial cell. Bacteria were following plated on Luria Bertani agarose plates supplemented with Ampicillin (Amp). In this way, only bacterial cells that were transformed with the prey plasmid grow because they express Amp resistance. On the contrary, those that were transformed with the bait plasmid have Chloramphenicol (Cam) resistance thus will not grow. The prey plasmids containing ScFv that gave the positive interaction were re-tested against each of the four baits separately in the secondary screening. The secondary screening was performed exactly like the primary screening.

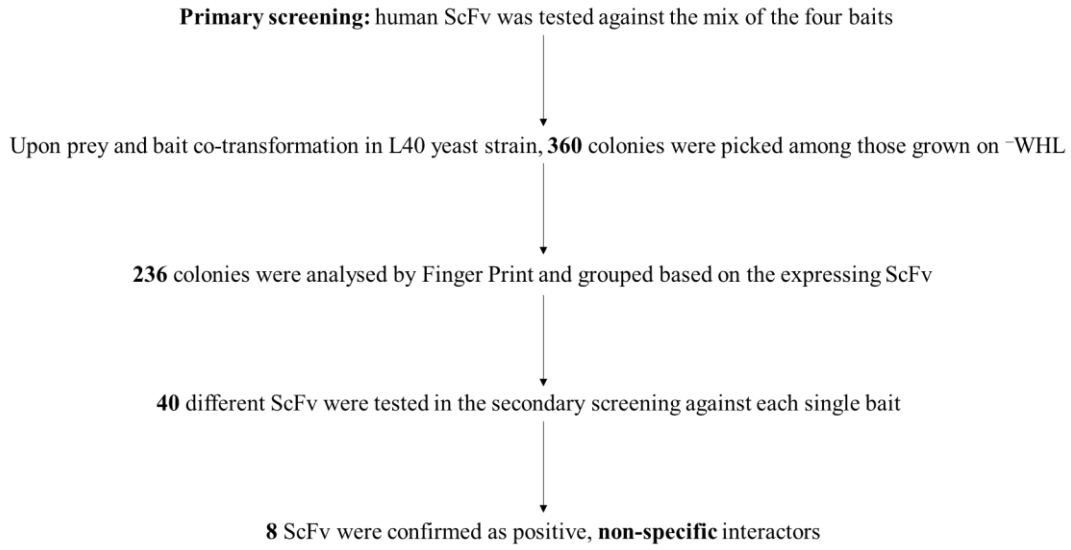



***Figure 38: Schematic representation of the main steps of the screening***

# 6 References


Abor G´, Os E″, Dosztányi Z & Dosztányi D (2018) IUPred2A: context-dependent prediction of protein disorder as a function of redox state and protein binding B ´ alint M ´ eszárosesz´eszáros. *Nucleic Acids Res* 46: 329–337

Anelli T, Bergamelli L, Margittai E, Rimessi A, Fagioli C, Malgaroli A, Pinton P, Ripamonti M, Rizzuto R & Sitia R (2012) Ero1α regulates Ca(2+) fluxes at the endoplasmic reticulum-mitochondria interface (MAM). *Antioxid Redox Signal* 16: 1077–1087

Anelli T & Sitia R (2008) Protein quality control in the early secretory pathway. *EMBO J* 27: 315–327

Araki K & Nagata K Protein Folding and Quality Control in the ER.

Arnould T, Kim E, Tsiokas L, Jochimsen F, Grü Ning W, Chang JD & Walz G (1998) The Polycystic Kidney Disease 1 Gene Product Mediates Protein Kinase C-dependent and c-Jun N-terminal Kinase-dependent Activation of the Transcription Factor AP-1*.

Asvapromtada S, Sonoda H, Kinouchi M, Oshikawa S, Takahashi S, Hoshino Y, Sinlapadeelerdkul T, Yokota-Ikeda N, Matsuzaki T & Ikeda M (2018) Characterization of urinary exosomal release of aquaporin-1 and-2 after renal ischemia-reperfusion in rats. *Am J Physiol Renal Physiol* 314: 584–601

Atochina-Vasserman EN, Biktasova A, Abramova E, Cheng DS, Polosukhin V V., Tanjore H, Takahashi S, Sonoda H, Foye L, Venkov C, *et al* (2013) Aquaporin 11 insufficiency modulates kidney susceptibility to oxidative stress. *Am J Physiol Renal Physiol* 304: 1295–1307

Bakunts A, Orsi A, Vitale M, Cattaneo A, Lari F, Tadè L, Sitia R, Raimondi A, Bachi A & van Anken E (2017) Ratiometric sensing of BiP-client versus BiP levels by the unfolded protein response determines its signaling amplitude. *Elife* 6

Belousov V V., Fradkov AF, Lukyanov KA, Staroverov DB, Shakhbazov KS, Terskikh A V. & Lukyanov S (2006) Genetically encoded fluorescent indicator for intracellular hydrogen peroxide. *Nat Methods* 3: 281–286

Bergmann C (2019) Experimental Nephrology and Genetics: Review Early and Severe Polycystic Kidney Disease and Related Ciliopathies: An Emerging Field of Interest. *Nephron* 141: 50–60

Bergmann C, Guay-Woodford LM, Harris PC, Horie S, Peters DJM & Torres VE (2018) Polycystic kidney disease. *Nat Rev Dis Primers* 4: 1–24 doi:10.1038/s41572-018-0047-y [PREPRINT]

Bergmann C, Senderek J, Küpper F, Schneider F, Dornia C, Windelen E, Eggermann T, Rudnik-Schöneborn S, Kirfel J, Furu L, *et al* (2004) PKHD1 mutations in autosomal recessive polycystic kidney disease (ARPKD). *Hum Mutat* 23: 453–463

Bertolotti M, Farinelli G, Galli M, Aiuti A & Sitia R (2016) AQP8 transports NOX2-generated H 2 O 2 across the plasma membrane to promote signaling in B cells . *J Leukoc Biol* 100: 1071–1079

Besse W, Chang AR, Luo JZ, Triffo WJ, Moore BS, Gulati A, Hartzel DN, Mane S, Torres VE, Somlo S, *et al* (2019) ALG9 Mutation Carriers Develop Kidney and Liver Cysts. *J Am Soc Nephrol* 30: 2091–2102

Besse W, Choi J, Ahram D, Mane S, Sanna-Cherchi S, Torres V & Somlo S (2018) A non-coding variant in GANAB explains isolated polycystic liver disease (PCLD) in a large family. *Hum Mutat* 39: 378

Besse W, Dong K, Choi J, Punia S, Fedeles S V., Choi M, Gallagher AR, Huang EB, Gulati A, Knight J, *et al* (2017a) Isolated polycystic liver disease genes define effectors of polycystin-1 function. *J Clin Invest* 127: 1772–1785

Besse W, Dong K, Choi J, Punia S, Fedeles S V., Choi M, Gallagher AR, Huang EB, Gulati A, Knight J, *et al* (2017b) Isolated polycystic liver disease genes define effectors of polycystin-1 function. *J Clin Invest* 127: 1772–1785

Bestetti S, Galli M, Sorrentino I, Pinton P, Rimessi A, Sitia R & Medraño-Fernandez I (2020) Human aquaporin-11 guarantees efficient transport of H2O2 across the endoplasmic reticulum membrane. *Redox Biol* 28: 101326

Bestetti S, Medraño-Fernandez I, Galli M, Ghitti M, Bienert GP, Musco G, Orsi A, Rubartelli A & Sitia R (2018) A persulfidation-based mechanism controls aquaporin-8 conductance. *Sci Adv* 4: 5770

Bienert GP, Schjoerring JK & Jahn TP (2006) Membrane transport of hydrogen peroxide.

Bilan DS & Belousov V V In Vivo Imaging of Hydrogen Peroxide with HyPer Probes.

Bockenhauer | & Bichet DG (2015) Pathophysiology, diagnosis and management of nephrogenic diabetes insipidus. *Nature Publishing Group* 11: 576–588

Cai Y, Maeda Y, Cedzich A, Torres VE, Wu G, Hayashi T, Mochizuki T, Park JH, Witzgall R & Somlo S (1999) Identification and characterization of polycystin-2, the PKD2 gene product. *J Biol Chem* 274: 28557–28565

Chapin HC, Rajendran V & Caplan MJ (2010) Polycystin-1 Surface Localization Is Stimulated by Polycystin-2 and Cleavage at the G Protein-coupled Receptor Proteolytic Site. *Mol Biol Cell* 21: 4338

Chauvet V, Qian F, Boute N, Cai Y, Phakdeekitacharoen B, Onuchic LF, Attié-Bitach T, Guicharnaud L, Devuyst O, Germino GG, *et al* (2002) Expression of PKD1 and PKD2 Transcripts and Proteins in Human Embryo and during Normal Kidney Development. *Am J Pathol* 160: 973–983

Chauvet V, Tian X, Husson H, Grimm DH, Wang T, Hieseberger T, Igarashi P, Bennett AM, Ibraghimov-Beskrovnaya O, Somlo S, *et al* (2004) Mechanical stimuli induce cleavage and nuclear translocation of the polycystin-1 C terminus. *J Clin Invest* 114: 1433

Choma DP, Vanacore R, Naylor H, Zimmerman IA, Pavlichenko A, Pavlichenko A, Foye L, Carbone DP, Harris RC, Dikov MM, *et al* (2016) Aquaporin 11 variant associates with kidney disease in type 2 diabetic patients. *Am J Physiol Renal Physiol* 310: 416–425

Cornec-Le Gall E, Olson RJ, Besse W, Heyer CM, Gainullin VG, Smith JM, Audrézet MP, Hopp K, Porath B, Shi B, *et al* (2018a) Monoallelic Mutations to DNAJB11 Cause Atypical Autosomal-Dominant Polycystic Kidney Disease. *Am J Hum Genet* 102: 832–844

Cornec-Le Gall E, Torres VE & Harris PC (2018b) Genetic complexity of autosomal dominant polycystic kidney and liver diseases. *Journal of the American Society of Nephrology* 29: 13–23 doi:10.1681/ASN.2017050483 [PREPRINT]

Dosztányi Z, Csizmok V, Tompa P & Simon I (2005) IUPred: web server for the prediction of intrinsically unstructured regions of proteins based on estimated energy content. *BIOINFORMATICS APPLICATIONS NOTE* 21: 3433–3434

Ellgaard L, Molinari M & Helenius A (1999) Setting the standards: Quality control in the secretory pathway. *Science (1979)* 286: 1882–1888

Feng Qian, Alessandra Boletta, Anil K. Bhunia, Hangxue Xue, Lijuan Liu, Ali K. Ahrabi, Terry J. Watnick, Fang Zhou & Gregory G. Germino (2002) Cleavage of polycystin-

1 requires the receptor for egg jelly domain and is disrupted by human autosomal-dominant polycystic kidney disease 1-associated mutations. *Proc Natl Acad Sci U S A* 99: 16981–16986

Fagioli C, Mezghrani A & Sitia R (2001) Reduction of Interchain Disulfide Bonds Precedes the Dislocation of Ig-Chains from the Endoplasmic Reticulum to the Cytosol for Proteasomal Degradation*. *J Biol Chem* 276: 40962–40967

Fagioli C & Sitia R (2001) Glycoprotein quality control in the endoplasmic reticulum. Mannose trimming by endoplasmic reticulum mannosidase I times the proteasomal degradation of unassembled immunoglobulin subunits. *J Biol Chem* 276: 12885–12892

Fassio A & Sitia R (2002) Formation, isomerisation and reduction of disulphide bonds during protein quality control in the endoplasmic reticulum. *Histochem Cell Biol* 117: 151–157

Fedeles S V, Gallagher A-R & Somlo S (2014) Polycystin-1: a master regulator of intersecting cystic pathways.

Fedeles S V., So JS, Shrikhande A, Lee SH, Gallagher AR, Barkauskas CE, Somlo S & Lee AH (2015) Sec63 and Xbp1 regulate IRE1α activity and polycystic disease severity. *J Clin Invest* 125: 1955–1967

Fedeles S V., Tian X, Gallagher AR, Mitobe M, Nishio S, Lee SH, Cai Y, Geng L, Crews CM & Somlo S (2011) A genetic interaction network of five genes for human polycystic kidney and liver diseases defines polycystin-1 as the central determinant of cyst formation. *Nat Genet* 43: 639–647

Gainullin VG, Hopp K, Ward CJ, Hommerding CJ & Harris PC (2015) Polycystin-1 maturation requires polycystin-2 in a dose-dependent manner. *J Clin Invest* 125: 607–620

Geng L, Segal Y, Pavlova A, Barros EJG, Löhning C, Lu W, Nigam SK, Frischauf AM, Reeders ST & Zhou J (1997) Distribution and developmentally regulated expression of murine polycystin. *https://doi.org/101152/ajprenal19972724F451* 272

Grieben M, W Pike AC, Shintre CA, Venturi E, El-Ajouz S, Tessitore A, Shrestha L, Mukhopadhyay S, Mahajan P, Chalk R, *et al* (2016) Structure of the polycystic kidney disease TRP channel Polycystin-2 (PC2). *Nature Publishing Group*

Han B, Wu X, Huang PP, Zhu FX & Liu S (2019) Aquaporin 11 rs2276415 variant and progression of chronic kidney disease. *Nephrology Dialysis Transplantation* 34: 970–973

Hardy E & Tsiokas L Polycystins as components of large multiprotein complexes of polycystin interactors.

Harris PC, Torres V; E, Adam MP, Feldman J & Mirzaa GM (2002) Polycystic Kidney Disease, Autosomal Dominant. 1993–2023

Harris PC & Torres VE (2014) Genetic mechanisms and signaling pathways in autosomal dominant polycystic kidney disease. *Journal of Clinical Investigation* 124: 2315–2324 doi:10.1172/JCI72272 [PREPRINT]

He J & Yang B Molecular Sciences Review Aquaporins in Renal Diseases.

Higo T, Hattori M, Nakamura T, Natsume T, Michikawa T & Mikoshiba K (2005) Subtype-Specific and ER Lumenal Environment-Dependent Regulation of Inositol 1,4,5-Trisphosphate Receptor Type 1 by ERp44. *Cell* 120: 85–98

Holmström KM & Finkel T (2014) Cellular mechanisms and physiological consequences of redox-dependent signalling. *Nat Rev Mol Cell Biol* 15: 411–421

Hopp K, Ward CJ, Hommerding CJ, Nasr SH, Tuan HF, Gainullin VG, Rossetti S, Torres VE & Harris PC (2012) Functional polycystin-1 dosage governs autosomal dominant polycystic kidney disease severity. *J Clin Invest* 122: 4257–4273

Hoshino Y, Sonoda H, Nishimura R, Mori K, Ishibashi K & Ikeda M (2019) Involvement of the NADPH oxidase 2 pathway in renal oxidative stress in Aqp11-/-mice.

Hughes J, Ward CJ, Peral B, Aspinwall R, Clark K, Millán JLS, Gamble V & Harris PC (1995) The polycystic kidney disease 1 (PKD1) gene encodes a novel protein with multiple cell recognition domains. *Nat Genet* 10: 151–160

Hussein A-AM, El-Dken ZH, Barakat N, Abol-Enein H & Hussein -A M Renal ischaemia/reperfusion injury: possible role of aquaporins.

Huynh VT, Audrézet MP, Sayer JA, Ong AC, Lefevre S, Le Brun V, Després A, Senum SR, Chebib FT, Barroso-Gil M, *et al* (2020) Clinical spectrum, prognosis and estimated prevalence of DNAJB11-kidney disease. *Kidney Int* 98: 476

Ibraghimov-beskrovnaya O, Dackowski WR, Foggensteiner L, Coleman N, Thiru S, Petry LR, Burn TC, Connors TD, Van Raay T, Bradley J, *et al* (1997) Polycystin: In

vitro synthesis, in vivo tissue expression, and subcellular localization identifies a large membrane-associated protein. 94: 6397–6402

Igarashi P & Somlo S (2002) Genetics and pathogenesis of polycystic kidney disease. *Journal of the American Society of Nephrology* 13: 2384–2398

Ilani T, Reznik N, Yeshaya N, Feldman T, Vilela P, Lansky Z, Javitt G, Shemesh M, Brenner O, Elkis Y, *et al* (2023) The disulfide catalyst QSOX1 maintains the colon mucosal barrier by regulating Golgi glycosyltransferases. *EMBO J* 42: e111869

Inoue Y, Sohara E, Kobayashi K, Chiga M, Rai T, Ishibashi K, Horie S, Su X, Zhou J, Sasaki S, *et al* (2014) Aberrant glycosylation and localization of polycystin-1 cause polycystic kidney in an AQP11 knockout model. *Journal of the American Society of Nephrology* 25: 2789–2799

Konno, Melo, Lopes, Mehmeti, Lenzen, Ron, Avezov. Ero1-independent production of $H_2O_2$ within the endoplasmic reticulum fuels Prdx4-mediatedoxidative protein folding. JCB Report (2015)

Karala AR, Lappi AK, Saaranen MJ & Ruddock LW (2009) Efficient peroxide-mediated oxidative refolding of a protein at physiological pH and implications for oxidative folding in the endoplasmic reticulum. *Antioxid Redox Signal* 11: 963–970

Konno T, Melo EP, Chambers JE, Avezov E & Lederkremer Z (2021) cells Intracellular Sources of ROS/H 2 O 2 in Health and Neurodegeneration: Spotlight on Endoplasmic Reticulum.

Kopito RR & Sitia R (2000) Aggresomes and Russell bodies - Symptoms of cellular indigestion? *EMBO Rep* 1: 225–231

Koulen P, Cai Y, Geng L, Maeda Y, Nishimura S, Witzgall R, Ehrlich BE & Somlo S (2002) Polycystin-2 is an intracellular calcium release channel. *Nat Cell Biol* 4

Lal M, Song X, Pluznick JL, Giovanni V Di, Merrick DM, Rosenblum ND, Chauvet V, Gottardi CJ, Pei Y & Caplan MJ Polycystin-1 C-terminal tail associates with b-catenin and inhibits canonical Wnt signaling.

Laurindo FRM, Araujo TLS & Abrahão TB (2014) Nox NADPH oxidases and the endoplasmic reticulum. *Antioxid Redox Signal* 20: 2755–2775

Lee SH & Somlo S (2014) Cyst growth, polycystins, and primary cilia in autosomal dominant polycystic kidney disease.

Lemoine H, Raud L, Le Meur Y, Audrézet M-P, Cornec-Le E, Correspondence G, Foulquier F, Sayer JA, Lambert B, Olinger E, *et al* (2022) Monoallelic pathogenic ALG5 variants cause atypical polycystic kidney disease and interstitial fibrosis Graphical abstract Authors Monoallelic pathogenic ALG5 variants cause atypical polycystic kidney disease and interstitial fibrosis. *The American Journal of Human Genetics* 109

Leonhard WN, Happe H & Peters DJM (2016) Variable cyst development in autosomal dominant polycystic kidney disease: The biologic context. *Journal of the American Society of Nephrology* 27: 3530–3538

Li A, Davila S, Furu L, Qian Q, Tian X, Kamath PS, King BF, Torres VE & Somlo S (2003) Mutations in PRKCSH Cause Isolated Autosomal Dominant Polycystic Liver Disease. *Am J Hum Genet* 72: 691

Li Y & Camacho P (2004) Ca2+-dependent redox modulation of SERCA 2b by ERp57. *J Cell Biol* 164: 35–46

Lin C-C, Kurashige M, Liu Y, Terabayashi T, Ishimoto Y, Wang T, Choudhary V, Hobbs R, Liu L-K, Lee P-H, *et al* A cleavage product of Polycystin-1 is a mitochondrial matrix protein that affects mitochondria morphology and function when heterologously expressed.

Low SH, Vasanth S, Larson CH, Mukherjee S, Sharma N, Kinter MT, Kane ME, Obara T & Weimbs T (2006) Polycystin-1, STAT6, and P100 Function in a Pathway that Transduces Ciliary Mechanosensation and Is Activated in Polycystic Kidney Disease. *Dev Cell* 10: 57–69

Lu H, Rondón Galeano MC, Ott E, Kaeslin G, Jaya Kausalya P, Kramer C, Ortiz-Brüchle N, Hilger N, Metzis V, Hiersche M, *et al* (2017) Mutations in DZIP1L, which encodes a ciliary-transition-zone protein, cause autosomal recessive polycystic kidney disease.

M Bertolotti, S Bestetti, JM Garcia-Manteiga, I Medrano-Fernandez, A Dal Mas, ML Malosio & R S (2013) Tyrosine kinase signal modulation: a matter of H2O2 membrane permeability? *Antioxid Redox Signal* 19: 1447–1451

Meng T-C, Fukada T & Tonks NK (2002) Reversible Oxidation and Inactivation of Protein Tyrosine Phosphatases In Vivo. *Mol Cell* 9: 387–399

Merrick D, Chapin H, Baggs JE, Yu Z, Somlo S, Sun Z, Hogenesch JB & Caplan MJ Developmental Cell The g-Secretase Cleavage Product of Polycystin-1 Regulates TCF and CHOP-Mediated Transcriptional Activation through a p300-Dependent Mechanism.

Miller EW, Dickinson BC & Chang CJ (2010) Aquaporin-3 mediates hydrogen peroxide uptake to regulate downstream intracellular signaling. *Proc Natl Acad Sci U S A* 107

Morishita Y, Matsuzaki T, Hara-chikuma M, Andoo A, Shimono M, Matsuki A, Kobayashi K, Ikeda M, Yamamoto T, Verkman A, *et al* (2005) Disruption of aquaporin-11 produces polycystic kidneys following vacuolization of the proximal tubule. *Mol Cell Biol* 25: 7770–7779

Mozzarelli A, Tishkov VI, Phillips RS, Temussi PA, Pollegioni L, Sacchi S & Murtas G (2018) Human D-Amino Acid Oxidase: Structure, Function, and Regulation. *Frontiers in Molecular Biosciences | www.frontiersin.org* 5: 107

Murata K, Mitsuoka K, Hirai T, Walz T, Agrek P, Bernard Heymann J, Engel A, Fujiyoshi Y & Mu ME (2000) Structural determinants of water permeation through aquaporin-1. *Nature* 407

Nordzieke DE & Medraño-Fernandez I (2018) The plasma membrane: A platform for intra-and intercellular redox signaling. *Antioxidants* 7 doi:10.3390/antiox7110168 [PREPRINT]

Okada S, Misaka T, Tanaka Y, Matsumoto I, Ishibashi K, Sasaki S & Abe K (2008) Aquaporin-11 knockout mice and polycystic kidney disease animals share a common mechanism of cyst formation. *The FASEB Journal* 22: 3672–3684

OM Woodward, Y Li, S Yu, P Greenwell, C Wodarczyk, A Boletta, WB Guggino & F Qian (2010) Identification of a polycystin-1 cleavage product, P100, that regulates store operated Ca entry through interactions with STIM1. *PLoS One* 5

Onuchic L, Padovano V, Schena G, Rajendran V, Dong K, Gresko NP, Shi X, Shen H, Somlo S & Caplan MJ (2021) The C-terminal tail of polycystin-1 suppresses cystic disease in a mitochondrial enzyme-dependent fashion. *bioRxiv*: 2021.12.21.473680

Onuchic LF, Furu L, Nagasawa Y, Hou X, Eggermann T, Ren Z, Bergmann C, Senderek J, Esquivel E, Zeltner R, *et al* (2002) PKHD1, the Polycystic Kidney and Hepatic Disease 1 Gene, Encodes a Novel Large Protein Containing Multiple

Immunoglobulin-Like Plexin-Transcription-Factor Domains and Parallel Beta-Helix 1 Repeats. *Am J Hum Genet* 70: 1305–1317

Padovano V, Mistry K, Merrick D, Gresko N & Caplan MJ A Cut Above (and Below): Protein Cleavage in the Regulation of Polycystin Trafficking and Signaling.

Pellegrini H, Sharpe EH, Liu G, Nishiuchi E, Doerr N, Kipp KR, Chin T, Schimmel MF & Weimbs T (2023) Cleavage fragments of the C-terminal tail of polycystin-1 are regulated by oxidative stress and induce mitochondrial dysfunction.

Piontek K, Menezes LF, Garcia-Gonzalez MA, Huso DL & Germino GG (2007) A critical developmental switch defines the kinetics of kidney cyst formation after loss of Pkd1.

Podrini C, Cassina L & Boletta A (2020) Metabolic reprogramming and the role of mitochondria in polycystic kidney disease. *Cell Signal* 67

Podrini C, Rowe I, Pagliarini R, Costa ASH, Chiaravalli M, Di Meo I, Kim H, Distefano G, Tiranti V, Qian F, *et al* (2018) Dissection of metabolic reprogramming in polycystic kidney disease reveals coordinated rewiring of bioenergetic pathways. *Communications Biology 2018 1:1* 1: 1–14

Porath B, Gainullin VG, Cornec-Le Gall E, Dillinger EK, Heyer CM, Hopp K, Edwards ME, Madsen CD, Mauritz SR, Banks CJ, *et al* (2016) Mutations in GANAB, Encoding the Glucosidase IIα Subunit, Cause Autosomal-Dominant Polycystic Kidney and Liver Disease. *Am J Hum Genet* 98: 1193–1207

Preston GM, Jungs11 JS, Gugginoll WB & Agre P (1993) THE JOURNAL OF BIOLOGICAL CHEMISTRY The Mercury-sensitive Residue at Cysteine 189 in the CHIP28 Water Channel*. 268: 17–20

Price ME, Fishler KP, Muff-Luett M, Mauch TJ, Brunelli L & Euteneuer JC (2023) Variants in AQP11 may result in autosomal recessive bilateral cystic renal dysgenesis. *Am J Med Genet A* 191

Qian F, Boletta A, Bhunia AK, Xu H, Liu L, Ahrabi AK, Watnick TJ, Zhou F & Germino GG Cleavage of polycystin-1 requires the receptor for egg jelly domain and is disrupted by human autosomal-dominant polycystic kidney disease 1-associated mutations.

Reichmann D & Jakob U (2013) The roles of conditional disorder in redox proteins.

Roitbak T, Ward CJ, Harris PC, Bacallao R, Ness SA & Wandinger-Ness A (2004) A Polycystin-1 Multiprotein Complex Is Disrupted in Polycystic Kidney Disease Cells D. *Mol Biol Cell* 15: 1334–1346

Roscoe JM & Sevier CS cells Pathways for Sensing and Responding to Hydrogen Peroxide at the Endoplasmic Reticulum.

Russo RJ, Herve´husson AE, Ae H, Joly D, Ae NOB, Patey N, Knebelmann B & Ibraghimov-Beskrovnaya O Impaired formation of desmosomal junctions in ADPKD epithelia.

Rützler M, Rojek A, Damgaard MV, Andreasen A, Fenton RA & Nielsen S (2017) Temporal deletion of Aqp11 in mice is linked to the severity of cyst-like disease. *Am J Physiol Renal Physiol* 312: F343–F351

Sacharow SJ, Picker JD, Levy H; L, Adam MP, Feldman J & Mirzaa GM (2004) Homocystinuria Caused by Cystathionine Beta-Synthase Deficiency. 1993–2023

Schwartz RS, Hildebrandt F, Benzing T & Katsanis N (2011) Mechanisms of Disease Ciliopathies. *n engl j med* 364: 1533–1576

Senum SR, Li YM, Benson KA, Joli G, Olinger E, Lavu S, Madsen CD, Gregory A V, Neatu R, Kline TL, *et al* Monoallelic IFT140 pathogenic variants are an important cause of the autosomal dominant polycystic kidney-spectrum phenotype.

Shen PS, Yang X, Decaen PG, Liu X, Bulkley D & Clapham DE (2016) The Structure of the Polycystic Kidney Disease Channel PKD2 in Lipid Nanodiscs Data Resources 5T4D Shen et al. *Cell* 167: 763–773

Sies H (2017) Hydrogen peroxide as a central redox signaling molecule in physiological oxidative stress: Oxidative eustress. *Redox Biol* 11: 613–619 doi:10.1016/j.redox.2016.12.035 [PREPRINT]

Sies H & Jones DP (2020) Reactive oxygen species (ROS) as pleiotropic physiological signalling agents. *Nat Rev Mol Cell Biol* 21: 363–383

Silberberg M, Charron AJ, Bacallao R & Wandinger-Ness A (2005) Mispolarization of desmosomal proteins and altered intercellular adhesion in autosomal dominant polycystic kidney disease. *Am J Physiol Renal Physiol* 288: 1153–1163

Simmen T, Lynes EM, Gesson K & Thomas G (2010) Oxidative protein folding in the endoplasmic reticulum: tight links to the mitochondria-associated membrane (MAM). *Biochim Biophys Acta* 1798: 1465–1473

Soheil S, Saravi S, Eroglu E, Waldeck-Weiermair M, Sorrentino A, Steinhorn B, Belousov V & Michel T (2020) Differential endothelial signaling responses elicited by chemogenetic H 2 O 2 synthesis.

Somlo S & Guay-Woodford LM (2009) Polycystic Kidney Disease. *Genetic Diseases of the Kidney*: 393–424

Sorrentino I, Galli M, Medraño-Fernandez I & Sitia R (2022) Transfer of H2O2 from Mitochondria to the endoplasmic reticulum via Aquaporin-11. *Redox Biol* 55

Su Q, Hu F, Ge X, Lei J, Yu S, Wang T, Zhou Q, Mei C & Shi Y (2018) Structure of the human PKD1-PKD2 complex. *Science (1979)* 361

Su W, Cao R, Zhang X & Guan Y (2020) Aquaporins in the kidney: physiology and pathophysiology. *Am J Physiol Renal Physiol* 318: 193–203

Ta CM, Vien TN, Ng LCT & Decaen PG (2020) Structure and function of polycystin channels in primary cilia.

Tanaka Y, Watari M, Saito T, Morishita Y & Ishibashi K Enhanced Autophagy in Polycystic Kidneys of AQP11 Null Mice. *International Journal of Molecular Sciences Article*

Tavender TJ, Springate JJ & Bulleid NJ (2010) Recycling of peroxiredoxin IV provides a novel pathway for disulphide formation in the endoplasmic reticulum. *EMBO Journal* 29: 4185–4197

Tchekneva EE, Khuchua Z, Davis LS, Kadkina V, Dunn SR, Bachman S, Ishibashi K, Rinchik EM, Harris RC, Dikov MM, *et al* (2008) Single Amino Acid Substitution in Aquaporin 11 Causes Renal Failure. *Journal of the American Society of Nephrology* 19: 1955–1964

Tempio T, Orsi A, Sicari D, Valetti C, Yoboue ED, Anelli T & Sitia R (2021) A virtuous cycle operated by ERp44 and ERGIC-53 guarantees proteostasis in the early secretory compartment. *iScience* 24: 102244

Törnroth-Horsefield S, Hedfalk K, Fischer G, Lindkvist-Petersson K & Neutze R (2010) Structural insights into eukaryotic aquaporin regulation. *FEBS Lett* 584: 2580–2588

Trudel M, Yao Q & Qian F cells The Role of G-Protein-Coupled Receptor Proteolysis Site Cleavage of Polycystin-1 in Renal Physiology and Polycystic Kidney Disease.

Tsiokas L (PDF) Homo- and heterodimeric interactions between the gene products of PKD1 and PKD2.

Tu BP, Ho-Schleyer SC, Travers KJ & Weissman JS (2000) Biochemical basis of oxidative protein folding in the endoplasmic reticulum. *Science* 290: 1571–1574

Tu BP & Weissman JS (2002) The FAD-and O 2-Dependent Reaction Cycle of Ero1-Mediated Oxidative Protein Folding in the Endoplasmic Reticulum in oxidative folding in bacteria (Kobayashi et al disulfide formation is driven by a flavin-dependent reaction (Tu et al., 2000). Depletion of riboflavin, a precursor of flavin adenine dinucleotide (FAD), rapidly leads to defects in the folding. *Mol Cell* 10: 983–994

Tu BP & Weissman JS (2004) Mini-Review Oxidative protein folding in eukaryotes: mechanisms and consequences. *The Journal of Cell Biology JCB The Journal of Cell Biology* 164: 341–346

V Padovano, IY Kuo, LK Stavola, HR Aerni, BJ Flaherty, HC Chapin, M Ma, S Somlo, A Boletta, BE Ehrlich, *et al* (2017) The polycystins are modulated by cellular oxygen-sensing pathways and regulate mitochondrial function. *Mol Biol Cell* 28: 261–269

Verkman AS (2011) Aquaporins at a glance. *J Cell Sci* 124: 2107–2112

Visintin M, Quondam M & Cattaneo A (2004) The intracellular antibody capture technology: towards the high-throughput selection of functional intracellular antibodies for target validation. *Methods* 34: 200–214

Visintin M, Settanni G, Maritan A, Graziosi S, Marks JD & Cattaneo A (2002) The intracellular antibody capture technology (IACT): towards a consensus sequence for intracellular antibodies. *J Mol Biol* 317: 73–83

Watanabe S, Amagai Y, Sannino S, Tempio T, Anelli T, Harayama M, Masui S, Sorrentino I, Yamada M, Sitia R, *et al* Zinc regulates ERp44-dependent protein quality control in the early secretory pathway.

Watanabe S, Moniaga CS, Nielsen S & Hara-Chikuma M (2016) Aquaporin-9 facilitates membrane transport of hydrogen peroxide in mammalian cells. *Biochem Biophys Res Commun* 471: 191–197

Wei W, Hackmann K, Xu H, Germino G & Qian F (2007) Characterization of cis-autoproteolysis of polycystin-1, the product of human polycystic kidney disease 1 gene. *Journal of Biological Chemistry* 282

Yi F, Jin S, Zhang F, Xia M, Bao JX, Hu J, Poklis JL & Li PL (2009) Formation of lipid raft redox signalling platforms in glomerular endothelial cells: An early event of homocysteine-induced glomerular injury. *J Cell Mol Med* 13: 3303–3314

Yu S, Hackmann K, Gao J, He X, Piontek K, González MAG, Menezes LF, Xu H, Germino GG, Zuo J, *et al* (2007) Essential role of cleavage of Polycystin-1 at G protein-coupled receptor proteolytic site for kidney tubular structure. *Proc Natl Acad Sci U S A* 104: 18688–18693

Yu Y, Ulbrich MH, Li M-H, Buraei Z, Chen X-Z, Ong ACM, Tong L, Isacoff EY & Yang J Structural and molecular basis of the assembly of the TRPP2/PKD1 complex.

Zhuo JL & Li XC Proximal Nephron.

Zito E, Melo EP, Yang Y, Sa Wahlander A˚, Neubert TA & Ron D (2010) Article Oxidative Protein Folding by an Endoplasmic Reticulum-Localized Peroxiredoxin.

